PROCEEDINGS

MMM 2008

Fourth International Conference

MULTISCALE MATERIALS MODELING

OCTOBER 27-31, 2008 ▪ TALLAHASSEE, FLORIDA, USA

Tackling Materials Complexities via Computational Science

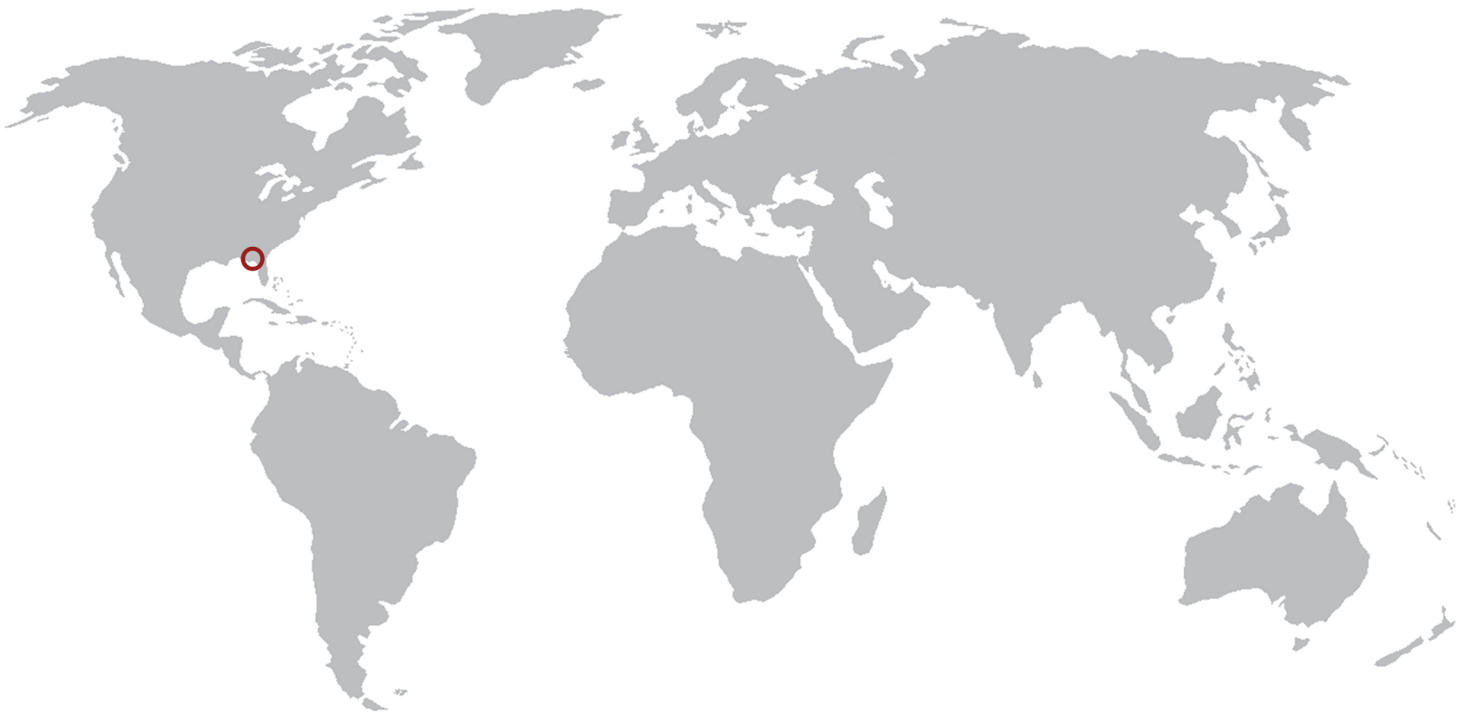

Hosted by the Department of Scientific Computing and Florida State University

DEPARTMENT OF Scientific COMPUTING

FLORIDA STATE UNIVERSITY 1851 VIRES ARTES MORES

Proceedings of

MMM 2008

Fourth International Conference

MULTISCALE MATERIALS MODELING

OCTOBER 27-31, 2008 ▪ TALLAHASSEE, FLORIDA, USA

Anter El-Azab
Editor

Organized and Hosted by
The Department of Scientific Computing and
Florida State University

DEPARTMENT OF Scientific COMPUTING

Papers published in this volume constitute the proceedings of the Fourth International Conference on Multiscale Materials Modeling (MMM-2008). Papers were selected by the program committee for oral or poster presentation. They are published as submitted, in the interest of timely dissemination.

ISBN 978-0-615-24781-6

Department of Scientific Computing
Florida State University
400 Dirac Science Library
P.O. Box 3064120
Tallahassee, FL 32306-4120

Printed in the United States of America

Forward

The field of multiscale modeling of materials promotes the development of predictive materials research tools that can be used to understand the structure and properties of materials at all scales and help us process materials with novel properties. By its very nature, this field transcends the boundaries between materials science, mechanics, and physics and chemistry of materials. The increasing interest in this field by mathematicians and computational scientists is creating opportunities for solving computational problems in the field with unprecedented levels of rigor and accuracy. Because it is a part of the wider field of materials science, multiscale materials research is intimately linked with experiments and, together, these methodologies serve the dual role of enhancing our fundamental understanding of materials and enabling materials design for improved performance.

The increasing role of multiscale modeling in materials research motivated the materials science community to start the Multiscale Materials Modeling (MMM) Conference series in 2002, with the goal of promoting new concepts in the field and fostering technical exchange within the community. Three successful conferences in this series have been already held:

- The First International Conference on Multiscale Materials Modeling (MMM-2002) at Queen Mary University of London, UK, June 17-20, 2002,
- Second International Conference on Multiscale Materials Modeling (MMM-2004) at the University of California in Los Angeles, USA, October 11-15, 2004, and
- Third International Conference on Multiscale Materials Modeling (MMM-2006) at the University of Freiburg, Germany, September 18-22, 2006.

The Fourth International Conference on Multiscale Materials Modeling (MMM-2008) held at Florida State University comes at a time when the wider computational science field is shaping up and the synergy between the materials modeling community and computational scientists and mathematicians is becoming significant. The overarching theme of the MMM-2008 conference is thus chosen to be "*Tackling Materials Complexities via Computational Science*," a theme that highlights the connection between multiscale materials modeling and the wider computational science field and also reflects the level of maturity that the field of multiscale materials research has come to. The conference covers topics ranging from basic multiscale modeling principles all the way to computational materials design. Nine symposia have been organized, which span the following topical areas:

- Mathematical basis for multiscale modeling of materials
- Statistical frameworks for multiscale materials modeling
- Mechanics of materials across time and length scales
- Multiscale modeling of microstructure evolution in materials
- Defects in materials
- Computational materials design based on multiscale and multi-level modeling principles

- Multiscale modeling of radiation effects in materials and materials response under extreme conditions
- Multiscale modeling of bio and soft matter systems

The first five topical areas are intended to cover the theoretical and computational basis for multiscale modeling of materials. The sixth topical area is intended to demonstrate the technological importance and industrial potential of multiscale materials modeling techniques, and to stimulate academia-laboratory-industrial interactions. The last two topical areas highly overlap with the earlier ones, yet they bring to the conference distinct materials phenomena and modeling problems and approaches with unique multiscale modeling aspects.

This conference would not have been possible without the help of many individuals both at Florida State University and around the world. Of those, I would like to thank the organizing team of MMM-2006, especially Professor Peter Gumbsch, for sharing their experience and much organizational material with us. I also thank all members of the International Advisory Board for their support and insight during the early organizational phase of the conference, and the members of the International Organizing Committee for the hard work in pulling the conference symposia together and for putting up with the many organization-related requests. Thanks are due to Professor Max Gunzburger, Chairman of the Department of Scientific Computing (formerly School of Computational Science) and to Florida State University for making available financial, logistical and administrative support without which the MMM-2008 would not have been possible. The following local organizing team members have devoted significant effort and time to MMM-2008 organization: Bill Burgess, Anne Johnson, Michele Locke, Jim Wilgenbusch, Christopher Cprek and Michael McDonald. Thanks are also due to my students Srujan Rokkam, Steve Henke, Jie Deng, Santosh Dubey, Mamdouh Mohamed and Jennifer Murray for helping with various organizational tasks. Special thanks are due to Bill Burgess and Srujan Rokkam for their hard work on the preparation of the proceedings volume and conference program.

I would like to thank the MMM-2008 sponsors: Lawrence Livermore National Laboratory (Dr. Tomas Diaz de la Rubia), Oak Ridge National Laboratory (Dr. Steve Zinkle) and Army Research Office (Drs. Bruce LaMattina and A.M. Rajendran) for the generous financial support, and thank TMS (Dr. Todd Osman) for the sponsorship of MMM-2008 and for advertising the conference through the TMS website and other TMS forums.

I would also like to thank all plenary speakers and panelists for accepting our invitation to give plenary lectures and/or serve on the conference panels. Lastly, I would like to thank the session chairs for managing the conference sessions.

Anter El-Azab
Conference Chair

International Advisory Board

Dr. Tomas Diaz de la Rubia	LLNL, USA
Prof. Peter Gumbsch	Fraunhofer Institute IWM, Freiburg, Germany
Dr. A.M. Rajendran	ARO, USA
Dr. Steve Zinkle	ORNL, USA
Prof. Anter El-Azab	FSU, USA
Prof. Michael Zaiser	Edinburgh, UK
Prof. Xiao Guo	Queens, London, UK
Prof. Shuichi Iwata	University of Tokyo, Japan
Prof. Jan Kratochvil	CTU, Prague, Czech Republic
Prof. Nasr Ghoniem (Chair)	UCLA, USA
Dr. Ladislas Kubin	ONERA-LEM, France
Prof. Shaker Meguid	Toronto, Canada
Prof. Alan Needleman	Brown, USA
Prof. Michael Ortiz	Caltech, USA
Prof. David Pettifor	Oxford, UK
Prof. Robert Phillips	Caltech, USA
Prof. Dierk Raabe	Max Planck Institute, Duesseldorf, Germany
Prof. Yoji Shibutani	Osaka University, Japan
Prof. Subra Suresh	MIT, Massachusetts USA
Prof. Yoshihiro Tomita	Kobe University, Japan
Prof. Erik Van der Giessen	University of Groningen, The Netherlands
Dr. Dieter Wolf	INL, USA
Prof. Sidney Yip	MIT, USA
Prof. David Bacon	Liverpool, UK
Dr. Michael Baskes	LANL, USA
Prof. Esteban Busso	Ecole des Mines, France
Prof. Timothy Cale	RPI, New York, USA
Dr. Moe Khaleel	PNNL, USA
Prof. David Srolovitz	Yeshiva, USA
Prof. Emily Carter	Priceton University, USA
Dr. Dennis Dimiduk	AFRL, USA
Prof. Rich Le Sar	Iowa State University, USA

International Organizing Committee

Weinan E	Princeton University, USA
Max Gunzburger	Florida State University, USA
Mitchell Luskin	University of Minnesota, USA
Rich Lehoucq	Sandia National Laboratories, USA
A.M. Rajendran	U.S. Army Research Office, USA
Stefano Zapperi	University of Rome, Italy
M.-Carmen Miguel	University of Barcelona, Spain
Mikko Alava	Helsinki University of Technology, Finland
Istevan Groma	Eötvös University, Hungary
Tom Arsenlis	Lawrence Livermore National Laboratory, USA
Peter Chung	Army Research Laboratory, USA

Marc Geers	Eindhoven University of Technology, The Netherlands
Yoji Shibutani	Osaka University, Japan
Dieter Wolf	Idaho National Laboratory, USA
Jeff Simmons	Air Force Research Laboratory, USA
Simon Phillpot	University of Florida, USA
Anter El-Azab (Chair)	Florida State University, USA
Daniel Weygand	University of Karlsruhe (TH), Germany
Zi-Kui Liu	Pennsylvania State University, USA
Hamid Garmestani	Georgia Institute of Technology, USA
Moe Khaleel	Pcific Northwest National Laboratory, USA
Mei Li	Ford Motor Company, USA
Fie Gao	Pacific Northwest National Laboratory, USA
Roger Stoller	Oak Ridge National Laboratory, USA
Pascal Bellon	University of Illinois, Urbana-Champaign, USA
Syo Matsumura	Kyushu University, Japan
Jeffery G. Saven	University of Pennsylvania, USA
Wei Yang	Florida State University, USA
T.P. Straatsma	Pacific Northwest National Laboratory, USA
L.P. Kubin	CNRS-ONERA, France
S.J. Zinkle	Oak Ridge National Laboratory, USA
Jaafar El-Awady	University of California, Los Angeles, USA
Shahram Sharafat	University of California, Los Angeles, USA
Hanchen Huang	Rensselaer Polytechnic Institute, USA
Yury N. Osetskiy	Oak Ridge National Laboratory, USA
Ron O. Scattergood	North Carolina State University, USA
Anna M. Serra	Universitat Politecnica de Catalunya, Spain

Local Organizing Committee (Florida State University, USA)

Prof. Anter El-Azab (Chair)
Prof. Max Gunzburger (Co-Chair)
Anne Johnson (Public relations and marketing)
Bill Burgers (Graphics and publications)
Srujan Rokkam (Proceedings and printing)
Michael McDonald (Webmaster)
Michele Locke (Finances)

Sponsors

Special thanks to the following sponsors:

- The Army Research Office
- Lawrence Livermore National Laboratory
- Oak Ridge National Laboratory

for their generous financial support, and to

- The Minerals, Metals & Materials Society (TMS)

for the sponsoring and advertising the conference through the TMS website.

Contents

Symposium 8

Symposium 8

Defects in materials

Honoring Professor Nasr Ghoniem
on the occasion of his 60th birthday

Materials, Energy and Climate: Requirements and Strategies for Sustainability in the 21st Century

Tomas de la Rubia

Lawrence Livermore National Laboratory, Livermore, CA 94550, USA
(E-mail: delarubia@llnl.gov)

ABSTRACT

Projections by the Department of Energy's Energy Information Administration and most other international studies show that worldwide electric power demand will increase from the current level of about 2 Terawatts (TW) to 5 TW by 2050 and likely to as much as 10 TW by 2100. A recent IEA 2006 Energy Technologies Perspectives report shows that for the next 30 to 50 years burning fossil fuels will continue to provide most of the world's electricity. In fact, in these baseline scenarios CO2 emissions will be almost two and a half times the current level by 2050. In addition, the most recent report from the Intergovernmental Panel on Climate Change has placed a 90% likelihood that human sources of carbon dioxide emissions are significantly affecting the global climate. Clearly, this increasing demand is placing enormous pressure on natural resources, the global ecosystem, and international political stability. Alternative sources of energy are required in order to meet increased energy demand, stabilize the increase of atmospheric carbon dioxide, and mitigate the concomitant climate change. In response, governments are urgently trying to develop new economical, sustainable, and environmentally friendly energy technologies. Materials will undoubtedly play a central role in the developments of these advanced energy technologies. In this talk, I will survey some of the key research challenges associated with the development of new materials with properties tailored to meeting the energy challenge. Specifically, I will focus on the development of advanced materials, fuels and new technologies for novel fission and inertial confinement fusion applications that will require extension of current performance parameters to the extreme conditions of temperature, stress and radiation present in these environments. Accelerated development of these new materials will require vast improvements in computational capabilities and in the ability of multiscale simulations to couple closely to experiments and produce predictive insights into the performance of real, complex materials in these extreme environments.

Defect Cluster Patterning in Irradiated Materials

Steven J. Zinkle[1], Lumin Wang[2]

[1]Oak Ridge National Laboratory, Materials Science and Technology Division, P.O. Box 2008, Oak Ridge, TN 37831-6132 USA, (E-mail: zinklesj@ornl.gov);
[2]University of Michigan, 2355 Bonisteel Blvd, Ann Arbor, MI 48109-2104 USA, (E-mail: lmwang@umich.edu)

ABSTRACT

Several experimental studies have found that particle irradiation of face centered cubic (FCC) metals can produce defect cluster patterning (self-organization) along crystallographic directions of the host lattice (e.g. {001} planes in nickel). Walgraef and Ghoniem have developed a theoretical model in which patterning is explained as a consequence of spatial fluctuations in the concentrations of point defects under irradiation conditions. These fluctuations couple with the growth/shrinkage rates of relatively immobile microstructure (e.g., dislocation loops, voids, etc.) to result in spatial self-organization. They concluded only a small fraction of glissile interstitial loops generated by collision cascades need to migrate along <111> directions in order for the defect patterns to attain an isomorphic relationship with the host lattice crystallography. We have performed several ion and neutron irradiation experiments on copper and nickel to obtain additional experimental information on defect cluster patterning. Pronounced defect cluster patterning was observed in nickel at doses above ~0.1 dpa for homologous irradiation temperatures near ~0.3 T_M at dose rates between 1e-6 and 1e-2 dpa/s. However, patterning was not observed in ion or neutron irradiated copper at the same homologous irradiation temperatures and dose rates. Comparing theory and experiments, possible explanations for the difference in self-organization behavior in irradiated copper and nickel are discussed. We will also summarize experimental data on the formation of ordered arrays of cavities in metals and ceramics during high dose irradiation, and discuss possible mechanisms for the formation of these ordered structures.

Research sponsored in part by the Office of Fusion Energy Sciences, U.S. Department of Energy under contract DE-AC05-00OR22725 with UT-Battelle, LLC.

Large-scale spin-lattice dynamics simulation of ferromagnetic iron

Leo P. W. Ma[1], C. H. Woo[1] and S. L. Dudarev[2]

[1]Department of Electronic and Information Engineering, The Hong Kong Polytechnic University, Hong-Kong, SAR, China, (E-mail: chung.woo@polyu.edu.hk)
[2]EURATOM/UKAEA Fusion Association, Culham Science Centre, Oxfordshire OX14 3DB, UK, and Department of Physics, Imperial College, Exhibition Road, London SW7 2AZ, UK, (E-mail: s.dudarev@imperial.ac.uk)

ABSTRACT

We report on the development of a spin-lattice dynamics simulation approach, in which the dynamics of an ensemble of ferromagnetic atoms are treated as classical particles with intrinsic spin. Both scalar many-body forces as well as spin-dependent forces of the Heisenberg form provide interactions among the atoms in the model. A coordinate-dependent exchange function provides the coupling between the lattice and spin degrees of freedom. Integration of the coupled spin-coordinate equations of motion is based on the 2^{nd} order Suzuki-Trotter decomposition for the non-commuting Liouville evolution operators for coordinates and spins. The notions of the spin thermostat and the spin temperature are introduced through the combined application of the Langevin spin dynamics and the fluctuation-dissipation theorem. Finite-temperature cases, where the interactions between atoms depend on the non-collinear relative orientations of their spins, can be treated. Several applications of the method have been performed. These include microcanonical ensemble simulations of adiabatic spin-lattice relaxation of periodic arrays of 180^{o} domain-walls, and isothermal-isobaric ensemble dynamical simulations of thermally equilibrated homogeneous systems at various temperatures. The resulting isothermal magnetization curve is well described by the mean-field approximation and agrees satisfactorily with the experimental data over a broad range of temperatures. Our results show that the spin degrees of freedom are very important to the properties of magnetic iron and iron-based alloys. The spin-lattice dynamics approach has been shown to be a viable scheme via which realistic large-scale dynamical simulations of magnetic materials can be performed.

Acknowledgement: This work is supported by the Grant PolyU5322/04E, and is performed in partial fulfillment of the requirements for the PhD degree of PWM at the Hong Kong Polytechnic University.

Dislocation Dynamics Modeling of Dislocation Cores in the Interaction with Precipitates

Akiyuki Takahashi[1], Mitsuru Kawanabe[1], Shotaro Hayashi[1], and Nasr M. Ghoniem[2]

[1]Department of Mechanical Engineering, Faculty of Science and Technology, Tokyo University of Science, 2641, Yamazaki, Noda-shi, Chiba 278-8510, Japan (takahash@rs.noda.tus.ac.jp, mitsuru@me.noda.tus.ac.jp, shota@me.noda.tus.ac.jp); [2]Department of Mechanical and Aerospace Engineering, University of California Los Angeles, Los Angeles, CA 90095-1597, USA (ghoniem@ucla.edu)

ABSTRACT

We describe here a computational method to investigate the influence of dislocation core structure and coherency strains on γ-precipitate strengthening in nickel-based superalloys. The method is a combination of the Parametric Dislocation Dynamics (PDD), an analytical solution to the spherical inclusion problem and a computational form of the Peierls-Nabarro (PN) model. Using the method, we studied the role of the shape and core structure of super-dislocations in a γ'-matrix on the strengthening resulting from γ-precipitates. Earlier analytical solution to stacking fault strengthening predicts slightly lower critical resolved shear stress (CRSS) in the comparison with the present results. This is attributed to super-dislocation shape changes during its interaction with the γ-precipitate. On the other hand, the analytical solution to coherency strain strengthening provides considerably larger CRSS compared to the results of the present simulations. This is attributed to the spreading of the dislocation core during the interaction process. The dislocation core is found to spread widely so that its interaction with the γ-precipitate is much "softer" than considered in previous analytical solutions, where core spreading is not accounted for. This remarkable effect is a direct result of the core structure of dislocations interacting with precipitates, and must be considered in future dislocation dynamics simulations of precipitate strengthening. We finally discuss the combined strengthening effects of the two mechanisms.

1. Introduction

Precipitation strengthening is one of the most effective ways to design alloys with for a required combination of strength and ductility.. The main mechanism is known to be the interaction between precipitates and dislocations, which plays a central role in plastic deformation of metals. Precipitates work as an impediment to dislocation motion, resulting in an increase in the flow stress, and a change in ductility that can be positive or negative. Up till now, the classical theory of precipitation strengthening has already been well established [1], and successfully applied to practical alloy design. However, the theory is based on many approximations, where the dislocation line is assumed to be straight, and the dislocation core is totally neglected. Therefore,

in order to improve the accuracy and reliability of the theory, it is important to incorporate the flexibility of the dislocation line and the effects of dislocation core on precipitation strengthening. One of the interesting examples of strengthening is the precipitation of a γ-phase (Ni-Al solid solution) in a γ'-(Ni3Al) matrix. This system has been investigated extensively because L12-type long-range ordered intermetallic compounds such as Ni3Al, Ni3Si and Co3Ti are considered for high-temperature structural applications, and this system is prototypical.
The dislocation dynamics (DD) computer simulation technique has been developed to study metal deformation from a fundamental perspective. Van der Giessen and Needleman utilized the superposition principle to account for the geometry of the material in DD simulations [2]. They employed the finite element method (FEM) to solve for the correction problem arising from the application of the superposition principle. Takahashi and Ghoniem extended the method to the general 3-dimensional dislocation-precipitate interaction problems [3]. They derived a set of boundary-volume integral equations for the correction problem, and solved the equations using the boundary element method (BEM) with a volume integral term.. On the other hand, Banerjee *et al*. developed a method to calculate the dislocation core structure within the continuum framework based on the well-known Peierls-Nabarro (PN) model [4]. They discretzed the PN model with a number of fractional dislocations having small Burgers vectors, and showed that the method has the potential to simulate the core structure of complicated dislocation lines.
The objective of this work is to develop a computational method to study the dynamics of the dislocation core and the effect of the dislocation core on the interaction between dislocations and precipitates. Using the method, the role of the dislocation core in precipitation strengthening, particularly the stacking fault and coherency strain strengthening, is investigated.

2. Computational Method

In this work, the Parametric Dislocation Dynamics (PDD) method developed by Ghoniem *et al*. is used[5]. In the method, flexible dislocation lines are discretized with a number of curved dislocation segments. The segment has two edge nodes, and the node has a generalized coordinate vector such as a combination of position and tangent vectors. The curved shape of the segments is described by a spline function that can preserve a high-order continuity condition. The equation of motion of each dislocation ensembles is given by

$$\int_{\Gamma} \left(F_k - B_{\alpha k} V_{\alpha}\right) \delta r_k \left| d\mathbf{s} \right| = 0 \tag{1}$$

where, F_k is the force on the dislocation segments, $B_{\alpha k}$ is the resistivity matrix and V_k is the velocity. The detail of the method can be found elsewhere [5]. In order to introduce the elastic field provided by the precipitates, the computational framework proposed by Takahashi and Ghoniem is employed [3]. In this paper, we as apply the method to an example of a γ-precipitate in a γ' phase in nickel base superalloys. In the material, the elastic constants of the matrix and the precipitate are almost identical, so we assume that both the matrix and the precipitate have the same elastic constants. Moreover, assuming that the shape of the precipitate is spherical, an analytical solution to the strain generated by the coherency strain of the spherical precipitate can be applied [6]. In this work, the PN model is discretized with a number of fractional dislocations, as originally proposed by Banerjee *et al*. [4]. In the method, if the dislocation core is represented with N fractional dislocations, each fractional dislocation has a Burgers vector of $\mathbf{b}/N$, where $\mathbf{b}$ is

the Burgers vector of the perfect dislocation. Then an additional force, lattice restoring force, is given to the fractional dislocations. The force can be calculated by taking a derivative of generalized stacking fault energy (GSFE), which can be computed by either the ab-inito method or reliable interatomic potentials.

3. Simulation Model

The size of the simulation volume is 50x50x20 nm, and each coordinate axis are along with crystal orientations of $[\bar{1}01]$, [111] and $[1\bar{2}1]$, respectively. A spherical precipitate is placed at the center of the volume. The diameter of the precipitate is changed in a range from 2 to 10 nm in order to examine the effect of the diameter on the interaction. Periodic boundary condition is applied to the $[1\bar{2}1]$ direction, assuming that there is an array of precipitate in the direction with 20 nm spacing between precipitates. A super-dislocation with the edge character is placed on a slip plane of (111), because, in γ' phases, a pair of dislocation must be appeared to terminate an anti-phase boundary (APB) in-between. The super-dislocation is then dicretized with 20 fractional dislocations. The position of the slip plane is also changed to see the dependence of the interaction on the position of the slip plane. To push the super-dislocation, a shear stress is applied, and is controlled to evaluate the CRSS for the interaction.

4. Dislocation Core Effects on Dislocation-Precipitate Interactions

Since the elastic constants of the γ' phase and the γ precipitate are almost identical, two different strengthening mechanisms work in the interaction, one is the stacking fault strengthening, and the other is the coherency strain strengthening. In the following, we will discuss the effect of the flexibility and the core structure of the dislocation on the each strengthening mechanisms first, and then study the combined strengthening mechanism of the two mechanisms.

4.1 Stacking Fault Strengthening

To study stacking fault strengthening alone, the coherency strain of the precipitate is first neglected. The GSFE for the γ' phase and γ precipitate is separately calculated using an interatomic potential for nickel-aluminum alloys developed by Mishin [7]. The derivatives of the two GSFEs are used to give the lattice restoring stress in the γ' phase and γ precipitate to the fractional dislocations. Fig. 1 shows the snap-shots of the PDD simulation of the dislocation precipitate interaction. In the figure, the leading super-partial attractively interacts with the precipitate, and goes through the precipitate to its edge. Then, the trailing super-partial penetrates the precipitate. The two super-partials extend the spacing between them in the precipitate. Finally, the leading super-partial breaks away from the precipitate. Following the leading super-partial, the trailing super-partial also breaks away from the precipitate. The CRSS can be found at Fig. 1(c), where the trailing super-partial is still in the precipitate, and is largely bent by the precipitate. Fig. 2 shows the variation of CRSS as the diameter of precipitate is changed. In the figure, an analytical solution to the stacking fault strengthening derived by Hirsch and Kelly [8] is also plotted as a line. It can be clearly seen in the figure that the results of the PDD simulation are slightly larger than the analytical solution. In the analytical solution, the flexibility of the

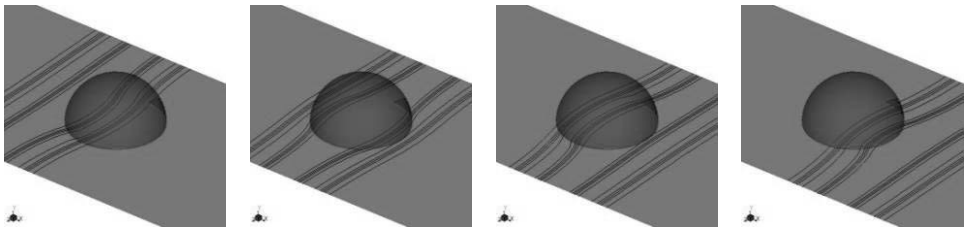

(a) (b) (c) (d)

Figure 1. Snap-shots of the dislocation-precipitate interaction only with the stacking fault strengthening. The diameter of the precipitate is 8 nm, and the slip plane is located at the center of the precipitate.

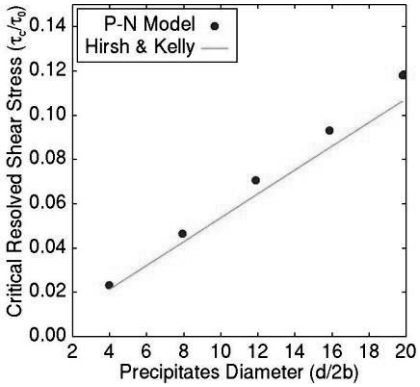

Figure 2. CRSS for various diameter of the precipitate

dislocation line is ignored, and then the length of the dislocation line in the precipitate at the CRSS is approximated to be the diameter of the precipitate. However, when the shear stress reaches the CRSS, the trailing super-partial is bent by the precipitate, which changes the length of the dislocation in the precipitate. (see Fig. 1(c)). Therefore, the difference between the analytical and numerical solution should arise from the flexibility of the dislocation, and the most importantly, the actual CRSS must be larger than the analytical solution. In the simulation, the precipitate is assumed to be isolated, and hence we do not consider the influence of precipitate density.

4.2 Coherency Strain Strengthening

Next, coherency strain strengthening is investigated. In order to remove stacking fault strengthening, the GSFE for the γ' phase is used not only in the matrix and also in the γ precipitate. The coherency strain stored in the precipitate is, in this case, negative. Fig. 3 shows the shape of the super-dislocation, when the CRSS is attained. In both cases, the CRSS appears, when the super-dislocation is placed at the edge of the precipitate, because the super-dislocation has an attractive interaction with the precipitate on a slip plane at the lower side of the precipitate, whereas the dislocation has a repulsive interaction with the precipitate on a slip plane at the upper side. Fig. 4 shows the variation of the CRSS as the position of the slip plane is changed. Also, an analytical solution to the problem [9] is plotted in the figure. The solution is derived with assumptions, such as the dislocation is straight, and has a line shape. In the figure, the results of the PDD simulations are much lower than the analytical solution. This must be related to the spreading of the dislocation core. In the analytical solution, the CRSS is calculated

by integrating the stress along a dislocation line locating at the edge of the precipitate, because the maximum stress works at the position. However, as can be seen in Fig. 3, the dislocation core actually widely spreads. Therefore, we must integrate the stress distribution in the dislocation core area spreading near the precipitate, which must lower the CRSS in the interaction.

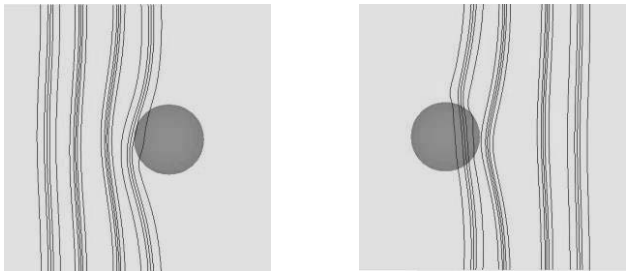

(a) (b)

Figure 3. Shapes of the super-dislocations interacting with a γ precipitate with a diameter of 8nm under CRSS. The positions of the slip plane are (a) 3 nm upper side and (b) 3 nm lower side in the [111] direction.

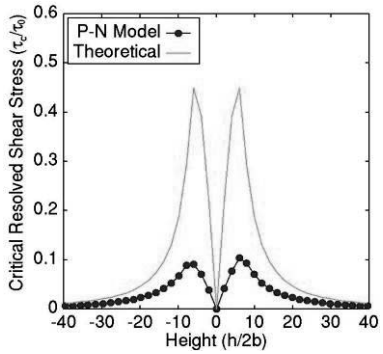

Figure 4. CRSS for various positions of the slip plane.

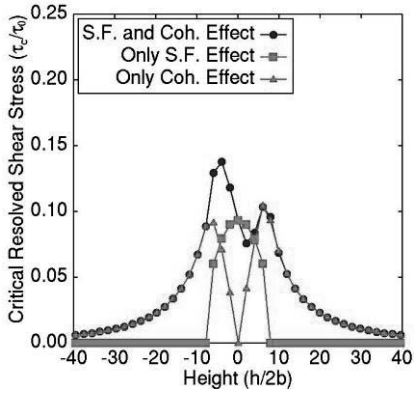

Figure 5. CRSS for various positions of the slip plane with several strengthening mechanisms

4.3 Combined Strengthening

The combined strengthening of the stacking fault and the coherency strain mechanisms is also of interest. Fig. 5 shows the CRSS for the dislocation-precipitate interaction with the combined strengthening. In the simulations, the position of the slip plane is changed in the [111] direction. The results of the stacking fault and coherency strain strengthening are also plotted in the figure. If only the stacking fault strengthening works, and the slip plane is outside the precipitate, there is no interaction. On the other hand, if the coherency strain strengthening works only, there is a long-range interaction. The CRSS shows two peaks near the edges of the precipitate. The CRSS for the combined strengthening is asymmetric with respect to the center of the precipitate. If the slip plane is within the precipitate, and the height is positive, the CRSS is very similar to that for the coherency strain strengthening. On the other hand, if the height of the slip plane is negative, the CRSS is significantly strengthened by the combined mechanism. The strengthening effect

can be explained as follows. When the height of the slip plane is negative, the coherency strain interaction is attractive as shown in Fig. 3(b), and also, due to the stacking fault strengthening, the dislocation is likely to be inside the precipitate. Therefore, the two effects are added, and provide enhanced strengthening.

5. Conclusions

A computational method to study the influenceof the flexibility and the core structure of dislocation lines on the precipitation strengthening was developed. The method is a combination of the PDD method, an analytical solution to the spherical inclusion problem and a computational form of the PN model. Applying the method to the interaction between a super-dislocation and a γ precipitate in a γ' phase, we could find that the flexibility and the dislocation core structure play a very important role in determining the strengthening by the precipitates.

1) In the stacking fault strengthening, due to the flexibility of the dislocation line, the CRSS becomes larger than the analytical solution to the problem.
2) In the coherency strain strengthening, the dislocation core spreads very widely under the CRSS. The spreading reduces the strength of the interaction with the precipitate.
3) In the combined strengthening, the CRSS is enhanced if the height of the slip plane is negative. The enhancement must be attributed to the combined effect of the stacking fault and the coherency strain strengthening.

Acknowledgements

This work is supported by the U.S. Air Force Office for Scientific Research (AFOSR), through Grant No. FA9550-07-1-0396, with UCLA.

References

[1] A.J. Ardell, "Precipitation Hardening", Metallurgical Transactions A, **16**, 2131 (1985).
[2] E. van der Giessen and A. Needleman, "Discrete dislocation plasticity: a simple plannar model", Modelling and Simulation in Materials Science and Engineering, **3**, 689 (1995).
[3] A. Takahashi and N.M. Ghoniem, "A computational method for dislocation-precipitate interaction", Journal of the Mechanics and Physics of Solids, **56**, 1534 (2008).
[4] S. Banerjee, N. Ghoniem, G. Lu and N. Kioussis, "Non-singular descriptions of dislocation cores: a hybrid ab-initio continuum approach", Philosophical Magazine, **87**, 4131 (2007)
[5] N.M. Ghoniem, S.-H. Tong and L.Z. Sun, "Parametric dislocation dynamics: a thermodynamics based approach to investigations of mesoscopic plastic deformations", Physical Review B, **61**, 913 (2000).
[6] S. Timoshenko and J.N. Goodier, *Theory of Elasticity*, (McGraw-Hill, 1951).
[7] Y. Mishin, "Atomistic modeling of the γ and γ'-phases of the Ni-Al system", Acta Materialia, **52**, 1451 (2004).
[8] P.B. Hirsch and A. Kelly, "Stacking-fault strengthening", Philosophical Magazine, **12**, 881 (1965).
[9] V. Gerald and H. Haberkorn, "On the Critical Resolved Shear Stress of Solid Solutions Containing Coherent Precipitates", Physica Status Solidi (b), **16**, 675 (1966).

The Influence of Focused Ion Beam Induced Damage on the Plasticity of Nano- and Micro-pillars

Jaafar A. El-Awady, Ming Wen, Nasr M. Ghoniem

Mechanical and Aerospace Engineering Department, University of California, Los Angeles, CA 90095-1597, USA (E-mail: jelawady@ucla.edu)

ABSTRACT

We present a computational study of the effects of radiation damage produced during focused ion beam (FIB) milling on the mechanical behavior of nano- and micro-pillars. We also investigate the influence of cross-slip on work hardening during the plastic deformation of micropillars. We conduct three-dimensional dislocation dynamics simulations of cylindrical Ni single-crystals under compression, using the parametric dislocation dynamics coupled with the boundary element method. A strengthening effect of this damaged surface layer is seen to become more prominent with decreasing specimen size. The flow strength can increase by over 20% when the damage layer is about 100 nm for micropillars having diameters below 0.5 μm. As the size of the micropillar increases, the induced damage is seen to have a small effect on the flow strength. In addition, the activation of cross-slip is shown to have a significant effect on work-hardening.

1. Introduction

With the recent interest in nano- and micro-technologies, attention has been directed towards determining material properties at such scales. Recently, the dependence of strength on size has been shown in numerous experiments [1-4], whichrevealed outstanding the dependence of flow strength on the diameter of the specimen. It was shown that the flow strength exhibits a strong size-dependency, with specimens in the submicron range exhibiting a flow strength that is an order of magnitude higher than bulk specimens. Another common observation is that the flow strength scaling with the dislocation density is different than that observed in bulk crystals.

Because of the wide-range of experimental observations, computer simulations can provide useful insights in understanding the origins of experimentally observed size effects. A number of two-dimensional (2-D) and three-dimensional (3-D) dislocation dynamics (DD) simulations have recently been performed to assess the mechanisms associated with the wide range of observations that we discussed earlier [5-7]. Such simulation results are in general agreement with several experimental observations. From these simulations it was concluded that the observed size effects on the flow strength are consistent with a "weakest-link activation mechanism".

In the following, we discuss two aspects that have been widely ignored in understanding the experimentally observed size effects. These two aspects are the effect of the induced damage due to focused ion been (FIB) milling of the micropillars, and the effect of cross-slip on work-hardening. To study the influence of these two aspects, we perform dislocation dynamics simulations that mimic the experimental setup of Dimiduk, Uchic, and Parthasarathy [1]. The computational method adopted here follows that developed in [5]. In this formulation, the Boundary Element Method (BEM) is coupled with the 3-D Parametric Dislocation Dynamics formulation to incorporate the influence of free and internal interfaces on dislocation motion, and hence to describe microscopic plastic flow in finite volumes. In the following, the simulations carried out in this work are performed on Ni cylindrical single crystals having an aspect ratio of 3:1. The initial dislocation density in all simulations is $\rho = 6 \times 10^{12}$ m^{-2}, and a compression stress is applied to the top surface of the cylinder while keeping the bottom surface fixed. The compression loading is performed under a constant strain rate $d\varepsilon/dt = 200$ s^{-1}, and the applied load is not allowed to decrease during the simulation.

2. Effect of Focused Ion Beam Induced Damage

Although it is well acknowledged that the FIB process introduces a damaged surface due to ion bombardment [8, 9], in all DD simulations of micropillar experiments, the effects of such damaged layer have been largely neglected. Kiener et. al. [8] reported that this damaged layer can be in the form of decoration of dislocations with Ga, vacancy clusters in the form of stalking fault tetrahedra, Ga-based precipitates, dislocation networks, and dislocation loops that resulted from the collapse of vacancy clusters. In addition, it is clear from TEM investigations that the penetration depth is dependent on the ion dose, and that it is in the range of 50 nm from the surface of the pillar for a dose of 30 keV [10].

In the following, we examine the effects of such FIB damage layer the observed size dependence of micro-pillar strength. Out of all forms of damage that may result from FIB ion implantation, Ga-based precipitates would have the largest effect of the flow strength. Thus, in our current analysis, we will confine our attention to the effects of the existence of such precipitates in the damaged layer. Marien et al. [11] reported the formation of precipitates with radius $\sim$ 1.4 nm, and an average spacing of 10.2 nm between precipitates [8]. We generate here a random distribution of nano-sized precipitates in the simulated micropillars with a depth d from the surface of the pillars, and an average spacing of 10.2 nm. When a dislocation propagates in the micropillar and meets a precipitate in the damaged layer it will get pinned. The dislocation will then be released and the precipitate destroyed when the resolved shear stress on the dislocation at the precipitate reaches a critical value, τ_p, equal to the strength of that precipitate. Although the strength of the precipitates may have a statistical distribution, for simplicity,we assume here a uniform precipitate strength. In addition, we assume that $\tau_p = 500.0$ MPa, which is equivalent to the theoretical estimate reported in [8].

In Figure 1, simulation results of microstructure evolution are shown for $D = 0.5$ μm micropillar having a FIB damage depth of 50 nm. It is observed that dislocation loops expanding in the damaged zone are pinned at precipitates. Due to dislocation pinning, the shear stress required to propagate the dislocation further will increase and thus the flow strength of the micropillar will be higher than a damage-free micropillar.

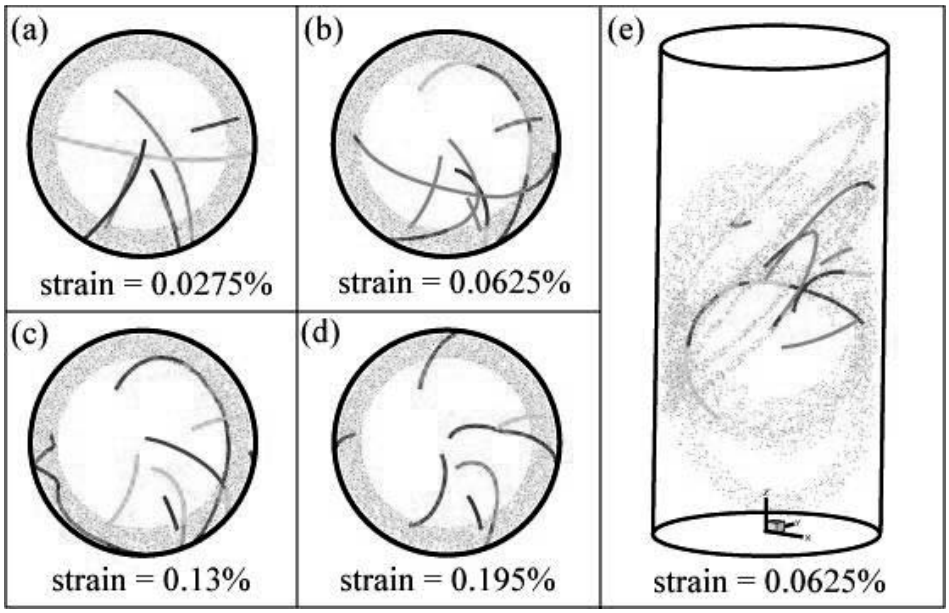

Figure 1. Top and 3-D views of microstructure evolution in a D = 0.5μm micropillar,having a 50 nm FIB damage depth. The precipitates are shown as dots and in the 3-D view only precipitates on the activated slip planes are shown.

The effect of the FIB damage depth on the overall flow strength for different micropillar sizes is shown in Figure 2. It is observed that as the size of the micropillar decreases, the effect of the damage depth increases. In fact, the flow strength can increase by over 20% when the damage layer is 100 nm. In addition, as the size of the micropillar increases, the induced damage is seen to have a minimal effect on the flow strength (e.g. ≤ 5% increase in the flow strength for $D \geq 1.0$ μm).

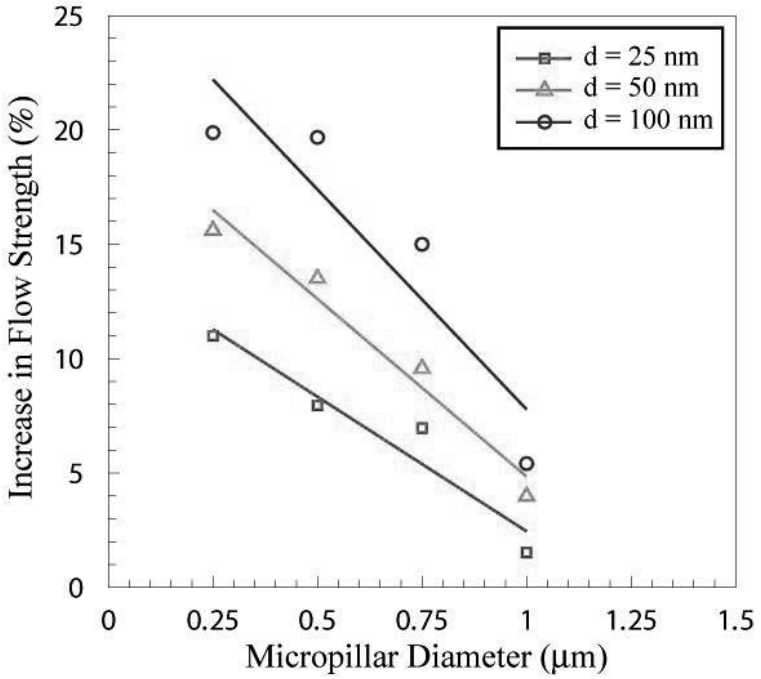

Figure 2. Increase in the overall flow strength as a function of the damage depth for different micropillar sizes.

3. Effects of Cross-Slip Activation

Some experimental observations indicate that the strain hardening rate increases as the micropillar size decreases [3, 4]. Dislocation cross-slip is generally recognized to have an important role in several aspects of material deformation. Cross-slip not only influences substructure morphology and evolution, but it is also known to control stage-III work-hardening in bulk metals. For the consideration of cross-slip in the PDD-BEM method, we adopt a stochastic probabilistic model developed for discrete dislocation dynamics simulations as discussed in [7].

In Figure 3, the engineering stress-strain response of three micropillar sizes D = 0.50, 0.75, and 1.00 μm are shown, respectively. Results from both simulations with and without cross-slip activation are shown as solid and dashed-dot-dot lines, respectively. From these results, distinct jumps in the stress-strain curves due to the activation of cross-slip activation are observed. In addition, between these jumps the material is observed to behave elastically.

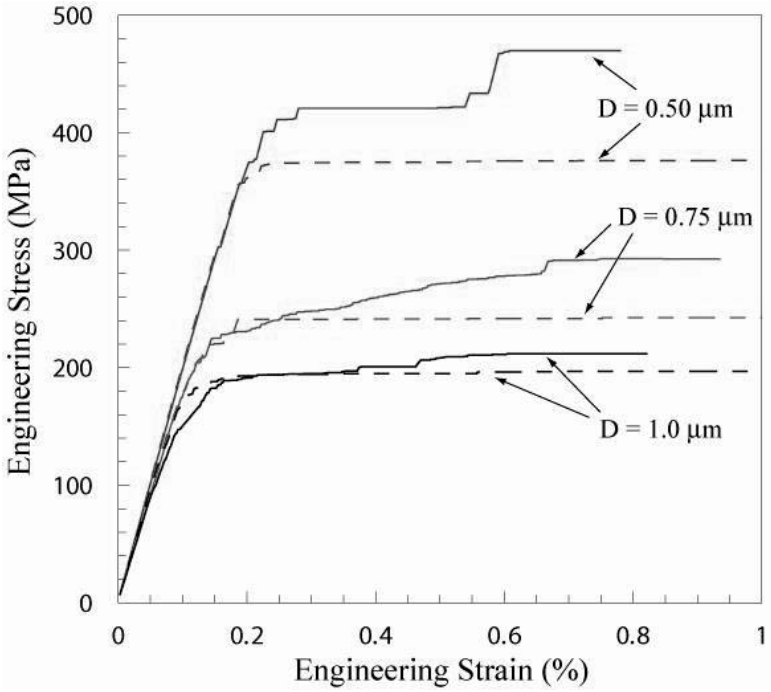

Figure 3. Engineering stress versus engineering strain for different micropillar sizes. The solid lines are with cross-slip activation while the dashed lines are without cross-slip activation [7].

The effect of cross-slip activation on the step formation can be explained as follows: when the resolved shear stress on the cross-slip plane of the screw segments of an activated dislocation link is much greater than on its original plane, the screw segment will cross-slip and thus, the length of the initial dislocation link length will be reduced. Since both the cross-slipped segment as well as the rest of the dislocation left on the original plane will have a smaller length than the original length, a higher stress is needed to activate these new sources and thus an increase in the strength is observed. In addition, it is observed that the activation of cross-slip leads to an

increase in the dislocation density as well as a reduction of the average size of activated dislocation lengths.

6. Conclusions

The effect of the induced FIB damage during the fabrication process of micropillars was examined by introducing a layer of nano-sized precipitates in the model. The influence of the depth of nano precipitates in the damaged surface layer on the computed flow strength was analyzed. We show here that the flow strength can increase by over 20% when the damage layer is about 100 nm for micropillars having diameters below 0.5 μm. As the size of the micropillar increases, the induced damage is seen to have a minimal effect on the flow strength (≤ 5% for $D \geq 1.0$ μm). In addition, the activation of cross-slip is shown to have a significant effect on work-hardening. Finally, the observed size effects are shown to be consistent with a "weakest-link activation mechanism".

Acknowledgements

We acknowledge the support of the U.S. Air Force Office for Scientific Research (AFOSR), through Grant No. FA9550-07-1-0396, with UCLA

References

[1] D.M. Dimiduk, M.D. Uchic, and T.A. Parthasarathy, “Size-affected single-slip behavior of pure nickel microcrystals”, Acta Materialia, **54**, 701, (2006).
[2] J.R. Greer, W.C. Oliver, and W.D. Nix, “Size dependence of mechanical properties of gold at the micron scale in the absence of strain gradients”, Acta Materialia, **53**, 1821, 2005.
[3] C.A. Volkert and E.T. Lilleodden, “Size effects in the deformation of submicron au columns”, Philosophical Magazine, **86**, 5567, (2006).
[4] C.P. Frick, B.G. Clark, S. Orso, A.S. Schneider, and E. Arzt, “Size effect on strength and strain hardening of small-scale [111] nickel compression pillars”, Material Science and Engineering A, **489**, 319, (2008).
[5] J.A. El-Awady, S.B. Biner, and N.M. Ghoniem, “A self-consistent boundary element, parametric dislocation dynamics formulation of plastic flow in finite volumes”, Journal of Mechanics and Physics of Solids, **56**, 2019, (2008).
[6] S.I. Rao, D.M. Dimiduk, T.A. Parthasarathy, M.D. Uchic, M. Tang, and C. Woodward, “Athermal mechanisms of size-dependent crystal flow gleaned from three-dimensional discrete dislocation simulations”, Acta Materialia, **56**, 3245, (2008).
[7] J.A. El-Awady, M. Wen, and N.M. Ghoniem, “The role of the weakest-link mechanism in controlling the plasticity of micropillars”, Journal of Mechanics and Physics of Solids, submitted, (2008).
[8] D. Kiener, C. Motz, M. Rester, M. Jenko, and G. Dehm, “FIB damage of Cu and possible consequences for miniaturized mechanical tests”, Material Science and Engineering A, **459**, 262, (2007).

[9] D. Kiener, C. Motz, T. Schöberl, M. Jenko, and G. Dehm, "Determination of mechanical properties of copper at the micron scale", Advanced Engineering Materials, **8**, 1119, (2006).
[10] B.N. Singh and S.J. Zinkle,"Defect accumulation in pure fcc metals in the transient regime: a review", Journal of Nuclear Materials, **206**, 212, (1993).
[11] J. Marien, J.M. Plitzko, R.-M. Keller, R. Spolenak, and J. Mayer, "Quantitative electron spectroscopic imaging studies of microelectronic metallization layers", Journal of Microscopy, **194**, 71, (1999).

In-reactor Deformation Experiments on FCC and BCC Pure Metals and Alloys

B.N Singh[1] and S. Tähtinen[2]

[1]Risø National Laboratory, P.O. Box 49, DK-4000 Roskilde, Denmark
[2]VTT Materials Performance, FIN-02044 VTT, Finland

ABSTRACT

Over a period of more than 40 years, the effect of neutron irradiation on mechanical properties of metals and alloys has been investigated using post-irradiation deformation experiments where the materials are irradiated in the absence of applied stress and deformed afterwards in the absence of neutron flux (i.e. radiation damage). These experiments have consistently demonstrated that the irradiation at temperatures below the recovery stage V causes not only an increase in the yield strength but leads to almost a complete loss of work hardening ability, induces plastic flow localization and causes a drastic decrease in the uniform elongation (i.e. ductility). It should be recognized however, that in reality the materials used in the structural components of a fission or fusion reactor will be exposed concurrently to a flux of neutrons and the internal and external forces. At present practically nothing is known about the dynamic response of materials under these conditions. Since the initial microstructure as well as the test conditions during a post-irradiation test are fundamentally different from those expected under in-reactor deformation experiments, the results of post-irradiation tests may not be representative of in-reactor deformation behaviour. In order to address this uncertainty, recently we have carried out a series of well controlled uniaxial tensile tests directly in a fission reactor on pure copper, CnCrZr alloy, pure iron and Fe-9% Cr alloy. In the present talk first of all the most crucial differences between post-irradiation and in-reactor tests will be highlighted. A brief description will be given of the important features of the test facilities and experimental procedure used in the present work. The main results will be presented to illustrate that (a) the mechanical response and (b) the damage accumulation and microstructural evolution are very different during in-reactor tests from those during the post-irradiation tests. Furthermore, both mechanical response and microstructural evolution in FCC crystals are found to be very different from that in the BCC crystals and even a very low level of irradiation dose leads to a drastic change in the dynamics and morphology of dislocations during in-reactor tests, particularly of BCC crystals. Finally, the importance of these results for theoretical and computational modelling of dislocation behaviour and the corresponding mechanical response under the realistic conditions of in-reactor deformation will be discussed.

Scale Transitions in the Plasticity of F.C.C. Single Crystals

Ladislas P. Kubin[1], Benoit Devincre[1] and Thierry Hoc[2]

[1]Laboratoire d'Etude des Microstructures, UMR 104 CNRS, CNRS-ONERA, 20 Av. de la Division Leclerc, BP 72, 92322 Chatillon Cedex, France (E-mails: ladislas.kubin@onera.fr, benoit.devincre@onera.fr).
[2]T. Hoc, Laboratoire MSSMat, UMR 8579 CNRS, Ecole Centrale Paris, Grande Voie des Vignes, 92295 Chatenay-Malabry Cedex, France (E-mail: hoc@ecp.fr).

ABSTRACT

A model for strain hardening in F.C.C. crystals [1] is presented and discussed from the viewpoint of scale transitions. This model is based on the storage – recovery framework expanded at the scale of slip systems and makes use of 3D dislocation dynamics (DD) simulations to guide modeling and measure parameter values. A first transition in scale is performed from elementary dislocation processes, notably short-range reactions, to collective intermittent behavior, as manifested by dislocation avalanches. Emphasis is put on the next transition, from intermittent to continuous behavior, which is performed through an implicit coarse-graining procedure. Using the information drawn from DD simulations, the continuous storage rate and the dislocation mean free paths are modeled in full detail and without any free parameter. The transition from dislocation-based modeling to the behavior of bulk single crystals is performed with the help of a crystal plasticity code. This route from single dislocations to strain hardening is efficient and yields realistic results in monotonic uniaxial deformation, especially regarding the orientation dependence of the classical hardening stages. The extension to polycrystal plasticity, stored energies and complex deformation conditions is now being investigated.

[1] B. Devincre, T. Hoc and L. Kubin, "Dislocation Mean Free paths and Strain Hardening of Crystals", Science, **320**, 1745 (2008).

Size Dependence in Constrained Plasticity: Discrete and Continuous Models of 3D Dislocation Dynamics

Michael Zaiser[1], N. Nikitas[1] and T. Hochrainer[2]

[1]The University of Edinburgh, Center for Materials Science and Engineering, The King's Buildings, Sanderson Building, Edinburgh EH11DT, UK (E-mail: M.Zaiser@ed.ac.uk); [2]Fraunhofer-Institute for Mechanics of Materials, Woehlerstr. 11, 79108 Freiburg, Germany (E-mail: thomas.hochrainer@iwm.fraunhofer.de).

ABSTRACT

We discuss three-dimensional density-based dislocation dynamics models and their application to size effects in constrained plasticity. Results are derived for thin film shearing and bending, and for the deformation of bi- and tricrystals. We evaluate the associated size effects and characterize the deformation patterns in terms of the dislocation density tensor fields. The results are compared with those obtained from phenomenological strain gradient plasticity and benchmarked against the results of 3D discrete dislocation dynamics simulations.

Determination of Micro-mechanical Constitutive Relations Using Dislocation Dynamics

Craig Hartley

El Arroyo Enterprises LLC, Sedona, AZ 86336, USA (ElArroyo_Enterprises @msn.com)

ABSTRACT

The widespread use of the Crystal Plasticity Finite Element Method (CPFEM) presently relies on empirical constitutive equations relating the local resolved shear stress and slip system geometry to rates of dislocation motion, multiplication and interaction. The form of these equations has been inferred from the observed behavior of dislocations intersecting the surface of single crystals and from the form of macroscopic constitutive equations based on micro-mechanical models. Values of parameters appearing in the micro-mechanical constitutive equations are generally obtained from fitting experimental data to macroscopic constitutive laws containing parameters based on dislocation geometry and behavior. Constitutive parameters obtained in this manner recently have been employed in CPFEM calculations of macroscopic material behavior and compared with experimental observations at the mesoscopic scale for verification. This kind of inference of microscopic constitutive parameters from meso- or macroscopic experiments is necessary because of the extreme difficulty of performing controlled experiments at the microscopic scale on actual materials. Recent advances in testing and imaging techniques at the micro-scale have mitigated this problem to some degree, but it still remains a formidable challenge to the experimentalist. Until better techniques are developed for examining materials at the microscopic scale in real time while they are undergoing controlled deformation under well-characterized boundary conditions, the computational tools provided by dislocation dynamics can provide useful information for the development of accurate constitutive equations for dislocation behavior at the micro-scale. These calculations have well-characterized material parameters for slip systems as well as well-known boundary conditions. Typically, the results are expressed in the form of "snapshots" of the evolution of dislocation structures at the micro-scale during various stages of a deformation process. In order for the output of dislocation dynamics calculations to provide useful information for constitutive models in continuum field theories of deformation, it is necessary to characterize the dislocation structure of the computational cell in terms of parameters that can be used in continuum calculations. In order to accomplish this, material points in the continuum are approximated by subdivisions of the dislocation dynamics cell called gauge volumes. For example, the Nye tensor, which describes the net flux of Burgers vectors due to dislocations crossing a plane of known orientation, can be directly measured in these gauge volumes within a computational cell after each computation step. Dislocation motion, the associated dislocation distortion rate and the plastic power dissipation associated with the gauge volume can be described in terms of vectors characterizing the edge and screw components of the dislocation density, a velocity vector that describe the rate of motion of the dislocation configuration and an effective virtual force on the configuration, based on the Peach-Koehler force on a single dislocation. The relationship between this force and the resulting velocity vector forms the basis for microscopic constitutive equations. This paper develops these ideas into a comprehensive procedure for extracting information on continuum parameters from dislocation dynamics calculations and gives some examples of the determination of microscopic constitutive equations.

Short-range Interactions in Continuum Dislocation Plasticity

Radan Sedláček[1], **Jan Kratochvíl**[2], **Cornelia Schwarz**[1]

[1]**Technische Universität München, Fakultät für Maschinenwesen**
Lehrstuhl für Werkstoffkunde und Werkstoffmechanik
Boltzmannstr. 15, 85747 Garching, Germany

[2]**Czech Technical University, Faculty of Civil Engineering,**
Department of Physics,
Thákurova 7, 166 29 Prague, Czech Republic

ABSTRACT

A model of mesoscale plasticity based on the continuum description of curved dislocations is presented. Glide dislocations are divided into groups which in the averaging process result in so-called single-valued dislocation fields. The averaged continuous distribution of the glide dislocations is treated as a superposition of these fields. The equations of the continuum model are derived from discrete dislocation dynamics. They contain constitutive functionals representing short-range dislocation interactions in and between the single-valued fields. The possibilities for specification and evaluation of the constitutive functionals are indicated. In a pragmatic approach, the short-range interactions are described by the self force, friction stress, and back stress.

1. Introduction

Plastic deformation is a multi-scale phenomenon, where the mechanisms and governing equations at the microscale (the level of order of nm), mesoscale (μm), and macroscale (specimen size) are strongly interrelated with each other. The elastoplastic behavior of crystalline materials at the scale of micrometers and below displays size effects, with the general tendency of smaller being harder. The standard approach to modeling the size dependent materials behavior is either the use of discrete dislocation dynamics approaches or the application of phenomenological strain gradient continuum models. An alternative approach that combines the advantages of both of them is a continuum dislocation-density based modeling. The objective of the present paper is to explore the possibility to generalize the continuum dislocation-based model [1, 2, 3] to include mutual short-range dislocation interactions by using a statistical approach to curved glide dislocations.

The first successful statistical approach leading to a continuum dislocation theory has been

proposed by Groma *et al.* [4]. He studied the idealized system of straight parallel edge dislocations of a single slip system represented by points of intersection of the dislocation lines with the plane of deformation. This approach led to statistics of point objects, to which the tools of standard statistical mechanics have been applied. The model revealed one of the main problems of this approach: an adequate description of the short-range dislocation correlations. In Groma's continuum model, the correlations result in non-local effects which play a decisive role in the modeling of dislocation pattering and size effects.

The standard tools of statistical mechanics are not directly applicable to glide dislocations treated as curved flexible lines, first of all because the connectivity of the infinitesimal dislocation segments forming the dislocation lines must be accounted for. Therefore, in the approach proposed here, the curved glide dislocations are separated into groups suitable for averaging. We use the approximation of single-valued dislocation fields introduced in [1, 2]. The glide dislocations in a reference configuration are sorted into groups in such a way that, for a sufficiently small volume element, the properties of the segments of the glide dislocations belonging to the same group remain sufficiently close. The dislocations form locally smooth line bundles, where the nearby dislocations are nearly parallel and have the same orientation. Thus, the quantities averaged over statistically equivalent systems of segments of the dislocations belonging to a given group, e.g. the dislocation density, can be expressed as single-valued fields of the position and time.

The equations of the continuum model are constructed from the equations of motion of discrete glide dislocations. A constitutive functional appears that represents the short-range dislocation interactions. Possibilities for specification and approximation of the functional are indicated, leading in general to nonlocal gradient terms [5]. This statistical approach is compared with a pragmatic one, where the short-range interactions are described phenomenologically by the self force, friction stress, and back stress [6].

2. Dynamics of Curved Dislocations

We consider N glide dislocations represented by planar curves lying in the slip planes. The i-th glide dislocation, $i = 1, \dots, N$, consists of infinitesimal segments identified by the arc length p. The position of a segment is $\boldsymbol{x}_i(p,t)$, and the segment orientation (character) is determined by the unit tangent vector $\boldsymbol{\xi}_i(p,t) = \boldsymbol{\xi}_i^{\mathrm{d}}(\boldsymbol{x},t)$. The velocity $\boldsymbol{V}_i(p,t)$ of an infinitesimal segment p of a glide dislocation i has always a direction parallel to the normal $\boldsymbol{\varsigma}_i(p,t)$ to the dislocation line in the glide plane. The velocity equation is considered in the commonly accepted linearized form with the assumption of an over-damped motion,

$$BV_i(p) = \begin{cases} b\,(\tau^{\mathrm{ext}}(\boldsymbol{x}_i(p)) + \tau^{\mathrm{int}}(\boldsymbol{x}_i(p)) - \tau_0) & \text{for} \quad \tau^{\mathrm{ext}}(\boldsymbol{x}_i(p)) + \tau^{\mathrm{int}}(\boldsymbol{x}_i(p)) \geq \tau_0\,, \\ b\,(\tau^{\mathrm{ext}}(\boldsymbol{x}_i(p)) + \tau^{\mathrm{int}}(\boldsymbol{x}_i(p)) + \tau_0) & \text{for} \quad \tau^{\mathrm{ext}}(\boldsymbol{x}_i(p)) + \tau^{\mathrm{int}}(\boldsymbol{x}_i(p)) \leq -\tau_0\,, \\ 0 & \text{for} \quad |\tau^{\mathrm{ext}}(\boldsymbol{x}_i(p)) + \tau^{\mathrm{int}}(\boldsymbol{x}_i(p))| < \tau_0\,, \end{cases} \tag{1}$$

where τ^{ext} denotes the resolved shear stress determined by applied boundary conditions, and τ_0 is some basic friction stress of the glide system. The dislocations are divided in K single-valued fields, each of them with N_I dislocations, so that

$$\tau^{\text{int}}(\boldsymbol{x}_i(p)) = \sum_{I=1}^{K} \sum_{j=1}^{N_I} \int_0^{l_j} \tilde{\tau}_{\text{D}}\big(\boldsymbol{x}_i(p) - \boldsymbol{x}_j(p'), \boldsymbol{\xi}_j^{\text{d}}(p')\big)\, \text{d}p' \,. \tag{2}$$

The term $\tilde{\tau}_{\text{D}}\big(\boldsymbol{x}_i(p) - \boldsymbol{x}_j(p'), \boldsymbol{\xi}_j^{\text{d}}(p')\big)\, \text{d}p'$ represents the resolved shear stress produced at $\boldsymbol{x}_i(p)$ by an infinitesimal segment $\text{d}p'$ located at $\boldsymbol{x}_j(p')$, l_j is the length of the j-th dislocation.

The statistical treatment [5] leads to the field equation for the flow of the glide dislocations of a single-valued field J,

$$B\rho_J V_J = \begin{cases} b\,(\tau + g_J^{\text{DD}} - \tau_0)\rho_J & \text{for} \quad \tau + g_J^{\text{DD}} \geq \tau_0 \,, \\ b\,(\tau + g_J^{\text{DD}} + \tau_0)\rho_J & \text{for} \quad \tau + g_J^{\text{DD}} \leq -\tau_0 \,, \\ 0 & \text{for} \quad |\tau + g_J^{\text{DD}}| < \tau_0 \,, \end{cases} \tag{3}$$

where ρ_J is the dislocation density of the field J and $\tau = \boldsymbol{s} \cdot \boldsymbol{\sigma} \boldsymbol{m}$ is the resolved shear stress on the slip system $(\boldsymbol{s}, \boldsymbol{m})$. The stress tensor $\boldsymbol{\sigma}$ results as a solution to a mesoscopic boundary-value problem with eigenstrain that is caused by the dislocation glide. The stress τ therefore comprises the externally applied loads as well as the stress due to long range dislocation interactions. The constitutive functional

$$g_J^{\text{DD}}(\boldsymbol{x}) = \sum_{I=1}^{K} \int_\Omega \tilde{\tau}_{\text{D}}(\boldsymbol{x} - \boldsymbol{x'}, \boldsymbol{\xi}_I(\boldsymbol{x'}))\rho_I(\boldsymbol{x'}) d_{JI}^{\text{DD}}(\boldsymbol{x}, \boldsymbol{x'})\, \text{d}v' \,, \tag{4}$$

represents the short-range interactions, where the correlation function d_{JI}^{DD} accounts for pair correlations due to the short-range effects, cf. [4, 5].

3. Specification of the Constitutive Functional

The functional g_J^{DD}, Eqn. (4), can be split into three contributions: $g_J^{\text{DD}} = g_J^{\text{self}} + g_J^{\text{A}} + g_J^{\text{B}}$. The contribution g_J^{self} represents the self stress, g_J^{A} the stress caused by the interaction between dislocations within the single-valued field J, and g_J^{B} the stress coming from the other dislocation fields $I \neq J$.

3.1 Self force

The interaction of a segment with its nearest neighbors forming the dislocation line, i.e. the self force, is the strongest and always present short-range interaction. It is the only one of

the dislocation interactions that was thoroughly analyzed in the past. The self stress can be written as

$$g_J^{\mathrm{self}}(\boldsymbol{x}) = \int_\Omega \tilde{\tau}_{\mathrm{D}}\big(\boldsymbol{x}-\boldsymbol{x}', \vartheta_J(\boldsymbol{x}')\big)\rho_J(\boldsymbol{x}')d_J^{\mathrm{self}}(\boldsymbol{x},\boldsymbol{x}')\,\mathrm{d}v'\,, \tag{5}$$

where Ω is the crystal volume. The self-correlation function d_J^{self} expresses in a statistical sense that glide dislocation segments are always connected to form dislocation lines and that only those segments at $\tilde{\boldsymbol{x}} \in \Omega$ that lie at the dislocation line contribute to the self stress. The angle ϑ_J describes the local dislocation orientation, its derivative along the line is the dislocation curvature κ. Using some approximations and the Taylor expansion of the integrand [5], the self force results in a form that corresponds to the classical result of deWit and Koehler [7], generally known as the line tension approach. For a planar dislocation in equilibrium with an external shear stress τ they found that $b\tau = \kappa T$, where the line tension $T(\vartheta) = E + \partial^2 E/\partial\vartheta^2$ has been derived using a variational approach and the energy per dislocation length $E(\vartheta)$. The force κT is a local approximation to the self force bg_J^{self}.

3.2 Interactions in a single-valued field

The stress caused by short-range interactions among the segments in a single-valued field J is

$$g_J^{\mathrm{A}}(\boldsymbol{x}) = \int_\Omega \tilde{\tau}_{\mathrm{D}}\big(\boldsymbol{x}-\boldsymbol{x}', \vartheta_J(\boldsymbol{x}')\big)\rho_J(\boldsymbol{x}')d_{JJ}^{\mathrm{A}}(\boldsymbol{x},\boldsymbol{x}')\,\mathrm{d}v'\,. \tag{6}$$

At a point $\boldsymbol{x}$ the segments belonging to the field J are parallel, having the same orientation. Therefore, assuming a small curvature, their interactions can be treated analogously to the interactions between parallel edge dislocations in the 2D statistics of Groma *et al.* [4]. This procedure [5] leads to a field expression for the stress $g_J^{\mathrm{A}}(\boldsymbol{x})$,

$$\begin{aligned} g_J^{\mathrm{A}}(\boldsymbol{x}) &= \rho_J(\boldsymbol{x}) \int_{\Omega_\perp(\boldsymbol{x})} \tilde{\tau}_{\mathrm{D}}\big(\boldsymbol{x}-\boldsymbol{x'}, \vartheta_J(\boldsymbol{x'})\big) d_{JJ}^{\mathrm{A}}(\boldsymbol{x}-\boldsymbol{x'})\;\mathrm{d}v' \\ &+ \operatorname{grad}_\perp \rho_J(\boldsymbol{x'})\big|_{\boldsymbol{x}} \cdot \int_{\Omega_\perp(\boldsymbol{x})} (\boldsymbol{x}-\boldsymbol{x'})\,\tilde{\tau}_{\mathrm{D}}\big(\boldsymbol{x}-\boldsymbol{x'}, \vartheta_J(x')\big) d_{JJ}^{\mathrm{A}}(\boldsymbol{x}-\boldsymbol{x'})\;\mathrm{d}v'\,. \end{aligned} \tag{7}$$

Here $\Omega_\perp(\boldsymbol{x})$ is a plane at $\boldsymbol{x}$ perpendicular to the dislocation lines. The first term in Eqn. (7) can be interpreted as a friction stress at $\boldsymbol{x}$ caused by the segments of the field J, whereas the second term approximates a non-local effect leading, along with the self force, to size dependence of the plasticity at the mesoscale.

3.3 Interactions between single-valued fields

The stress caused by the interaction with dislocation segments of other single-valued fields $I \neq J$ in the constitutive functional (4) is

$$g_J^{\mathrm{B}}(\boldsymbol{x}) = \sum_{I\neq J}^{K} \int_\Omega \tilde{\tau}_{\mathrm{D}}(\boldsymbol{x}-\boldsymbol{x'}, \vartheta_I(\boldsymbol{x'})\rho_I(\boldsymbol{x'})d_{JI}^{B}(\boldsymbol{x},\boldsymbol{x}')\,\mathrm{d}v'\,. \tag{8}$$

The statistical treatment [5] of this equation results in

$$g_J^{\mathrm{B}}(\boldsymbol{x}) = \sum_{I\neq J}^{K} \cos(\Delta\vartheta_{IJ}(\boldsymbol{x})) \Bigg(\rho_I(\boldsymbol{x}) \int_{\Omega_\perp(\boldsymbol{x})} \tilde{\tau}_{\mathrm{D}}\big(\boldsymbol{x}-\boldsymbol{x'},\vartheta_{IJ}(\boldsymbol{x})\big) d_{IJ}^{\mathrm{B}}(\boldsymbol{x}-\boldsymbol{x'})\,\mathrm{d}v' + \operatorname{grad}_\perp \rho_I(\boldsymbol{x'})\big|_{\boldsymbol{x}} \cdot \int_{\Omega_\perp(\boldsymbol{x})} (\boldsymbol{x}-\boldsymbol{x'})\,\tilde{\tau}_{\mathrm{D}}\big(\boldsymbol{x}-\boldsymbol{x'},\vartheta_{IJ}(\boldsymbol{x})\big) d_{IJ}^{\mathrm{B}}(\boldsymbol{x}-\boldsymbol{x'})\,\mathrm{d}v' \Bigg), \quad (9)$$

where $\Delta\vartheta_{IJ}(\boldsymbol{x})$ is the difference in the orientations between the segments of the fields I and J at $\boldsymbol{x}$, whereas $\vartheta_{IJ}(\boldsymbol{x})$ is the orientation of the locally adjusted parts of the flexible dislocations [5]. Equation (7) thus appears to be a special case of Eqn. (9) for $\Delta\vartheta_{IJ}=0$.

4. Back Stress in the Continuum Dislocation-Based Model

In the standard continuum dislocation-based model [1, 2, 3], the short-range dislocation interactions are represented by the self force κT and the Taylor-type friction stress $\hat{\tau} = \alpha\mu b\sqrt{\varrho}$. The latter corresponds to the first terms in Eqns. (7) and (9). Since it is not yet clear how to transform these equations in a form suitable for practical calculations, we have introduced gradient terms into the model [6] phenomenologically. Inspired by Groma *et al.*, we define the 'back stress' for parallel dislocations (i.e. within a single-valued field J) as

$$\tau_{\mathrm{b}} = \frac{\mu b D}{2\pi(1-\nu)\rho}\,\boldsymbol{\varsigma}^{(J)} \cdot \operatorname{grad}\rho_J\,, \quad (10)$$

with the constant factor $D=0.8$, cf. [4]. To consider non-parallel dislocations as well (i.e. the short-range interactions between single-valued fields) the definition of back stress has been generalized [6] to

$$\tau_{\mathrm{b}}^{(J)} = \frac{\mu b}{2\pi(1-\nu)\varrho} \sum_{I=1}^{K} D(\Delta\vartheta_{IJ})\,\boldsymbol{\varsigma}^{(J)} \cdot \operatorname{grad}\rho_I\,, \quad (11)$$

where $\varrho = \sum_I \rho_I$. The gradient is calculated in perpendicular direction to the field J for which the effective back stress is required, that is $\boldsymbol{\varsigma}^{(J)}$, as this is the direction of motion and thus the sense of the repulsive back stress, too. However, for the effect which 'the other' fields have on the field J, this gradient is applied to their respective density field. The orientation-dependent factor $D(\psi_{IJ})$ is considered in the form,

$$D(\psi) = 0.8\cdot\cos(\psi) = \begin{cases} 0.8 & \text{for} \quad \psi = 0 \\ 0 & \text{for} \quad \psi = \frac{\pi}{2} \\ -0.8 & \text{for} \quad \psi = \pi \end{cases}. \quad (12)$$

The character of the numerical solution of the model was found to have improved compared to the standard model. Especially, the convection dominance of the original convection-diffusion problem has been suppressed by the back stress [6]. It was observed that the

standard model without back stress can be interpreted as a limit case of the enhanced model for high dislocation densities, as the effect of the back stress for moderate loading can be neglected in this case. On the other hand, for a low initial dislocation density, the effect of the back stress surmounts that of the Taylor-type friction stress by far. Using the back stress in the application of the model to the benchmark problem 'shearing of a thin crystalline strip' shows, that the short-range interactions of both types contribute to the source-shortening effect, that is the narrowing of glide channels in the course of plastic deformation, and the subsequent additional hardening.

5. Conclusions

The evaluation of the constitutive functional (4) is the main problems when applying the statistical approach to dynamics of curved glide dislocations. Therefore, phenomenological models, here represented by the back-stress[1] concept, are currently being developed and used for practical calculations.

References

[1] R. Sedláček, J. Kratochvíl, and E. Werner. "The importance of being curved: Bowing dislocations in continuum description", Philosophical Magazine, **83**, 3735 (2003).

[2] J. Kratochvíl and R. Sedláček. "Pattern formation in the framework of the continuum theory of dislocations", Physical Review B, **67**, 094105 (2003).

[3] R. Sedláček, C. Schwarz, J. Kratochvíl, and E. Werner. "Continuum theory of evolving dislocation fields", Philosophical Magazine, **87**, 1225 (2007).

[4] I. Groma, F. F. Csikor, and M. Zaiser. "Spatial correlations and higher-order gradient terms in a continuum description of dislocation dynamics", Acta Materialia, **51**, 1271 (2003).

[5] J. Kratochvíl and R. Sedláček. "Statistical foundation of continuum dislocation plasticity", Physical Review B, **77**, 134102 (2008).

[6] C. Schwarz, R. Sedláček, and E. Werner. "Refined short-range interactions in the continuum dislocation-based model of plasticity at the microscale", Acta Materialia, **56**, 341 (2008).

[7] G. deWit and J. S. Koehler. "Interaction of dislocations with an applied stress in anisotropic crystals", Physical Review, **116**, 1113 (1959).

[1] The 'back stress' due to the short-range dislocation interactions should not be confused with the hardening variable 'back stress' that is responsible for kinematic hardening in the standard continuum plasticity.

On the Gradient Theory of Elasticity and Dislocation Dynamics

Daniel Walgraef and Elias C. Aifantis

Laboratory of Mechanics and Materials, Aristotle University of Thessaloniki, 54124 Thessaloniki, Greece, (E-mail: mom@mom.gen.auth.gr)

ABSTRACT

Higher order gradients in dislocation dynamics, in formal analogy to the Brusselator, were introduced by the authors about twenty five years ago in order to describe dislocation patterning phenomena observed during cyclic deformation of single Cu crystals. The resulting W-A model was based on "effective mass" balance type equations for dislocation populations containing both "flux" and "source" terms, on the distinction between "mobile" and "immobile" positive and negative dislocations, as well as on the techniques of nonlinear stability analysis. Even though the model was criticized as treating dislocations as "particles" rather than as "lines" (an acceptable view only for single slip of straight dislocation segments that the model was originally developed for), a number of authors have used and extended it to various other cases. Moreover, the model has motivated a large number of articles on statistical mechanics and discrete dislocation simulation aspects of general curved dislocation lines, as well as stochastic dislocation dynamics. It has also triggered related developments in gradient plasticity and, more recently, on gradient elasticity. Despite of these efforts, the problem of dislocation patterning is still an open issue requiring further work and attention. The paper addresses two apparently different topics along this direction. The first topic is concerned with the use of gradient elasticity in producing nonsingular dislocation fields that may be more efficient to use in simulations. The second topic is concerned with a re-examination of the original W-A model to consider multislip and stochastic effects.

1. Introduction

The problem of bridging material length and time scales (nanoscopic 10^{-9} m and femtosecs; microscopic 10^{-6} m and picosecs; mesoscopic 10^{-4} m and nanosecs; macroscopic 10^{-2} m and millisecs) is still open. The recently developed strategy of multiscale modeling (quantum chemistry/QC and density functional theory/DFT; molecular dynamics/MD and monte carlo/MC; discrete dislocation dynamics/DDD; finite elements/FE) is a "configuration"- rather than a "process"-oriented approach, not designed for describing simultaneously the material response at all scales. Moreover, it does not account for recently developed revolutionary concepts and powerful techniques (fractals, wavelets, cellular automata) in nonlinear science and complexity theory.

As an alternative, a number of researchers (e.g. Aifantis / Fleck-Hutchinson / Gao-Huang / Gurtin and their co-workers) have advanced the so-called gradient theory paradigm. This may be viewed as a compromise between classical continuum and discrete multiscale formalisms, since the new material parameters measuring the effect of gradient terms of the state variables (order parameters) can be calculated, in principle, through multiscale modeling. Moreover, the approach is perfectly suited for taking advantage of recent developments in bifurcation/instability theory and statistical physics. Examples of this approach for the description of dislocation densities and associated patterning phenomena, the elimination of singularities in dislocation lines and elastic crack tips, and the nucleation and evolution of shear bands in plastically deforming materials have been advanced with reasonable success over the last twenty five years. Two particular examples are further considered in this paper. The first example is concerned with the implications of gradient elasticity to eliminate classical dislocation singularities and describe the "core" region. The second example is concerned with a reformulation of the W-A model to consider multislip and stochastic effects.

This contribution was prepared in relation to honoring Professor Nasr Ghoniem on the occasion of his 60th birthday. His pioneering work on using molecular dynamics type simulations for describing dislocation clustering phenomena during creep deformation started almost at the same time that the gradient approach was introduced to describe macroscopic shear banding phenomena during monotonic deformation and microscopic persistent slip band phenomena during cyclic deformation [1]. In our opinion, the subsequent voluminous work on discrete dislocation dynamics simulations was motivated by these initial works on "dislocation patterning", a term originally introduced by the authors for dislocation clusters and periodic structures derived within a nonlinear selforganization framework, along the same philosophy used later by Walgraef and Ghoniem to describe pattern formation in irradiated films [2].

2. Outline of Gradient Theory

A robust generalization of classical theory to include higher order gradient terms is provided here. Two types of co-existing scales are assumed: one scale is accounted for by standard constitutive equations, while its interaction with the second scale is accounted for through second-order (Laplacian) spatial terms resulting from an appropriate "averaging" procedure. More specifically, the modified gradient-dependent Hooke's law and the governing differential equations for the evolution of dislocation density may be written as follows:

$$\bar{\sigma}_{ij} = \lambda \bar{\varepsilon}_{\kappa\kappa}\delta_{ij} + 2\mu\bar{\varepsilon}_{ij} \quad ; \quad \bar{\sigma}_{ij} = \sigma_{ij} + c_\sigma \nabla^2 \sigma_{ij} \ , \ \bar{\varepsilon}_{ij} = \varepsilon_{ij} + c_\varepsilon \nabla^2 \varepsilon_{ij}, \tag{1}$$

$$\dot{\bar{\rho}}_\alpha + \mathrm{div}\bar{\mathbf{j}}_{\boldsymbol{\alpha}} = g\left(\bar{\rho}_{\alpha,\beta}\right) \quad ; \quad \bar{\rho}_\alpha = \rho_\alpha + c_\rho \nabla^2 \rho_\alpha \ , \quad \bar{\mathbf{j}}_{\boldsymbol{\alpha}} = \mathbf{j}_{\boldsymbol{\alpha}} + c_j \nabla^2 \mathbf{j}_{\boldsymbol{\alpha}} \ . \tag{2}$$

The field variables in Eqns. (1)-(2) are as follows: ρ denotes dislocation density and $\mathbf{j}$ the corresponding flux vector; $(\sigma_{ij}, \varepsilon_{ij})$ denote the stress and strain tensors for elastic deformation. The quantity g, which depends on the effective stress, denotes the standard source term of dislocation dynamics (the indexes α, β denote different dislocation families), while (λ, μ) are the Lamé constants. The bars denote the values of the respective variable in one scale (say the macroscale), while the corresponding quantity without bar denotes its value in the second scale

(say the microscale). The sign and values of the gradient coefficients depend on the deformation state at hand (hardening or softening), the governing substructure that brings this deformation about, as well as the scale at which the relevant field quantity is determined.

3. Elimination of Elastic Singularities

The strain energy per unit dislocation length for a cylinder of radius R surrounding the dislocation line within the simplest version of gradient elasticity theory [3] is given by

$$W_s = A_s\left\{\gamma + \ln\frac{R}{2\sqrt{c}} + K_0\left(\frac{R}{\sqrt{c}}\right)\right\}, W_e = A_e\left\{\gamma + \frac{1}{2} + \ln\frac{R}{2\sqrt{c}} + 2K_0\left(\frac{R}{\sqrt{c}}\right) + 2\frac{\sqrt{c}}{R}K_1\left(\frac{R}{\sqrt{c}}\right) - \frac{2c}{R^2}\right\}, \quad (3)$$

where γ denotes the Euler constant, K_0 and K_1 denote Bessel functions of the 2nd kind, and (A_s, A_e) are prelogarithmic factors (for screw, edge dislocations) depending on the Burgers vector and the elastic constants. The above non-singular expressions were adopted to calculate the self-energy of a $1/6<20\bar{2}3>$ partial dislocation in wurtzite GaN [4]. They provide an estimate for the dislocation core r_0 of the form $W_{core}\sqrt{c}/r_0 \simeq 0.33$ eV/Å independently of the particular core structure considered, and they give the variation of the self-energy with distance from the dislocation line in agreement with atomistic simulations (for $r \to 0$) and with linear elasticity (for $r >> r_0$). It also turns out that for a screw dislocation, the appropriate component of the dislocation density tensor varies as $\sim (b/2\pi c)K_0\left(r/\sqrt{c}\right)$, which departs significantly from the delta-type distribution of its classical elasticity counterpart. For a 2nd gradient elasticity theory it turns out that the value of the relevant component of the dislocation density tensor is finite $\sim\left(b/4\pi d^2\right)$ at $r = 0$ (where d is a new gradient coefficient). It is finally pointed out that non-singular dislocation models have been proposed in the literature before. Reference is made, in particular, to the classical Peirls-Nabarro atomistic model, to Li's hollow disclocation model, and to a more recent dislocation core-spreading model [5]. It turns out that the shear stress $\sigma_{xy}(x,0)/[\mu b/2(1-\nu)]$ on the glide plane under the assumption of same peak stress for these models varies according to the following distributions: $x/\left[x^2 + (a^2/4(1-\nu)^2)\right]$ for the Peirls-Nabarro; $1/x - r_0^3/x^3$ for Li's; $1/x - 4c/x^3 + (2/x)K_2\left(x/\sqrt{c}\right)$ for gradient elasticity; $x/(x^2+\alpha^2)$ for core spreading, with $r_0 \simeq 0.6a$, $\alpha = 0.76a$ where a denotes the lattice parameter.

4. Dislocation Patterning

Without presenting an argument to show how Eqn. (2) can be used to generate the original W-A model, we briefly discuss here an extension of this model in the case of two coexisting slip systems (say, in the directions x and y, orthogonal to each other) by restricting attention to one

scale (mesoscale) only [6]. The model consists of coupled rate equations for the stationary or forest (slow moving) and mobile dislocation densities ρ_s, ρ_{mx} and ρ_{my}. They read

$$\begin{aligned} &\partial_t\rho_s = D_s\nabla^2\rho_s + \upsilon_s\rho_s\sqrt{\rho_s} - \upsilon_s d_c\rho_s^2 - \left(\beta_x+\beta_y\right)\rho_s + \gamma\rho_s^2\left(\rho_{mx}+\rho_{my}\right), \\ &\partial_t\rho_{mx} = D_{mx}\nabla_x^2\rho_{mx} + \beta_x\rho_s - \gamma\rho_s^2\rho_{mx}\,, \quad \partial_t\rho_{my} = D_{my}\nabla_y^2\rho_{my} + \beta_y\rho_s - \gamma\rho_s^2\rho_{my}\,, \end{aligned} \tag{4}$$

which is a direct generalization of the original W-A model. It turns out that near bifurcation (as the external stress is increased) the governing equation for the slow mode or order-like parameter of the system is of Ginzburg-Landau type of the form

$$\tau_0\partial_t\rho = \left[\varepsilon - d_0\left(q_c^2+\nabla^2\right)^2 - d_\perp\nabla_x^2\nabla_y^2\right]\rho + \upsilon\rho^2 - u\rho^3, \tag{5}$$

where $\tau_0 = \left(\gamma\rho_s^{0^2}\right)\Big/\left(q_c^2 D_m\beta_c\right)$, $q_c = \left[\left(\gamma\rho_s^{0^2}\upsilon_s\right)\Big/\left(2d_c D_m D_s\right)\right]^{1/4}$, $\beta_c = \left(\sqrt{\upsilon_s/2d_c} + \sqrt{\gamma\rho_s^{0^2} D_s/D_m}\right)$, $\varepsilon = \left(\beta-\beta_c\right)/\beta_c$, $d_\perp = \left(\gamma\rho_s^{0^2}\right)\Big/\left[q_c^4\left(\gamma\rho_s^{0^2}+D_m q_c^2\right)\right]$, $d_0 = D_m\Big/\left(q_c^2\gamma\rho_s^{0^2}\right)$, and the kinetic coefficients υ and u are explicitly determined from their slow-mode dynamics procedure (center manifold theorem). The numerical analysis of Eqn. (5) leads [6] to the evolution of the dislocation patterns or "labyrinth structures", in qualitative agreement with observed experimental micrographs.

An alternative to the above deterministic dislocation density evolution framework may be obtained with the use of statistical/stochastic arguments of the type advanced in [7]. By denoting with $(\tau^{int}/\tau^{ext}, b)$ internal/external resolved shear stress and Burgers vector (B denotes a mobility constant) one arrives at the following differential equations for the sum $\rho = \rho_+ + \rho_-$ and the difference $k = \rho_+ - \rho_-$ dislocation densities (which are now defined in terms of the respective probability densities)

$$\partial_t\rho(\mathbf{r},t) = -\left(b_i\nabla\right)\left\{Bk(\mathbf{r},t)\left[\tau^{int}(\mathbf{r}) + \tau^{ext}\right]\right\}, \; \partial_t k(\mathbf{r},t) = -\left(b_i\nabla\right)\left\{B\rho(\mathbf{r},t)\left[\tau^{int}(\mathbf{r}) + \tau^{ext}\right]\right\}, \tag{6}$$

which may be viewed as the relevant Langevin equations for stochastic variables. On considering the mean field version described by Eqn. (6), and computing the total internal stress induced by the dislocation ensemble for a system of parallel edge dislocations, it turns out that linear stability analysis for a constant external stress around the homogeneous stationary solution gives for small perturbations $\hat{\rho}(\mathbf{r},t) = \rho(\mathbf{r},t) - \rho^0$, $\hat{k}(\mathbf{r},t) = k(\mathbf{r},t)$, the following expression for the growth rate ω

$$\omega^2 + \omega\left[q_x^2 q_y^2/q^4\right]\Lambda + q_x^2\left(bB\tau^{ext}\right)^2 = 0, \tag{7}$$

where $\Lambda = \mu b^2 B\rho^0/[2\pi(1-\nu)]$ with (μ,ν) denoting shear and Poisson moduli. It can easily be seen that the real part of the eigenvalues is never positive and that the uniform solution is stable.

As a result, elastic dislocation interaction is not sufficient to induce dislocation patterning. However, uniform dislocation densities are only marginally stable for perturbations with wavevectors parallel or perpendicular to the glide direction. In fact, $\omega = 0$ for spatial modulations perpendicular to the glide direction $\left(q_x = 0\right)$, which thus do not decay, at least linearly. On the other hand, $\omega = \pm i q_x bB\tau^{ext}$ for modulations parallel to the glide direction $\left(q_y = 0\right)$, which thus propagate along it.

This suggests that the evolution of the dislocation densities is expected to be extremely sensitive to nonlinear couplings and fluctuations; thus a stochastic analysis may be unavoidable. In this case it turns out that the appropriate equations for the perturbations read

$$\begin{aligned}
\partial_t \hat{\rho}(\mathbf{r},t) &= -(bB\nabla)\left[\hat{k}(\mathbf{r},t)\tau^{ext} + \rho^0 \int d\mathbf{r}_1 \hat{\rho}(\mathbf{r}-\mathbf{r}_1,t)\, d_\Delta(\mathbf{r}_1)\tau^{ind}(\mathbf{r}_1)\right], \\
\partial_t \hat{k}(\mathbf{r},t) &= -(bB\nabla)\left[\hat{\rho}(\mathbf{r},t)\tau^{ext} + \rho^0 \int d\mathbf{r}_1 \hat{k}(\mathbf{r}-\mathbf{r}_1,t)\left[1 + d_\sigma(\mathbf{r}_1)\right]\tau^{ind}(\mathbf{r}_1)\right].
\end{aligned} \tag{8}$$

where $2d_\sigma(\mathbf{r},\mathbf{r}_1) = d_{++}(\mathbf{r},\mathbf{r}_1) + d_{+-}(\mathbf{r},\mathbf{r}_1)$ and $2d_\Delta(\mathbf{r},\mathbf{r}_1) = d_{++}(\mathbf{r},\mathbf{r}_1) - d_{+-}(\mathbf{r},\mathbf{r}_1)$, since $d_{++} = d_{--}$ and $d_{+-} = d_{-+}$; where $d_{\alpha\beta}(\mathbf{r},\mathbf{r}_1)$ is the scaled pair correlation function of dislocations of sign α and β [$\tau^{ind}(\mathbf{r}) \equiv \mu b \partial^3_{xy^2} g(r) \big/ 2\pi(1-\nu)$; $g(r) = 1/2\, r^2 \ln r$]. Since the dislocation densities are expected to vary smoothly with respect to the correlation functions, the integrals in Eqn. (8) may be evaluated through an expansion of the dislocation densities around $\mathbf{r}$, yielding the following expression for the eigenvalue ω of the linear evolution matrix

$$\omega = \frac{\Lambda}{2}\left[q_x^2 D_+ - q_x^4 E_+ - q_x^2 q_y^2 F_+ - \frac{q_x^2 q_y^2}{q^4}\right] \pm \sqrt{\frac{\Lambda^2}{4}\left[q_x^2 D_- - q_x^4 E_- - q_x^2 q_y^2 F_- - \frac{q_x^2 q_y^2}{q^4}\right]^2 - q_x^2 \left(bB\tau^{ext}\right)^2}, \tag{9}$$

where $D_\pm = D_\Delta \pm D_\sigma \simeq D_\Delta$, $E_\pm = E_\Delta \pm E_\sigma \simeq E_\Delta$ and $F_\pm = F_\Delta \pm F_\sigma \simeq F_\Delta$, since $d_\Delta >> d_\sigma$; and the coefficients $(D,E,F)_{\Delta,\sigma}$ are given in terms of surface integrals involving products of $d_{\Delta,\sigma}$ with third partial derivatives of $g(\mathbf{r})$. It can easily be seen that both $\hat{\rho}$ and $\hat{k}$ have positive growth rates for finite wavevectors, and that $\hat{\rho}$ has a maximum growth rate which corresponds to $q_y = 0$ and $q_x = \sqrt{D_\Delta/(2E_\Delta)} \propto \sqrt{\rho^0}$. Dislocation walls perpendicular to the glide direction are thus expected to grow first, as obtained in previous numerical simulations. In the presence of an applied external stress, it can easily be established that perturbations with $q_x = 0$ are always marginally stable. Perturbations with $q_y = 0$ are unstable for $0 < q_x^2 < q_M^2 = D_+/E_+$, with a growth rate given by $\omega \simeq \Lambda/2\left[q_x^2 D_+ - q_x^4 E_+\right] \pm i q_x \left(bB\tau^{ext}\right)$, which is strictly valid for $\tau^{ext} > (\Lambda/bB) q_x \sqrt{D_- - q_x^2 E_-}$. For each wave number between 0 and q_M, there is thus a threshold for the external stress above which the instability is of the wave type and below which it is of the spinodal decomposition type. For sufficiently large external stress, when the bifurcation is of the

wave type, walls perpendicular to the glide direction and traveling in this direction are linearly selected; the maximum growth rate occurs for $q_x^2 = q_0^2 = D_+/(2E_+)$ and the corresponding propagation velocity is $\upsilon_0 \simeq \pm q_c bB\tau^{ext}$. Perturbations with $q_y \neq 0$ may be unstable. These results hold for the case that source terms are not included. The corresponding results for the more realistic case where dislocation reactions are included, as in the W-A model, will be presented in a forthcoming article, along with related details pertaining to the discussion of this section.

Due to space limitations shear banding problems in gradient plasticity, as well as the competition between deterministic gradients and stochastic effects will not be discussed. Preliminary work on this topic has been reported by Aifantis in [3], as well as by Zaiser and Aifantis [8]; the results of the second paper have been recapitulated by Zaiser and Moretti in [9], and further extended by Zaiser and Aifantis in [10].

Acknowledgments

The support of EU under the RTN DEFINO Program HPRN-CT-2002-00198, as well as NSF under the NIRT Grant DMI-0532320 is gratefully acknowledged.

References

[1] E.C. Aifantis, D. Walgraef and H. Zbib (Editors), "Material Instabilities", Special Issue of Res. Mechanica **23**, Vols. 2&3 (Elsevier Appl. Sci. Publ., 1988).
[2] N. Ghoniem and D. Walgraef, *Instabilities and Self-Organization in Materials* (Oxford University Press, 2007).
[3] E.C. Aifantis, "Update on a class of gradient theories", Mech. Mater., **35**, 259 (2003).
[4] J. Kioseoglou, G.P. Dimitrakopulos, Ph. Komninou, Th. Karakostas, I. Konstantopoulos, M. Avlonitis and E.C. Aifantis, "Analysis of partial dislocations in wurtzite GaN using gradient elasticity", Phys. Stat. Sol. A, **203**, 2161 (2006).
[5] W. Cai, A. Arsenlis, C.R. Weinberger, V.V. Bulatov, "A non-singular continuum theory of dislocations", J. Mech. Phys. Solids, **54**, 561 (2006)
[6] J. Pontes, D. Walgraef and E.C. Aifantis, "On dislocation patterning: Multiple slip effects in the rate equation approach," Int. J. Plasticity, **22**, 1486 (2006).
[7] M. Zaiser, M.-C. Miguel and I. Groma, "Statistical dynamics of dislocation systems: The influence of dislocation-dislocation correlations", Phys. Rev. B, **64**, 224102 (2001).
[8] M. Zaiser and E.C. Aifantis, "Avalanches and slip patterning in plastic deformation," J. Mech. Beh. Mat., **14**, 255 (2003).
[9] M. Zaiser and P. Moretti, "Fluctuation phenomena in crystal plasticity - a continuum model", J. Stat. Mech., P08004 (2005).
[10] M. Zaiser and E.C. Aifantis, "Randomness and slip avalanches in gradient plasticity", Int. J. Plasticity, **22**, 1432 (2006).

Phase Field Theory of Dislocations Obtained by Coarse Graining

Istvan Groma

Eotvos University Budapest, Department of Materials Physics, Pazmany P. setany 1/A, Budapest, 1117 Hungary (E-mail: groma@metal.elte.hu)

ABSTRACT

In the past decade there has been a increasing activity to develop a continuum theory of dislocations. Theoretical investigations are largely motivated by the experimental finding that if the characteristic size of a specimen is less than about $10\mu m$ the plastic response of the crystalline materials depends on the size (size effect). The continuum theory should be built up from the properties of individual dislocations. For a system of parallel edge dislocations with single slip Groma et al. have established a systematic way to derive a continuum theory from the equation of motion of individual dislocations. The most important feature of this theory is that gradient terms appear naturally in the evolution equations of the different dislocation densities. At the moment, however, it is not clear how to extend the model for more complicated dislocation geometries and configurations. Recently, several new promising frameworks have been proposed for treating curved dislocations with statistical methods, but there are many open issues to be resolved before we can say we have a well established 3D continuum theory of dislocations. Constructing a continuum theory even for 2D multiple slip is far from straightforward. A dislocation ensemble is a system of objects with long range interaction. So the traditional methods developed for atomic systems to derive a continuum theory from the equation of motion of the individual objects cannot be directly applied. In the investigations presented we consider a set of parallel edge dislocations representing the simplest possible, but already rather complex system. In the first part of the paper the 3D field theory of individual dislocations developed by Kröner is reformulated into a variational problem. Since the general 3D problem is extremely complicated the variational formalism is simplified for the 2D edge dislocation case. It is shown, that if one simple replaces the different discrete dislocation density fields by their coarse grained counterparts in the energy functional this results in a continuum theory of dislocation that completely neglect dislocation-dislocation correlation effects. To account for correlations an energy correction term is proposed. The evolution equations of the different dislocation densities are obtained from this corrected functional by applying the standard formalism of phase field theories. In order to check if the continuum theory derived is able to account for the collective properties of dislocations its predictions were compared with discrete dislocation dynamics simulations for different static cases. The problem of induced geometrically necessary dislocation density developing around an extra dislocation added to the system (Debye screening) is discussed in details.

A Perspective on the Development of Density-Based Models of Dislocation Dynamics

Anter El-Azab

School of Computational Science (and Materials Science Program), Florida State University, Tallahassee, FL 32306; E-mail: anter@scs.fsu.edu

ABSTRACT

We discuss the statistical dislocation modeling approach and the importance of this approach in establishing mesoscale models of crystal plasticity. A general mathematical description of dislocation density evolution in deforming crystals will be briefly discussed in order to highlight the need for statistical modeling of dislocations in both space and time. The presentation then focuses on the recent work on the quantitative characterization of the statistics of the dislocation system and their internal elastic fields in deformed crystals. Both the spatial and temporal statistics of dislocation systems in model BCC and FCC crystals will be discussed. In particular, we show that the 3D dislocation correlations exhibit an oscillatory behavior and significant anisotropy in the crystal space, with surprisingly long correlation length that decays as function of strain and strain rate. We also show that temporal statistical analysis of the cross slip and junction formation and annihilation events can help us establish temporal coarse graining strategies for such dynamical events and, as a result, fix the source terms of the dislocation kinetic equations. The methodology used to model dislocation statistics here is based on stochastic fiber process for spatial statistics, and on time series analysis and marked point process for the temporal statistics. In both cases, the method of dislocation dynamics simulation has been used to collect statistical realizations of the dislocation system. The presentation concludes with highlighting a number of open questions related to the statistical modeling of dislocations and to the connection of the resulting density-based dislocation evolution models with the basic laws of crystal mechanics.

This work is performed in collaboration with my doctoral student, Jie Deng. The work is supported by the U.S. Department of Energy, Office of Basic Energy Sciences, Division of Materials Science and Engineering under contract number DE-FG02-08ER46494 at Florida State University.

3D Simulations of Evolving Dislocation Microstructures: Connection to Coarse Graining

Richard LeSar[1], Jeffrey Rickman[2]

[1]Iowa State University, Ames, IA 50011, USA (E-mail: lesar@iastate.edu)
[2]Lehigh University, Bethlehem, PA, USA (E-mail: jmr6@lehigh.edu)

ABSTRACT

Recent advances in our ability to directly simulation complex dislocation response is enabling a new view of an old problem -- dislocation-based plasticity. The complexity of the simulations as well as the computational burden, especially as the dislocation density increases, limits the ability of such simulations to model large-scale plastic flow. One path forward is to develop explicit coarse-graining strategies that describe the evolution of locally-averaged quantities, thus reducing the number of degrees of freedom in the problem. In this talk we will discuss our recent work using dislocation simulations to define coarse-grained variables and to develop evolution equations.

Self Learning Kinetic Monte Carlo Simulations: application to hetero- and homo-epitaxial growth processes

Talat Rahman

University of Central Florida, Orlando, FL 32828, USA
(E-mail: talat@physics.ucf.edu)

ABSTRACT

Coupled with advances in ab initio methods for the calculation of activation energy barriers, the kinetic Monte Carlo (KMC) method is proving itself to be an important tool for computational studies of phenomena such as epitaxial growth, surface diffusion and surface morphological evolution. However, despite its ability to carry out simulations for time and length scales that are relevant to experiments, in its nascent form the method has limited predictive power because of its reliance on predetermined atomic events and their energetics as input. To overcome this handicap, we have developed a self learning method (SLKMC), in which we combine standard KMC with automatic generation of a table of microscopic events, facilitated by a pattern recognition scheme. Each time the system encounters a new configuration, the algorithm initiates a procedure for saddle point search around a given energy minimum. Nontrivial paths are thus selected and the fully characterized transition path is permanently recorded in a database for future usage. The system thus automatically builds up all possible single and multiple atom processes that it needs for a sustained simulation. Results of the application of the method to examination of the diffusion and coalescence of 2-dimensional Cu and Ag adatom and vacancy clusters on Cu(111) and Ag(111) will be presented. I will highlight the key role played by specific diffusion processes revealed during the simulation. Of particularly interest are multiple atom processes whose presence may have been ignored otherwise. As we will see the importance of such processes is dependent on both cluster size and surface temperature. For adatom clusters varying in size from 2 to 1000, I will discuss the size dependence of the diffusion coefficient and the effective energy barrier. The rate limiting processes will also be discussed for island coalescence. Results will be compared with those from experiments, where available, and with those from KMC simulations based on a fixed catalogue of diffusion processes. I will also provide some details of an extension of the techniques to “off-lattice” case and its application to examine the case of hetero-epitaxial growth. *Work done in collaboartion with O. Trushin, A. Kara, H. Yildirim and A. Karim *Work supported in part by NSF and CRDF

Anomalous Relaxation in Strained (110) fcc Layers

Klaus Schwarz

IBM Research Yorktown Heights, NY 10598, USA
(E-mail: kws@us.ibm.com)

ABSTRACT

Current efforts to extend the performance of semiconductor devices depend heavily on strain engineering, using strained Si layers on relaxed SiGe substrates, strained SiGe embedded in Si, and other more complicated schemes. In this technology, dislocation-mediated strain relaxation is a major concern, either as something to be promoted and controlled, or as something to be avoided. Although past development efforts have been focussed exclusively on the type of SiGe/Si heteroepitaxy in which the interface-normal is in the [001] direction, recent observations of higher carrier mobilities in (110) Si, pseudomorphically grown on relaxed (110) SiGe, have stimulated interest in (110) or, more generally, hybrid-oriented technology (HOT), and the associated plasticity effects. In the present talk, we report on a large-scale Discrete Dislocation Dynamics study of plastic behavior in biaxially strained (110) fcc layers. Since the glide planes are no longer symmetrically distributed about the layer normal, such a layer relaxes in a highly unusual way. Taking the two perpendicular crystal directions lying in the layer plane to be in the [100] and [-110] directions, we find that relaxation of strain in the [001] direction is driven by the sum of the biaxial strain components, whereas relaxation in the [-111] direction is driven by their difference. Consequently, strain relaxes primarily in the [001] direction, relaxation in the [-111] direction not commencing until a sufficient imbalance in the strain components has been created. The resulting anisotropic relaxation behavior, and the peculiar configuration of the resulting misfit dislocations will be described in detail.

Dislocation Dynamics Simulation in Heterogeneous Elastic Thin Films

E.H. Tan and Lizhi Sun

University of California – Irvine, Irvine, CA 92697-2175, USA
(E-mails: tan_enhui@hotmail.com, lsun@uci.edu)

ABSTRACT

A novel dislocation dynamics framework is developed to simulate dislocation evolutions in thin film heterostructures. It is based on 3-D dislocation motion together with its physical background by adding the solid viscous effect. As the numerical simulation results demonstrate, this new model solves a long-standing paradoxical phenomenon with which the simulation results were dependent on dislocation-segment lengths in the classical discrete dislocation dynamics theory. The proposed model is applied to simulate the effect of dislocations on the mechanical performance of thin films. The interactions among the dislocation loop, free surface and interface are rigorously computed by decomposing this complicated problem into two relatively simple sub-problems. This model is allowed to determine the critical thickness of thin films for a surface loop to nucleate and to simulate how a surface loop evolves into two threading dislocations. Furthermore, the relationship between the film thickness and yield strength is constructed and compared with the conventional Hall-Petch relation.

The Behavior of Dislocations in Bulk and Nano-layered Crystals: An *ab initio*-based Parametric Dislocation Dynamics Approach

Mutasem Shehadeh[1], Sauvik Banerjee[2], Gang Lu[3], Nickolas Kioussis[3], Nasr Ghoneim[4]

[1]Villanova University, Villanova, PA 19085, USA
(E-mail: mutasem.shehadeh@villanova.edu)
[2]Saint Louis University, Saint Louis, MO 63103, USA (E-mail: sbanerje@slu.edu)
[3]California State University Northridge, Northridge, CA 91330, USA
(E-mail: gang.lu.35@csun.edu, nick.kioussis@csun.edu)
[4]University of California, Los Angeles, CA, USA (E-mail: ghoniem@ucla.edu)

ABSTRACT

The behavior of dislocations in bulk and nano-layered materials are investigated using a hybrid approach that links the parametric dislocation dynamics method with ab initio calculations. The model takes into account all three components of atomic displacements of the dislocation and utilizes the entire generalized stacking fault energy surface (GSFS) to capture the essential features of dislocation core structure. This model is used to study two classes of problems: First; The strengthening mechanisms in bimetallic Cu/Ni nanolyers where the dislocation spreading over the interface is explicitly accounted for. The effects of the mismatch in the elastic properties, GSFS and lattice parameters on the spreading of the dislocation onto the interface and the transmission across the interface are studied in detail. Our results show that the strength of the bimaterial can be greatly enhanced by the spreading of the glide dislocation, and also increased by the pre-existence of misfit dislocations. In contrast to other available PN models, dislocation core spreading in the two dissimilar nano-materials and on their common interface must be simultaneously considered because of the significant effects on the transmission stress. Second; Multiplane-induced widening of stacking faults in fcc metals. We show that Shockley partials on successive glide planes greatly assist the widening of stacking faults (SFs) in Al and Ag. This effect is amplified when all trailing partials are pinned. Subsequent placement of Shockley partials on adjacent planes enhances further the widening of the SF width. In sharp contrast, dislocations with zero net Burgers vector across three successive planes form very compact cores in both Al and Ag, in agreement with recent experiments.

A New Characteristic Length Scale

Hanchen Huang

**Department of Mechanical, Aerospace, and Nuclear Engineering,
Rensselaer Polytechnic Institute
(http://www.rpi.edu/~huangh; E-mail: hanchen@rpi.edu)**

ABSTRACT

If it is challenging to model *N* length scales, it must be more challenging to model *N+1* length scales. This talk presents a new characteristic length scale – the $(N+1)^{th}$ length scale, which has always existed but has been discovered only recently. During materials processing such as synthesis, length scales develop as a result of kinetics and thermodynamics. Following the discovery of three-dimensional Ehrlich-Schwoebel barrier, we have discovered a new length scale – the length of surface islands bounded by multiple-atomic-layer steps. This presentation starts with the physics origin of such length scale, and continues with atomistic simulations demonstrating the variation of the length scale and validation experiments, and ends with design of nanosynthesis based on the knowledge of this new length scale & its experimental validation. It is interesting to note that this length scale is the very reason that nanorods synthesis is possible, even though nanorods had been realized long time ago (and it was patented a decade ago).

Tracking Acoustic Emission and Spatial Configurations of Dislocations during the Portevin-Le Chatelier Effect

G. Ananthakrishna

Materials Research Centre, Indian Institute of Science
Bangalore 560012, India
(E-mail: garani@mrc.iisc.ernet.in)

ABSTRACT

Acoustic emission studies on plastic deformation have established a definite correlation between the nature of the signal and collective effects of dislocations. From a theoretical point of view, modeling acoustic emission during plastic deformation poses serious challenges. A major source of difficulty is the lack of dislocation based models that describe the desired collective effects. More importantly, one needs to bridge widely separated time scales corresponding to the inertial time scale and the time scale corresponding to collective effects of dislocations. Currently, the Ananthakrishna model that uses dislocation densities offers a platform to discuss the collective effects for describing the *Portevin – Le Chatelier* effect. However, bridging the widely separated time scales remains a major obstacle. Here, we suggest a formal way of describing the inertial time scale and the collective modes of plastic deformation in the context of the Ananthakrishna model. We show that the nature of acoustic emission is quite different for the type C, B and A bands. We will also outline a method of tracking dislocation configurations corresponding to the three types of bands. While most dislocations are in the pinned state for the type C and B bands, for the type A band, most dislocations are at threshold of unpinning.

Meshfree Approaches for Modeling Grain Structure Evolution

J. S. Chen[1], X. Zhang[1], S. Osher[2]

[1]Civil & Environmental Engineering Department, 5713 Boelter Hall, University of California, Los Angeles (UCLA), Los Angeles, CA 90095-1593.
E-mail: jschen@seas.ucla.edu
[2] Mathematics Department, Math Sciences 7617F, University of California, Los Angeles (UCLA), Los Angeles, CA 90095-1593.
E-mail: sjo@math.ucla.edu

ABSTRACT

The process of stressed grain growth involves both grain boundary migration (moving interfaces) and topological changes of grain geometry, and it can not be effectively modeled by the standard finite element method without continuous remeshing. We introduce two meshfree approaches for modeling grain structure evolution. In the first approach [1,2], a meshfree method combined with front-tracking is proposed for modeling stressed grain growth. In this approach, a uniform set of meshfree points are employed to discretize the material domain, while the grain boundary evolution is treated as moving weak discontinuity discretized by finite elements. The second approach [3] is based on a combined level set and meshfree method for modeling topological changes in the evolving grain network without the need of front-tracking.

[1] J. S. Chen, V. Kotta, H. Lu, D. Wang, D. Moldovan, and D. Wolf, "A Variational Formulation and a Double-grid Method for Meso-scale Modeling of Stressed Grain Growth in Polycrystalline Materials", Computer Methods in Applied Mechanics and Engineering, **193**, 1277 (2004).
[2] J. S. Chen and S. Mehraeen, "Variationally Consistent Multi-scale Modeling and Homogenization of Stressed Grain Growth", Computer Methods in Applied mechanics and Engineering, Vol. 193, pp. 1825-1848, 2004.
[3] X. Zhang, J. S. Chen, and S. Osher, "A Multiple Level Set Method for Modeling Grain Boundary Evolution of Polycrystalline Materials," Interaction and Multiscale Mechanics, **1**, 178 (2008).

Mode II Loading Behaviour of Intergranular Cracks Lying on Symmetrical Tilt Boundaries in Cu

A. Luque, J. Aldazabal, J.M. Martínez-Esnaola, J. Gil Sevillano

CEIT and TECNUN (University of Navarra)
Paseo de Manuel Lardizabal, 15. 20018 San Sebastián, Spain (E-mail: jgil@ceit.es)

ABSTRACT

We present Molecular Dynamics (MD) simulations of the shear-coupled migration behaviour of symmetrical tilt boundaries in presence of nano-cracks lying on the boundary plane. The simulations have been performed for copper bicrystals at room temperature. Shear-coupled migration occurs ahead of the mode II loaded crack tips, but the tilt boundary gets pinned by the crack tip. The bulging of the tilt boundary reduces the shear stress on the boundary surface near the tip and hinders mode II crack propagation; in fact, some crack healing is observed. The applied stress growths until depinning of the boundary takes place or until another deformation mechanism (emission of dislocations from the crack tip vicinity, grain boundary sliding) is activated.

1. Introduction

First references to grain boundary (GB) movement as a consequence of applied mechanical loads go back to the fifties [1], but only recently this phenomenon has attracted much attention [2-4]. Shear-coupled migration (SCM) of tilt boundaries has been acknowledged as a particular plastic strain mechanism that can complement or compete with the other intra- or inter-granular mechanisms in a wide temperature range. SCM is diffusion-less but thermally activated; it can occur at low temperatures. The shear strain effectiveness of the migration of a tilt boundary can be characterized by a shear coupling factor, β, the ratio of the shear displacement parallel to the GB surface to the GB migration normal to its surface. The factor β is determined by the tilt GB misorientation, θ, either $\beta = 2tg(\theta/2)$ (positive coupling, "small" misorientations) or $\beta = -2\tan(\varphi/2)$, $\varphi = (\pi/2) - \theta$ (negative coupling, "large" misorientations).

In this work MD simulations of shear-coupled migration of several symmetrical tilt boundaries in copper at room temperature have been carried out aiming to compare the behaviour of perfect boundaries with that of boundaries containing (nano-) cracks lying on their surface. The mode II stress field near the crack tip was expected to modify the migration response of the GB although it could also modify the local activity of the other strain mechanisms: dislocation emission, GB sliding.

2. Simulation technique, specimens and tests

Details of the MD technique, the Embedded Atom Method and the copper potential employed in the simulations are given elsewhere [5]. The Nosé-Hoover thermostat [6] was implemented for temperature control. Simulations have been carried out at $T = 300^{o}$ C using time increments $\Delta t = 2.5\times10^{-15}$ s.

The response of three symmetrical high-angle [001] tilt boundaries has been studied (Tab. 1). Prior to virtual testing of the samples, the cracked or un-cracked bicrystals were constructed at 0 K, the cracks being formed by removing the atoms located in a band of 0.55 nm centred in the GB along 1/3 of the specimen size in the x direction (the cut-off radius of the atom interactions was 0.55 nm). They were relaxed during 12.5 ps under no constraints at 300 K for the GB to acquire its metastable configuration, after relaxing 5 ps at 0 K and during a linear T increase to 300 K during 7 ps. Surface tension leads to some global and local (at the crack tip) geometrical distortion of the initial shape of the bicrystals. All three GB tested showed negative shear coupling, in agreement with published results that report negative coupling for $\theta \geq 35^{o}$ in [001] tilt boundaries [3].

Table 1. Crystallographic orientation and size of the investigated bicrystals.

Tilt boundary designation	**Tilt axis**	**Tilt angle θ (º)**	**Specimen size, $L_x\times L_y\times L_z$ (nm^3)**	**Shear coupling factor β**
Σ 5(310)	[001]	36.9	13.7×2.9×17.8	-1
Σ 17(530)	[001]	61.9	14.8×2.2×21.0	-0.5
Σ 41(540)	[001]	77.3	13.9×2.2×18.4	-0.222

After relaxation, two rigid zones 0.55 nm thick were established in the upper and lower layers of the samples. During the virtual shear test, the lower rigid zone remained fixed, the upper part being displaced at a constant rate of 2.12 ms^{-1} (Σ41, Σ17) or 2.85 ms^{-1} (Σ5) equivalent to a mean shear strain rate of the sample of about 10^8 s^{-1}. Periodic boundary conditions were set along the x and y axes. The applied shear force and the imposed displacement are stored during the simulations, in order to compute the shear stress – shear strain curves. Atomic positions are also periodically stored for analyzing any structural changes.

4. Results and discussion

Figure 1 shows the nominal shear stress, τ_{nom}, calculated as the sum of shear forces applied to the upper rigid layer along the x axis divided by the layer area, as a function of the nominal shear strain, γ_{nom}. The average shear stress in the ligament of the cracked specimens is 1.5 times higher than that value.

For the uncracked tilt boundaries the results reproduce the behaviour observed at similar homologous temperature by other authors [3, 4], characterized by a stick-slip phenomenon

associated to the boundary migration when certain shear stress (≈ 0.3 GPa) is overcome. The slopes of the intermittent elastic loading stages range from 27 GPa for the Σ41 and Σ17 boundaries to 37 GPa for the Σ5 one. The presence of a crack affects the mechanical response of the samples. The cracked specimens show similar stick-slip behaviour but the shear stress increases monotonically with strain till values of 1 to 1.5 GPa at about $\gamma_{nom} \approx 0.1$, where a sudden drop of the stress occurs.

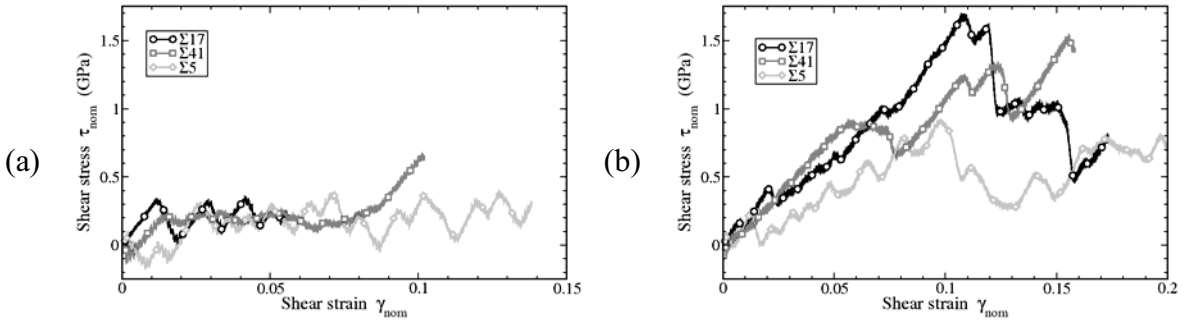

Figure 1. Nominal shear stress, τ_{nom}, vs. nominal shear strain, γ_{nom}, curves of (a) the un-cracked bicrystals and (b) the cracked bicrystals. The $\Sigma 41$ GB travels much faster than the other two because of its small coupling factor β; the stress rise of observed beyond $\gamma_{nom} \cong 0.07$ is an artifact due to the interaction of the GB, detached from the cracks, with the lower rigid slab of the sample.

This is at first sight a surprising result, the bicrystal being strengthened by the presence of intergranular cracks, although the situation is similar to the strengthening of a crystal by a dispersion of nanovoids in dislocation-mediated plasticity. The shear strain-induced structural changes explain this anomalous behaviour, fig. 2. In the cracked bicrystals, although the crack strongly amplifies the shear stress in the vicinity of the tip, the GB is pinned by the crack. In our case shear coupled migration occurs away from the crack tip, the GB bowing out (downwards in this case, $\beta < 0$). The shear stress applied on the GB surface close to the crack tip weakens because of the progressive GB misorientation; migration of the GB becomes progressively more difficult until GB depinning from the crack (small $|\beta|$, helped by partial dislocation emission from the crack tip) or grain boundary sliding (large $|\beta|$, fig. 3) occurs, locally releasing the stress and producing the observed applied stress drop.

The same effects are expected to occur if precipitates or nanograins, instead of cracks, interrupt the continuity of the tilt boundary. Simulations of the encounter of a migrating tilt boundary with strong nano-precipitates confirm this expectation [7]. Quasi-rigid precipitates have been simulated attributing to their atoms (and to the interaction between the Cu atoms and the precipitate atoms) an interatomic potential 10 times stronger than that of copper. The migrating boundary is pinned by the precipitates and its movement hindered in the same way done by the nano-cracks.

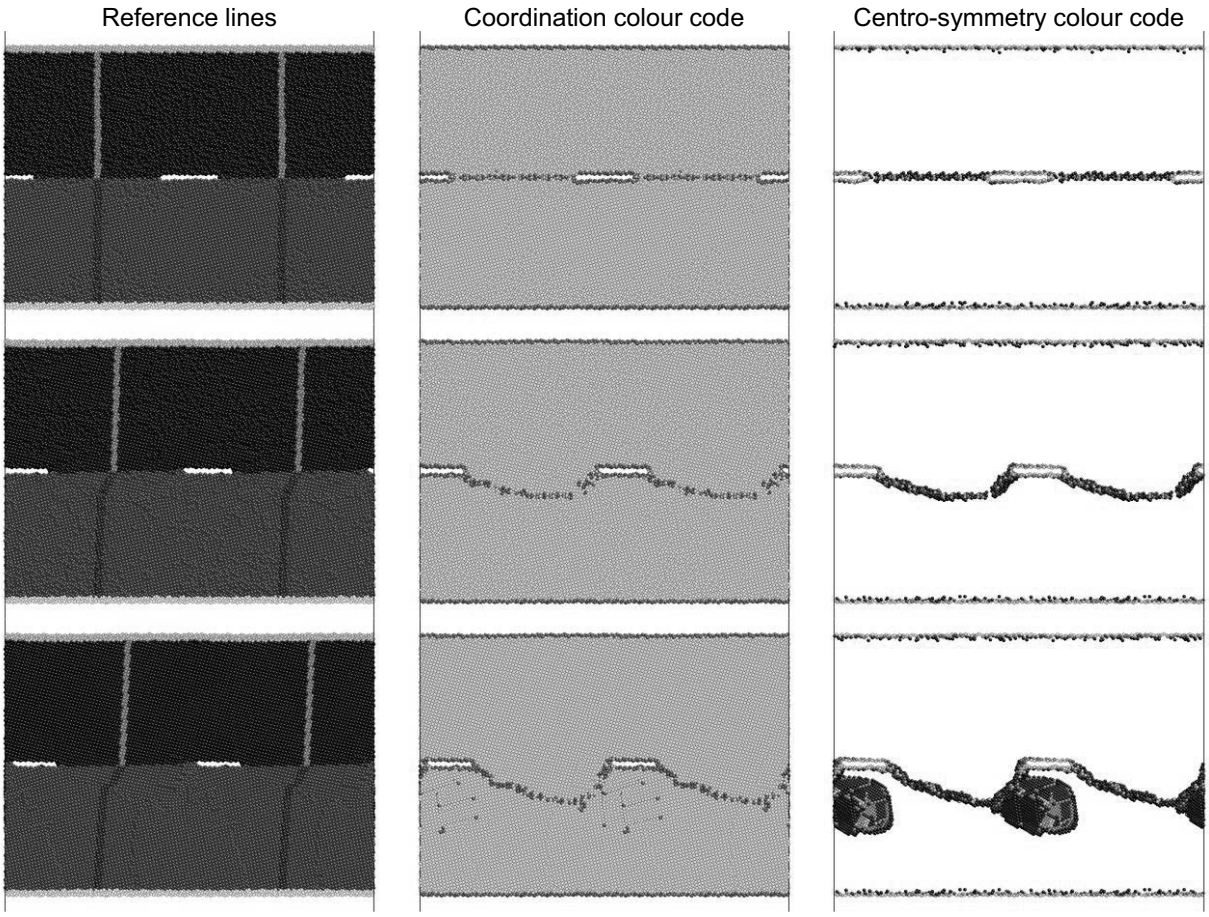

Figure 2. Copper bicrystal (Σ17 [001] tilt boundary) under imposed shear displacement parallel to the (530) boundary plane. The tilt axis is perpendicular to the figure. The bicrystal contains periodically spaced through-thickness intergranular cracks. Images are snapshots at macroscopic strain $\gamma_{nom} = 0$, $\gamma_{nom} = 0.08$ and $\gamma_{nom} = 0.12$. Depinning of the GB occurs shortly after the last strain. Coordination makes visible the GB and partial dislocations, centro-symmetry, the stacking faults.

Of course the effect of interactions of the migrating tilt boundary with cracks, precipitates, etc. will be dependent on their size and spacing. A shear stress τ applied on a flat tilt GB with a shear-coupling factor β induces on it a virtual pressure

$$P = \beta\tau \tag{1}$$

A free to move flat tilt GB will start its migration for $P_c = \beta\tau_c$. If pinned by cracks, precipitates, etc. spaced a distance L on the boundary, ignoring the deviation of the GB plane from its initial symmetrical position (i.e., ignoring the effect of the angle α in the nomenclature of ref. [4]), the crack will bow to a semicircular shape (in our 2-D approximation) of radius R,

$$R = \frac{E_S}{P - P_c} = \frac{E_S}{\beta(\tau - \tau_c)} \tag{2}$$

where E_S is the specific energy of the boundary. A limit condition for depinning would be reached if the critical condition $2R = L$ was attained provided other deformation mechanisms do not intervene before,

$$\tau_{depinning} \leq \tau_c + \frac{2E_S}{\beta L} \tag{3}$$

The shear stress-strain behaviour of the perturbed bicrystal can easily be obtained from eqs. (2) and (3) on account of the volume swept by the bowing GB. The bowing is interrupted by grain boundary sliding for the $\Sigma 5$ boundary or by escaping from the obstacles without almost any bowing for the $\Sigma 41$ boundary. Migration of a tilt boundary attached to other grain edges indeed offers a richer casuistic [7]

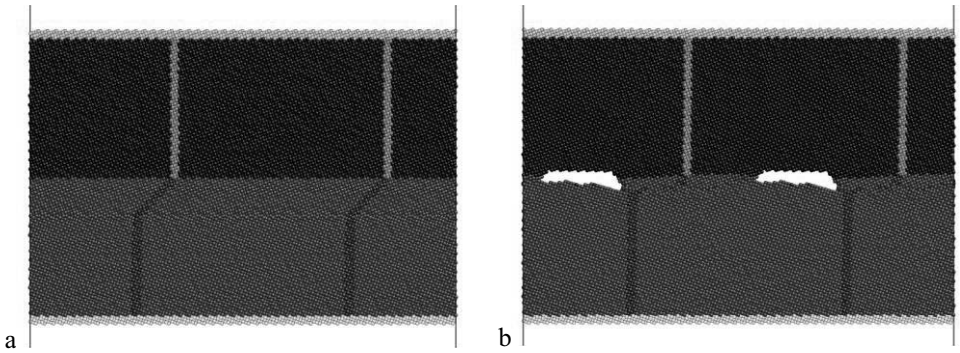

Figure 3. Copper bicrystal, $\Sigma 5$ symmetrical tilt boundary ([001] tilt axis perpendicular to the figure). Colours of the image correspond to the initial bicrystal regions and vertical strain marker. (a) Uncracked bicrystal after an imposed nominal shear strain $\gamma_{nom} = 0.14$; uniform shear coupled migration. (b) Bicrystal with intergranular cracks after an imposed nominal shear strain $\gamma_{nom} = 0.20$. Boundary trapped by nanocracks. Some downward GB migration has occurred, followed by grain boundary sliding accompanied by crack propagation.

5. Conclusions

- Shear-coupled migration of symmetrical tilt boundaries is hindered by the presence of intergranular cracks. Intergranular crack propagation in mode II is not enhanced by the shear-coupled migration.
- The tilt boundary is pinned by the crack tip and migration occurs with boundary bulging. The applied stress grows above the value needed for migration of a perfect boundary until either depinning takes place with emission of lattice dislocations from the crack tip vicinity or grain boundary sliding occurs.

- Similar effects are observed if the continuity of the GB is broken by precipitates or by other disturbances of the bi-crystallinity.

Acknowledgements

Work supported by the Department of Industry, Commerce and Tourism of the Basque Government and the Provincial Council of Gipuzkoa (projects NANOTRON, UET 1210/06 and ETORTEK inanoGUNE). A. Luque also acknowledges the Spanish Ministry of Science and Innovation and the European Social Fund (Torres Quevedo Programme).

References

[1] C.H. Li, E.H. Edwards, J. Washburn, E.R. Parker, "Stress-induced movement of crystal boundaries", Acta Metall., **1**, 223 (1953).
[2] M. Winning, G. Gottstein, L.S. Shvindlerman, "Stress induced grain boundary motion", Acta Mater., **49**, 211(2001).
[3] J.W. Cahn, Y. Mishin, A. Suzuki, "Coupling grain boundary motion to shear deformation", Acta Mater., **54**, 4953 (2006).
[4] H. Zhang, D. Du, D. Srolovitz, "Effects of boundary inclination and boundary type on shear-driven grain boundary migration", Philos. Mag., 88, 243 (2008).
[5] A. Luque, J. Aldazabal, J.M. Martínez-Esnaola, J. Gil Sevillano, "Molecular dynamics simulation of crack tip blunting in opposing directions along a symmetrical tilt grain boundary of copper bicrystal", Fatigue Fract. Engng. Mater. Struct., **30**, 1008 (2007).
[6] S. Nosé, "A unified formulation of the constant temperature molecular dynamics methods", J. Chem. Phys., **81**, 511 (1984).
[7] A. Luque, J. Aldazabal, J.M. Martínez-Esnaola, J. Gil Sevillano, in preparation.

Local Chemistry Effect on Dislocation Mobility: Sequential and Concurrent Multi-scale Approaches

Nicholas Kioussis[1], Zhengzheng Chen[1] , Nasr Ghoniem[2]

[1]California State University Northridge, Northridge
[2]University California Los Angeles
(E-mails: nick.kioussis@csun.edu, satchel1979@gmail.com, nghoniem@gmail.com)

ABSTRACT

The challenge in computational materials science and engineering is that real materials usually exhibit phenomena on one scale that require a very accurate and computationally expensive description, and phenomena on another scale for which a coarser description is satisfactory and, in fact, necessary to avoid prohibitively large computations. I will discuss two multiscale approaches that seek to link different length scales sequentially and concurrently, respectively. The first approach is based on a hybrid approach which employs an ab initio parameterization of the inter-row potential in bcc systems. The second approach involves concurrent coupling of electronic degrees of freedom via the density functional theory with classic atomic degrees of freedom via the empirical embedded-atom-method. The unified approach that combines quantum mechanics and classic atomistic simulations, allows us to study materials behavior at larger length-scales with desirable accuracy and predictive power. We will present two applications of these approaches on the effect of local chemistry on the dislocation core and mobility in bcc metals. These include: 1) Cu or Cr precipitates in αFe and 2) W solutes/precipitates in Ta.

From electrons to finite elements: quantum mechanical simulations at macroscales

Gang Lu

California State University, Northridge, CA 91330-8268, USA
(E-mail: ganglu@csun.edu)

ABSTRACT

We present a novel multiscale modeling approach that can simulate millions (or even billions) of electrons effectively with density functional theory (DFT). The method is based on a full formulation of quasicontinuum (QC) approach, including both local and nonlocal contributions. The only energetic formulation is the present method is Orbital-Free DFT (OFDFT). The local QC contribution is handled by Cauchy-Born rule with OFDFT calculations. The quantum mechanical problem of the nonlocal electrons is solved in the presence of the local electrons and nuclei. The coupling between the local/nonlocal atoms is calculated quantum mechanically via OFDFT. The method is demonstrated with a nano-indentation study of Al thin film (the entire system contains more than 60 millions atoms). The results are compared with those determined from EAM-based QC simulations.

Study of dislocation nucleation activation from surface step by atomistic calculations

P. Hirel, S. Brochard, J. Godet, L. Pizzagalli

Laboratoire PHYMAT, UMR 6630 CNRS/Université de Poitiers
Bvd M. & P. Curie, BP 30179
86962 Futuroscope Chasseneuil Cedex, FRANCE
(E-mail: sandrine.brochard@univ-poitiers.fr)

ABSTRACT

The plasticity of nanostructured materials is mainly governed by the nucleation of extended defects from surfaces or interfaces. Indeed, such nanomaterials are too small, and often free of pre-existing defects, for usual dislocation sources (such as Frank-Read sources) to operate. Defects on surfaces are thus potential sources of extended defects, which can modify in a drastic way the standard properties of nanomaterials. Dislocation nucleation from cleavage surface defects can also play a key role in the propagation of cracks, and more generally in the brittle to ductile transition in semiconductors.
We present here an analysis of the dislocation nucleation activation from a surface step in a crystal under stress, studied by atomistic calculations. Two prototypical materials are considered: a face centered cubic metal (aluminum) and a diamond-like semiconductor (silicon). Both of them can be modeled with semi-empirical interatomic potentials, but care must be taken in the case of silicon and comparison with *ab initio* calculations are used to validate the results.
The simulations in aluminum allow the determination of the saddle-point configurations and the associated activation energies. In order to obtain them for a wide range of applied stress, different methods have been used: both direct molecular dynamics simulation, and relaxation using the nudged elastic band method. The obtained results are then compared with those deduced from elasticity.
In the case of silicon, the determination of the saddle-point configuration and associated activation energy is rendered complicated by the numerous different types of dislocation that can be obtained, depending essentially on the temperature. Nevertheless, the simulations bring important information on a possible change of nucleation mechanisms with temperature, namely nucleation of perfect dislocations in the shuffle set at low temperatures and partial dislocations in the glide set at high temperatures.

We greatfully acknowledge the Agence Nationale de la Recherche for financing the project (number ANR-06-blan-0250), and the IDRIS for providing computing resources.

Smooth Versus Jerky Motion of Dislocations Across Fields of Obstacles

R.C. Picu, R. Li, Z. Xu

Department of Mechanical, Aerospace and Nuclear Engineering, Rensselaer Polytechnic Institute, Troy, NY 12180, USA (E-mail: picuc@rpi.edu)

ABSTRACT

We report on the transition from smooth ("unzipping") to jerky motion of a dislocation moving across a field of obstacles under constant applied stress [1]. The transition is controlled by the stress, by the obstacle strength and distribution. Comparison of the simulation results with experimental data indicates that the jerky motion is more relevant for plastic deformation of real crystals than unzipping. The strain rate sensitivity parameter, *m*, decreases sharply when the dislocation enters the jerky mode and becomes independent of the obstacle strength, presence of obstacles of various strengths and the way those are mixed, and of temperature. It depends exclusively on the applied stress and the distribution of obstacles in the glide plane. These observations have implications for the superposition rule of contributions to the flow stress of various sub-populations of obstacles. Finally, the scaling behavior of the jerky motion will be discussed.

[1] Z. Xu, R.C. Picu, "Thermally activated motion of dislocations in fields of obstacles: The effect of obstacle distribution," Physical Review B, **76**, 094112 (2007).

Acknowledgment: This work was supported by the NSF through grant No. CMS-0502891.

Quantitative Aspects of Microstructure Formation in Solidification

Michal Beneš[1,2], Pavel Strachota[1] and Zdeněk Čulík[1]

Affiliations: [1]Department of Mathematics, Faculty of Nuclear Sciences and Physical Engineering, Czech Technical University in Prague, Trojanova 13, 120 00 Prague, (michal.benes@fjfi.cvut.cz)**; [2]Institute of Thermomechanics, Czech Academy of Sciences, Dolejškova 5, 186 00 Prague.**

ABSTRACT

For the modelling of microstructure growth in metal solidification the modified anisotropic phase-field model is used. The numerical algorithm is based on finite-difference spatial discretization together with the higher-order time solvers. Numerical analysis of the discrete scheme justifies the use of the model in the description of the pattern formation in solidification. A series of qualitative studies demonstrating ability of the model is presented. A special attention is paid to the implementation issues such as handling of high CPU-cost parts of the code and parallelization. As a quantitative result, we present the convergence studies for the dendritic growth.

1. Model description

The aim of the contribution is to present numerical convergence of non-convex patterns for the system of phase-field equations endowed by anisotropy. The equations represent a mathematical model of solidification of pure crystallic substances at microscale. The mentioned physical phenomenon is accompanied by presence of an interface between phases which can move in space and is determined intrinsically by the state of the physical system, its boundary and initial data. Among various approaches to the mathematical treatment of the problem the diffuse-interface model yields a well controlled smooth approximation of the characteristic function of phase as a part of the solution. This fact originally observed in the form of a wave-like solution of reaction-diffusion systems (see [1]) leads to the formulation of a model of solidification with additional consequences in understanding physics of phase transitions ([2]). The model equations consist of the heat equation with nearly singular heat source coupled to a semilinear or quasilinear parabolic equation for the order parameter known as the Allen-Cahn equation or equation of phase. The equations in various setting were studied in, e.g. [3], and applied in simulation of physical phenomena ([4], [5]). The application of models based on the phase-field theory rose several quantitative questions concerning relation to the sharp-interface analogue ([5]). Problems of choice of the small parameter versus mesh size, and problems with interface stability lead to various modifications mainly in the Allen-Cahn equation (see [5]). Quantitative comparison, performed especially in case of curve motion (or hypersurface motion) driven by mean curvature (see [6]) showed a satisfactory agreement of numerical computations with the analytical solution (where it was possible) or with results

obtained by numerical solution of other models, and rised a question about how the anisotropy can be incorporated into the Allen-Cahn equation without loosing a possibility of weak formulation which requires a second-order space differential operator in the divergence form (see [7]). This has been done e.g. in [6] for the case of mean-curvature flow, and in [7] for the full phase-field model.

We follow the scope of [7], [8] where the anisotropic model has been presented in the following form:

$$\begin{aligned} \frac{\partial u}{\partial t} &= \nabla^2 u + L\chi'(p)\frac{\partial p}{\partial t}, \\ \xi\frac{\partial p}{\partial t} &= \xi\nabla\cdot T^0(\nabla p) + \frac{1}{\xi}f_0(p) + F(u)\xi\Phi^0(\nabla p), \end{aligned} \tag{1}$$

with initial conditions

$$u|_{t=0} = u_0\,, \quad p|_{t=0} = p_0,$$

and with boundary conditions of Dirichlet type

$$u|_{\partial\Omega} = 0\,, \quad p|_{\partial\Omega} = 0,$$

for simplicity. Here, $\xi > 0$ is the "small" parameter (thickness of the interface), and f_0 the derivative of double-well potential. The coupling function $F(u)$ is bounded and continuous, or even Lipschitz-continuous. The anisotropy is included using the monotone operator T^0 converting the gradient (see below). We consider $f_0(p) = ap(1-p)(p-\frac{1}{2})$ with $a > 0$. The enthalpy is given by $\mathcal{H}(u) = u - L\chi(p)$, where the coupling function χ is monotone with bounded, Lipschitz-continuous derivative: $\chi(0) = 0$, $\chi(0.5) = 0.5$, $\chi(1) = 1$, $supp(\chi') \subset \langle 0, 1\rangle$. For the sake of simplicity, Ω is rectangle. Obviously, the extension to higher dimensions, and to other boundary conditions is possible. Similarly, the forcing term $F(u)\xi\Phi^0(\nabla p)$ can be modified into $F(u)\xi\tilde{\Phi}^0(\nabla p)$ where $\tilde{\Phi}^0$ is another anisotropy - see [7].

The analysis presented in this article has been motivated by numerical studies obtained by the model both for the case of curve dynamics in the plane (see [6], and [7]), and for the case of microstructure growth in solidification (see [7]). The model works with an anisotropy rigorously implemented into the equations. Finally, the model gives reasonable results even in case of non-convex anisotropies, when the mentioned theory is not applied. Our aim is to present numerical convergence results for the onset of dendritic growth.

2. Computational results

The anisotropy is incorporated into the phase-field model according to the approach developed by the author in [7] and [6], which also is influenced by the literature cited therein. Main idea is in replacing isotropic Euclidean norm in $\mathbb{R}^2$ by another norm exhibiting the desired anisotropy, and in replacing derivatives in a corresponding way.

For this purpose, we introduce a nonnegative function $\Phi^0 : \mathbb{R}^2 \to \mathbb{R}_0^+$ which is smooth, strictly convex, $\mathcal{C}^2(\mathbb{R}^n \setminus \{\Theta\})$ and satisfies:

$$\Phi^0(t\eta) = |t|\Phi^0(\eta), \quad t \in \mathbb{R}, \eta \in \mathbb{R}^2, \tag{2}$$

$$\lambda|\eta| \leq \Phi^0(\eta) \leq \Lambda|\eta|, \tag{3}$$

where $\lambda, \Lambda > 0$. The function satisfies the following relation

$$\Phi^0(\eta) = \Phi^0_\eta(\eta) \cdot \eta, \quad \eta \in \mathbb{R}^2,$$

where the index η denotes derivative of Φ^0 (i.e., $\Phi^0_\eta = (\partial_{\eta_1}\Phi^0, \partial_{\eta_2}\Phi^0)$). We define the map $T^0 : \mathbb{R}^2 \to \mathbb{R}^2$ as

$$\begin{aligned} T^0(\eta) &:= \Phi^0(\eta)\Phi^0_\eta(\eta) \text{ for } \eta \neq 0, \\ T^0(0) &:= 0. \end{aligned}$$

The Φ^0-normal vector (the Cahn-Hoffmann vector - see [8]) and velocity of a level set

$$\Gamma(t) = \{x \in \mathbb{R}^2 \mid P(t,x) = const.\},$$

given by a suitable field P depending on time and space are

$$\mathbf{n}_{\Gamma,\Phi} = -\frac{T^0(\nabla P)}{\Phi^0(\nabla P)}, \quad v_{\Gamma,\Phi} = \frac{\partial_t P}{\Phi^0(\nabla P)}.$$

The anisotropic curvature is given by the formula

$$\kappa_{\Gamma,\Phi} = div(\mathbf{n}_{\Gamma,\Phi}).$$

In [6], the law

$$v_{\Gamma,\Phi} = -\kappa_{\Gamma,\Phi} + F,$$

has been studied by the phase-field method, in particular by the Allen-Cahn equation as in (1).

Example. In case of $\mathbb{R}^2$, we may use the polar coordinates of a vector $\eta \in \mathbb{R}^2$ denoted by ϱ and θ to define

$$\Phi^0(\eta) = \varrho f(\theta),$$

for a suitable 2π-periodic function f (we choose $f(\theta) = 1 + A\cos(m(\theta - \theta_0))$ where A is the anisotropy strength and $m \in \mathbb{N}_0$ the anisotropy type). Φ^0 therefore belongs to $\mathcal{C}^1(\mathbb{R}^2)$ and $\mathcal{C}^2(\mathbb{R}^2 \setminus \{0\})$ provided Ψ belongs to $\mathcal{C}^2(\langle 0, 2\pi\rangle_{per})$. Note that in case of m being odd, the rule (2) does not hold, but Φ^0 still can be used in the model.

We have performed a series of computations by using (1) to show that it yields a good approximation of the original problem and to investigate the solution itself. Quantitative results for the dendritic growth have been achieved (see [8]).

We set $F(u) = \beta(u-1)$, $\beta > 0$ with a suitable cut-off, r_{crit} is the diameter of the initial crystallization seed. In the computations, the spatial grid has $N_1 \times N_2$ meshes, the parameter Δt means

the period of the data output, N_T number of such outputs, N_τ total number of time steps performed by the adaptive time solver, tol tolerance for the adaptive Mersn time stepping (see also [6]) and DoF total number of degrees of freedom, $DoF = N_\tau \times (N_1 - 1) \times (N_2 - 1)$.

Example 1 shows the growing dendrite with imposed weak (convex) anisotropy. We compare the solution on four grids with the solution on a very fine mesh by measuring their difference. The problem setting is indicated in Table 1. The shape of the solution is presented in Figure 1, the level-set is projected below the graph of p.

Table 1. Table of the computational parameters for Example 1.

L	β	m	A	ξ	Ω	r_{crit}	Θ_0
1.0	200.0	4	0.06300	0.00400	(0,3)x(0,3)	0.05	1.0000

Δt	N_T	N_τ	tol	mesh	DoF	CPU
0.015	10	33226	0.001	0.00375	242423023252	708520.60

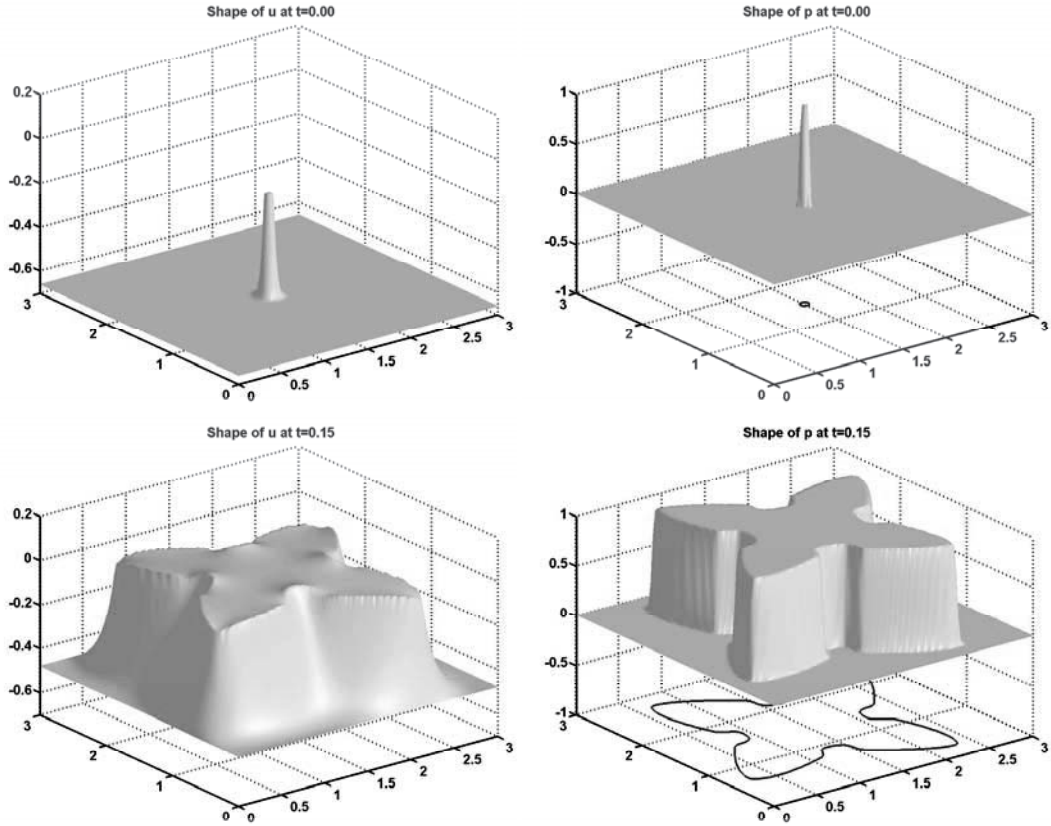

Temperature field Phase field

Figure 1. Shape of the solution for Example 1.

Example 2 shows the growing dendrite with imposed stronger (non-convex) anisotropy. We compare the solution on four grids with the solution on a very fine mesh by measuring their difference.

The problem setting is indicated in Table 2. The shape of the solution is presented in Figure 2, the level-set is projected below the graph of p.

Table 2. Table of the computational parameters for Example 2.

L	β	m	A	ξ	Ω	r_{crit}	Θ_0
1.0	200.0	4	0.09000	0.00400	(0,3)x(0,3)	0.05	-1.0000

Δt	N_T	N_τ	tol	mesh	DoF	CPU
0.015	10	36230	0.001	0.00375	46258536460	1474862.00

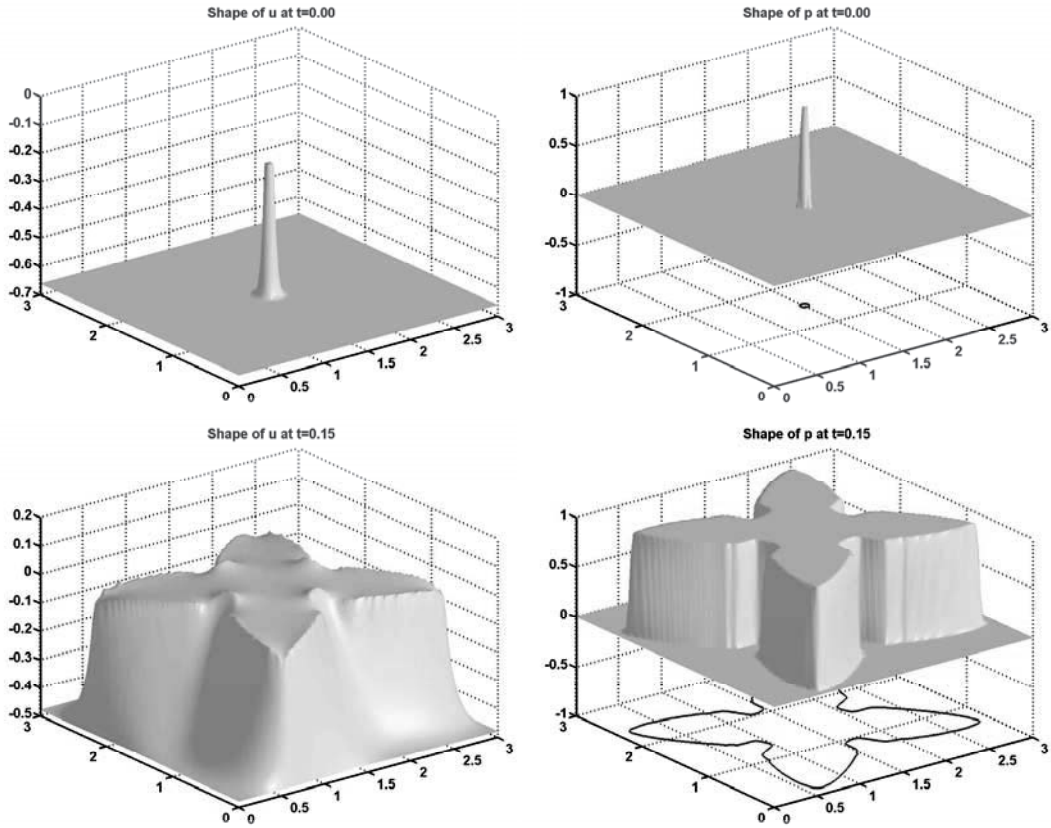

Temperature field Phase field

Figure 2. Shape of the solution for Example 2.

Acknowledgments

This work was partly supported by the research branch of ČVUT No. MSM 6840770010 *"Applied Mathematics in Technical and Physical Sciences"*.

References

[1] T. Ohta, M. Mimura, and R. Kobayashi, "Higher-dimensional localized patterns in excitable media", Physica D, **34**, 115–144 (1989).

[2] D. A. Kessler, J. Koplik, and H. Levine, "Geometrical models of interface evolution. III. Theory of dendritic growth", Phys. Rev. A, **31**, 1712–1717 (1985).

[3] G. Caginalp, "An analysis of a phase field model of a free boundary", Arch. Rational Mech. Anal., **92**, 205–245 (1986).

[4] J.A. Warren and J.S. Langer, "Prediction of dendritic spacings in a directional-solidification experiment", Phys. Rev. E, **47**, 2702–2712 (1993).

[5] M. Beneš, "Mathematical and computational aspects of solidification of pure substances", Acta Mathematica Universitatis Comenianae, **70**, No. 1, 123–152, (2001).

[6] M. Beneš, "Diffuse-interface treatment of the anisotropic mean-curvature flow", Applications of Mathematics, **48**, No. 6, 437–453 (2003).

[7] M. Beneš, "Anisotropic phase-field model with focused latent-heat release", in *FREE BOUNDARY PROBLEMS: Theory and Applications II*, edited by N. Kenmochi, GAKUTO International Series Mathematical Sciences and Applications (Chiba, Japan, 2000), Vol.14, 18–30.

[8] M. Beneš, "Computational studies of anisotropic diffuse interface model of microstructure formation in solidification", Acta Mathematica Universitatis Comenianae, **76**, No. 1, 39–50 (2007).

Material Deformation under High Rate: Atomistic, Dislocation Dynamics Simulations and Constitutive Modeling

Zhiqiang Wang[1] , Irene Beyerlein[1], Richard LeSar[2]

[1]Los Alamos National Laboratory, Los Alamos, New Mexico, USA,
[2]Iowa State University, Ames, Iowa, USA
(E-mail: zhiqiang@lanl.gov)

ABSTRACT

Plastic behavior of materials under high strain rate attracts a lot of research interests. However, compared to low rate deformation, we still have less fundamental understanding of defect and microstructure evolution at single crystal level, which is crucial for the development of models to predict material deformation. We apply molecular dynamics (MD) and dislocation dynamics (DD) simulations to understand fundamental dislocation mechanisms and to predict the collective dislocation behavior in single crystals in high rate deformation. Dislocation inertial effects and dislocation cross-slip are shown to be important, affecting dislocation generation, annihilation and interaction, hence changing the macroscopic material behavior. The method allows us to directly simulate dislocation microstructures and quantitatively analyze the mobile dislocation density, cross slip, annihilation, slip activities on single planes, etc. It is shown that there is more anisotropy and more heterogeneity in microstructure at higher strain rates. We have predicted slip band formation along the most active slip planes and the transition of the rate sensitivity of flow stress of metals, which compares well to various experimental observations. Based on microscale information obtained from DD, we present a theoretical framework for single crystal constitutive laws applicable for high rate deformation. Our results provide critical linkages between material microstructure and flow stress and work hardening

A Description of Helium Bubble Growth in ODS Alloys using Monte Carlo Simulation

Shahram Sharafat[1] , Akiyuki Takahasi[2], Koji Nagasawa[2], Nasr Ghoniem[1]

[1]University of California-Los Angeles, Los Angeles, CA 90095-1597, USA
[2]Tokyo University of Science, Yamazaki, Noda-shi, Chiba, 278-8510, Japan
(E-mail: shahrams@ucla.edu)

ABSTRACT

There is experimental evidence that Oxide Dispersion Strengthened (ODS) alloys suppress helium bubble growth when compared with non-ODS alloys. Based on these observations, the oxide particles provide stable trapping sites for helium bubbles and thus inhibit free migration of bubbles. Helium bubbles remain finely dispersed and small in size, resulting in reduction of coalescence-driven growth. Recently we have developed a Monte Carlo Simulation code, called McHEROS, which successfully modeled helium bubble evolution of low energy helium implanted tungsten. The McHEROS code is used to investigate the impact of the finely dispersed nano-sized oxides on the migration and growth of helium bubbles. The helium bubble migration, coalescence and growth in a typical ODS alloy are simulated and compared with non-ODS alloys.

On The Dynamics of Cleavage Fracture: Atomic-Dislocation Scale Mechanisms Leading to A Universal Toughness-Temperature Shape

Michael Hribernik, G. Robert Odette, Takuya Yamamoto

University of California Santa Barbara
(E-mails: Michael.Hribernik@pw.utc.com, odette@engineering.ucsb.edu, yamataku@engineering.ucsb.edu)

ABSTRACT

Fundamental understanding of the brittle to ductile transition (BDT) and multiscale models of fracture toughness have long been elusive scientific and technical grand challenges. In this work we focus on the characterizing the locally semi-brittle fracture of unalloyed cleavage oriented iron single crystals, as a foundation for building understanding and physical models of the fracture toughness of the complex structural alloys that underpin our technological civilization. We report here the first reliable measurements of initiation and arrest fracture toughness in unalloyed iron single crystals oriented for cleavage. The data show that cleavage fracture dynamics are controlled by atomic scale processes that are associated with double kink nucleation on screw dislocations. We show that the semi-brittle cleavage toughness depends on the total yield strength of a material in a way that controls the much higher macroscale fracture toughness of complex structural steels, giving rise to a universal master toughness-temperature curve shape. We propose simple dislocation confinement model to explain this behavior.

THE ROLE OF SOLUTE SEGREGATION ON THE EVOLUTION AND STRENGTH OF DISLOCATION JUNCTIONS

S. Bulent Biner[1,2], Q. Chen[1,2], X-Y Liu[1]

[1]Ames Laboratory (USDOE), [2]Iowa State University
(E-mails: sbbiner@iastate.edu, qianchen@iastate.edu, xyliu@ameslab.gov)

ABSTRACT

In this study, the role of solute segregation on the strength and the evolution behavior of dislocation junctions is studied by utilizing kinetic Monte Carlo and 3D dislocation dynamics simulations. The different solute concentrations and the character of the junctions are all included in the simulations in an effort to make a parametric investigation. The results indicate that the solutes have a profound effect on the strength of the junctions. Solute segregation can lead to both strengthening and weakening behavior depending upon the evolution of the dislocation junctions. The local solute concentration seems to be the more relevant parameter to characterizing the solute and dislocation interactions, due to the short-range stress field of solutes; and its bounds are set by the unconstrained volume dilatation.

* This work at the Ames Laboratory was supported by the Department of Energy-Basic Energy Sciences under Contract No. DE-AC0207CH11358.

Self-forces on Moving Defects with Inertia

Xanthippi Markenscoff, Luqun Ni

University of California- San Diego, La Jolla, CA 92093
(E-mail : xmarkens@ucsd.edu, luqunni@sbcglobal.net)

ABSTRACT

Self-forces on moving defects,namely dislocations and inclusions are calculated, based on near-field solutions obtained for defects moving in a generally accelerating motion. For dislocations a smearing of the core is required, which is achieved on the basis of Eshelby smearing and theory of distributions.The self-force is also calculated for a suddenly expanding inclusion with eigenstrain, and a relation between moving dislocations and phase boundaries is obtained.

Why is the Peierls stress lower in experiments than in simulations?

David Rodney[1], Laurent Proville[2]

[1]SIMAP – INP Grenoble, FRANCE, (david.rodney@grenoble-inp.fr);
[2]SRMP – CEA Saclay, FRANCE, (Laurent.proville@cea.fr).

ABSTRACT

The thermally-activated glide of dislocations in high-Peierls stress crystals is ubiquitous. Here, we study the velocity law of dislocations through a combination of Molecular Dynamics (MD) and Molecular Static (MS) simulations. In the thermally-activated regime, the dislocation velocity is expected to depend exponentially on the activation ratio between the enthalpy to form a kink pair on the dislocation line and the thermal energy. This relation is checked at the atomic scale by comparing the dislocation velocity observed in MD simulations at constant strain rate and varying temperatures with the velocity predicted by the above relation using kink-pair formation enthalpies computed from MS simulations based on the Nudged Elastic Band (NEB) method. The shape of the kink-pair formation enthalpy versus stress curve is then analyzed using a Line Tension (LT) model. Two dimensional NEB calculations on straight dislocations are used to compute the Peierls potential seen by the dislocations between Peierls valleys. In contrast with classical LT models, the Peierls potential is found to depend on the applied stress and to stiffen with the latter. Using this stress-dependent potential in a LT model, the enthalpy curve is well reproduced over the entire stress range, from zero up to the Peierls stress. These results, tested on different high-Peierls stress crystals, are discussed with respect to classical theories of thermal-activated glide.

Experimental Measurements of Nucleation Rates Near Critical Conditions of Binary Vapor-Gas Systems

M.P. Anisimov, E.G. Fominykh, and A.B. Trilis

Institute of Chemical Kinetics and Combustion, Siberian Division of the Russian Academy of Sciences. 3 Institutskaja Ave., 630090 Novosibirsk, Russia,
(E-mail: anisimovmp@mail.ru)

ABSTRACT

Nanomaterial generation begins with a new phase embryo formation within an initial metastable media. Passing of a supercritical system to subcritical state is accompanied of nucleation events. Gas supercritical solutions of substances are widely used for different nanomaterial generation even the theory of that process is not fully understood. As result a computer modeling of nucleation rates near critical conditions meets some basic problems which have no reasonable theoretical solution up to now. The nucleation experiment conditions are usually far enough from the critical states of system under investigation. High-pressure flow diffusion chamber is designed for the nucleation rate measurements in the critical conditions vicinity of binary solution on example of glycerin vapor – carbon dioxide systems. The sensitivity of the measuring system is enough to detect melting points for continuum of glycerin-carbon dioxide systems. New phase transition in critical embryos of condensate was found at nucleation near critical condition line for series of glycerin vapor – carbon dioxide binary solutions. Nucleation rate measurements were provided within of pressures from atmospheric to near critical one. Total number of the single experimental points is over two thousands. That data volume permits to resolve folds on the nucleation rate surfaces. The experimental results are extremely new. Obviously that computer modeling of nucleation within the phase transition parameters for critical embryos of condensed phase should take in to account a nonlinear behavior of the nucleation rate surfaces at the phase transition conditions in critical embryos.

1. Introduction

Nucleation is the first step in nanomaterial production. However, the theory of nucleation is not sufficiently well developed. Supercritical solutions of some substance in gas are widely used for nanomaterial generation even the theory of that process is not fully understood. Nucleation rate theory does not reliable enough for calculation of the embryo generation kinetics for the critical conditions of binary systems. Some researchers believe that there are no effects of the nature and pressure of the carrier gas on the nucleation rate [1, 2]. There have been a limited number of publications of the role of carrier gas and the effect of its pressure on vapor nucleation rates. Heist and co-workers [3-4] have reported, for example, effects of pressure and nature of the (mistakenly called) non-condensable carrier gas on nucleation rate for series of short-chain alcohols. Measurements have made in these experiments with a

thermal diffusion cloud chamber using pressures up to 0.4 MPa of H_2, He, N_2, and Ar as the carrier gas. They observed a strong effect of both pressure and gas nature. The discrepancies of measurement results made with different experimental systems [5] should be noted as the largest problem for nucleation science for present time. A theory of nucleation from any supercritical solutions does not be developed practically. The topology of nucleation rate surfaces will be illustrated for some selected cases following the idea formulated in publication [6]. There are no experimental data on nucleation rate for near critical parameters currently because the routine experiments are out of the critical conditions of a system under investigation. Both problems make the considerable constraints for computer modeling of near critical nucleation. To measure the near critical nucleation rates one needs to create a nucleation rate measuring tool for near critical pressures. Rate of measurements should be high enough to make a systematic research of near critical nucleation. A high-pressure flow diffusion chamber was designed in the frame of present study. Binary solution of glycerin vapor and carbon dioxide was used as a system under investigation of near critical nucleation kinetics.

2. Results and Discussion

Glycerin vapor – carbon dioxide system nucleation was studied using a high-pressure flow diffusion chamber (HP-FDC). The main idea of the experimental device is described in detail elsewhere, for example [7]. New high-pressure aerosol counter is the key part for HP-FDC. A set-up pressure limit is enough to reach critical conditios up to several hundred bars in the present research.

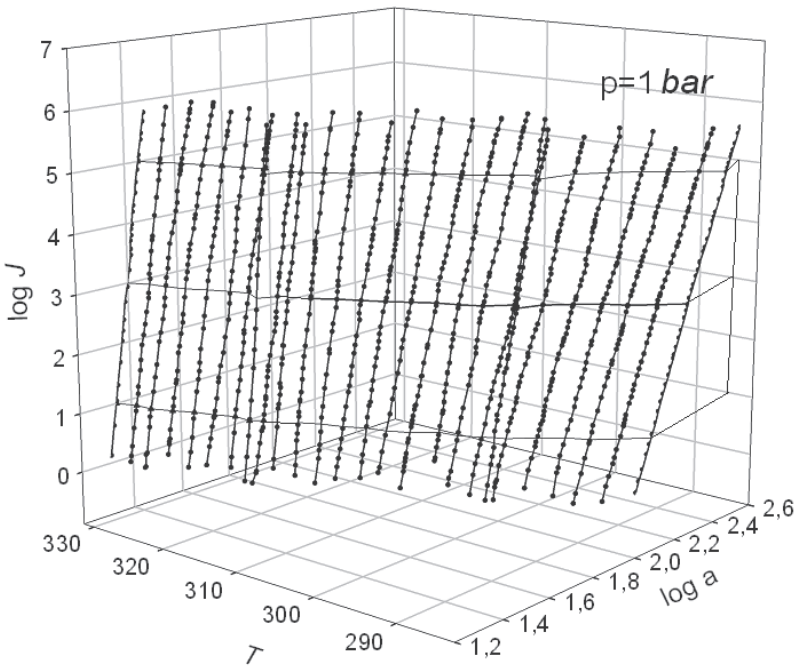

Fig. 1. Nucleation rates, *J*, for glycerin vapor – carbon dioxide system on glicerin vapor activity, *a*, and series of constant nucleation temperatures, *T* at total pressure 1 bar.

Fig. 1 shows an example of the experimental nucleation rate surface. One can easely see a surface discontinuity at nucleation temperature 295 *K*, which is associated with glycerin melting. Other discontinuity is appeared at temperature of 317 *K*. That phase transition is appeared near critical conditions of the nucleated system. Nonody has observed that phase transition before. The experimental nucleation rate levels of log*J* = 1; 3; 5 are presented in Fig. 2 to get better view of the nucleation rate surface profiles.

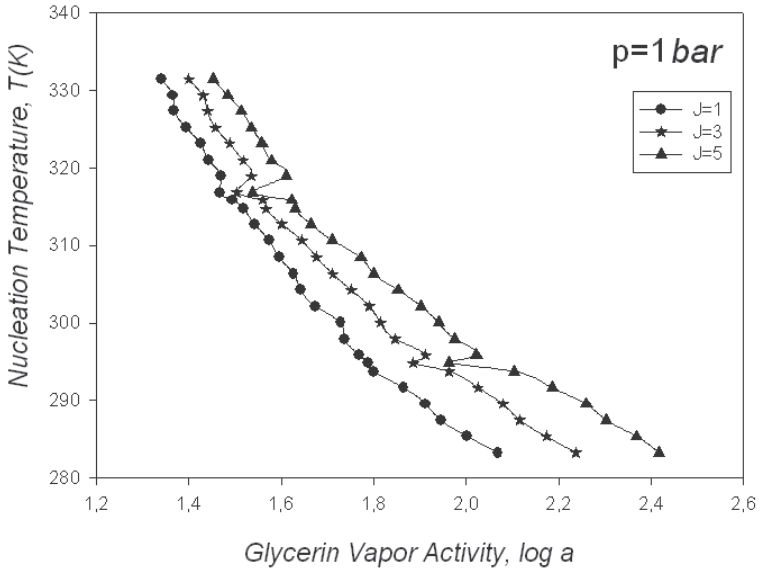

Fig. 2. The experimental surface profiles for the nucleation rate levels of log*J* = 1; 3; 5

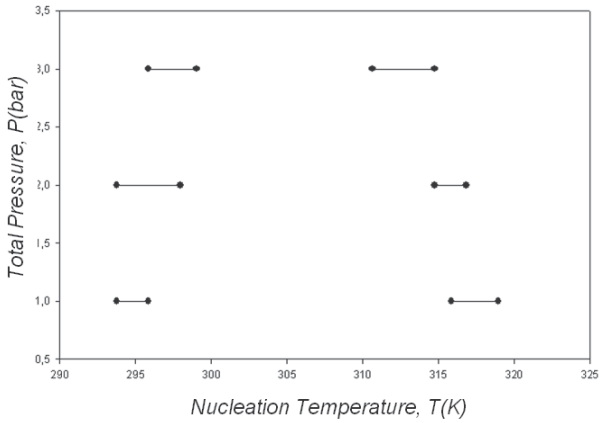

Fig. 3. Phase transitions temperature intervals drifts on a total nucleation pressure.

Fig. 3 illustrates a phase transition temperature drifts on the total pressures of vapor-gas system. One can see the opposite temperature trends for both phase transitions. That lucky case shows that pressure and temperature trends are presenting the real effects whith magnitude which is higher the unsertances appeared in the result of computer calculation inaccuracy.

3. Summary

This study is designed to clarify several important issues in nucleation using computer construction of the nucleation rate surface of systems with phase transitions in the critical embryos of condensate. It was shown experimentally for the first time that these phase transitions make folders on the experimental nucleation rate surfaces. These folders were not predicted theoretically. A computer modeling of nucleation rates near critical conditions meets some basic problems as a result. High-pressure flow diffusion chamber is designed for the nucleation rate measurements near the critical conditions of binary solution on example of glycerin vapor – carbon dioxide systems. New phase transition in critical embryos of condensate was found at nucleation near critical condition line. The total number of the single experimental points is over two thousands. That data volume permits to resolve folds on the nucleation rate surfaces. The experimental results are extremely new. Obviously that computer modeling of nucleation within the phase transition parameters for critical embryos of condensed phase should take in to account a nonlinear behavior of the nucleation rate surfaces at the phase transition conditions in critical embryos. It may be possible to simplify the experimental measurements, as a result of outrun computer optimizing the empirical data collection and using measurements for easily available experimental conditions. An obvious advantage of the computer design of nucleation rate surfaces is the ability to build any nucleation rate surface over the full interval of nucleation parameters that are unavailable for laboratory experiments.

4. Acknowledgements

Research is under support of the Russian Foundation for Basic Research through grant numbers of 07-08-13529-ofi and 07-03-00587-a.

References

[1] R. Strey, and P.E. Wagner, "Homogeneous Nucleation of 1-Pentanol in a Two-Piston Expansion Chamber for Different Carrier Gases", J. Chem. Phys. **86**,1013-1015 (1982).
[2] J. Wedekind, K. Iland, P. Wagner, and R. Strey, "Homogeneous Nucleation of 1-Alcohol Vapors", in *Nucleation and Atmospheric Aerosols 2004*. Eds. M.Kasahara&M.Kulmala. (Kyoto University Press, Kyoto, 2004) 49-52.
[3] R.H. Heist, J. Ahmed, and M. Janujua, "Effects of Background Gases on the Homogeneous Nucleation of Vapors. 1", J. Chem. Phys. **98**, 4443-4453 (1994).
[4] A. Berttelsmann, R. Stuczynski, and R.H. Heist, " Effects of Background Gases on the Homogeneous Nucleation of Vapors. 3", *J.Phys.Chem*. **100**, 9762-9773 (1996).
[5] D. Brus, A. Hyvarinen, V. Zdimal, H. Lihavainen, "Homogeneous nucleation rate measurements of 1-butanol in helium: A comparative study of a thermal and laminar flow diffusion chamber", J. Chem. Phys. **122**, 214506 (2005).
[6] M.P. Anisimov, P.K. Hopke, D.H. Rasmussen, S.D. Shandakov, V.A. Pinaev, "Relation of phase state diagrams and surfaces of new phase nucleation rates", J. Chem. Phys., **109**, 1435-1444 (1998).
[7] M.P. Anisimov and A.G. Cherevko, "Gas-flow diffusion chamber for vapor nucleation studies. Relations between nucleation rate, critical nucleus size and entropy of transition from a metastable into a stable state", J. Aerosol Sci., **16**, 97-107 (1985).

Numerical Simulation of Dislocation Dynamics – The Stress Field Evaluation Threshold

Vojtěch Minárik[1], Jan Kratochvíl[2], Michal Beneš[1]

[1]Dept. of Mathematics, Faculty of Nuclear Sciences and Physical Engineering, Czech Technical University in Prague, Trojanova 13, 120 00 Praha 2, Czech Republic, *minarikv@kmlinux.fjfi.cvut.cz*, *benes@kmlinux.fjfi.cvut.cz*, [2]Dept. of Physics, Faculty of Civil Engineering, Czech Technical University in Prague, Thákurova 7, 166 29 Praha 6, Czech Republic, *kratochvil@fsv.cvut.cz*

ABSTRACT

The aim of this contribution is to present the current state of our research in the field of numerical simulation of dislocation motion in crystalline materials. The simulation is based on recent theory treating dislocation curves and dipolar loops interacting by means of forces of elastic nature and hindered by the lattice friction. The motion and interaction of a single parametrically described dislocation curve and one or more dipolar loops placed in 3D space is considered. The complexity of the stress fields of dipolar loops as well as of the dislocation curve necessitates application of advanced numerical algorithms to successfully solve the problem. The present numerical algorithm is based on analytical formulae for stress tensor of interaction between dislocation curve and dipolar loop, analytical interaction formulae for dipolar-to-dipolar loop interaction, parametric description of the dislocation curve (i.e. 1D description of a fully 3D problem), and the flowing finite volume method. It is showing up, that despite of using analytical formulae in the numerical algorithm, it is necessary to introduce distance thresholds for evaluation of these formulae.

1. Numerical Model

In our model of dislocation dynamics, discrete solution of the dislocation curve is represented by a moving polygon given, at any time t, by plane points $\vec{X}_i, i = 0, ..., M$. The values $\vec{X}_0$ and $\vec{X}_M$ of the end points are prescribed in case of fixed ends of the curve, i.e. the values do not depend on time. The segments $\left[\vec{X}_{i-1}, \vec{X}_i\right]$ are called flowing finite volumes. The evolution equation of the dislocation curve has the form of intrinsic diffusion equation [1], [2], [4]. By integrating in dual volumes and using some other straightforward steps described in [7] we get a system of ordinary differential equations for the points of the polygon:

$$B\frac{\mathrm{d}\vec{X}_i}{\mathrm{d}t} = \varepsilon\frac{2}{d_i + d_{i+1}}\left(\frac{\vec{X}_{i+1} - \vec{X}_i}{d_{i+1}} - \frac{\vec{X}_i - \vec{X}_{i-1}}{d_i}\right) + \frac{2}{d_i + d_{i+1}}F_i\frac{\vec{X}^{\perp}_{i+1} - \vec{X}^{\perp}_{i-1}}{2}\,, \qquad (1)$$
$$i = 1, \ldots, M-1\,.$$

In the above ODE system, d_i denote distances between neighbouring nodes of the dislocation curve's discretization. Obviously, we have to complete the ODE system by including differentials $\frac{\mathrm{d}\vec{X}_0}{\mathrm{d}t}$ and $\frac{\mathrm{d}\vec{X}_M}{\mathrm{d}t}$. The exact form of these differentials depends on the particular model we use.

The governing equations for the motion of dipolar loops, that are allowed to move only along the x-axis, consist of another system of ODE:

$$\frac{\mathrm{d}x^{(j)}(t)}{\mathrm{d}t} = \frac{1}{BP} F^{(j)}_{x,total}(\vec{X}_0(t), \ldots, \vec{X}_M(t), x^{(0)}(t), \cdots, x^{(N)}(t)), \quad j = 1, \cdots, N\,, \tag{2}$$

where $x^{(j)}(t)$ denotes the x-axis position of the j-th dipolar loop, and $F^{(j)}_{x,total}$ (depending on positions of the dislocation curve and all the other dipolar loops) denotes the total forces acting on the j-th dipolar loop.

The complete discrete problem consists of (1) and (2) with accompanying initial and boundary conditions. The initial conditions simply describe positions and shapes of the dislocation curve and dipolar loops at the beginning of the computation. The boundary conditions differ depending on the particular model (both mathematical and numerical) we solve. The terms F_i in Eqn (1) and $F^{(j)}_{x,total}$ in Eqn (2) are very complex and include stress fields of dipolar loops as well as the interactions among the dipolar loops, which both are also very complex.

The interaction between two dipolar loops in stable configurations is described by analytical formulae which were presented in [5]. The analytical formula for the stress field generated by a single dipolar loop of type V_1, V_2, I_1, or I_2[1] is based on the formula presented by Kroupa in [3]. Due to some special arrangements of our model it reads:

$$\begin{aligned}
\sigma_{xy}(x,y,z) &= -\frac{\mu h b}{2\pi(1-\nu)} \left\{ \left[\frac{l-z}{\varrho_-} + \frac{l+z}{\varrho_+} \right] \left[\frac{x \pm y}{(x^2+y^2)^2} (\pm x + y - 8\frac{x^2 y}{x^2+y^2} \right] \right. \\
&\quad + \left[\frac{l-z}{{\varrho_-}^3} + \frac{l+z}{{\varrho_+}^3} \right] \left[\pm\nu + \frac{xy}{(x^2+y^2)^2} (y^2 - 3x^2 \mp 4xy) \right] \\
&\quad \left. + \left[\frac{l-z}{{\varrho_-}^5} + \frac{l+z}{{\varrho_+}^5} \right] \left[-\frac{3x^2 y(x \pm y)}{x^2+y^2} \right] \right\}, \\
\varrho_- &= \sqrt{x^2+y^2+(l-z)^2}, \quad \varrho_+ = \sqrt{x^2+y^2+(l+z)^2}\,,
\end{aligned} \tag{3}$$

where σ_{xy} stands for the xy-component of the stress field tensor, x, y, z is the relative position of the point we want to evaluate the stress in, μ is shear modulus, h and l are the half-width and half-length of a dipolar loop, b is Burgers vector, and ν is Poisson's ratio.

2. Stress Field Evaluation Threshold

Having the analytical formula for the stress field σ_{xy} and the interaction force of a pair of dipolar loops may seem to be enough for fast computation. However, this is not true. According to the

[1] Each dipolar loop is described by a letter and a subindex. Letters V and I stand for vacancy and interstitial dipolar loops, subindices 1 and 2 denote stable configurations as presented in [7], [6].

profiling results of disdyn[2] code for a test case having 10 dipolar loops and single dislocation curve consisting of 2000 segments, about 93% of CPU time was spent in computation of σ_{xy} and about 5% in computation of interactions among dipolar loops. The rest was spent in Runge-Kutta and other supplemental algorithms.

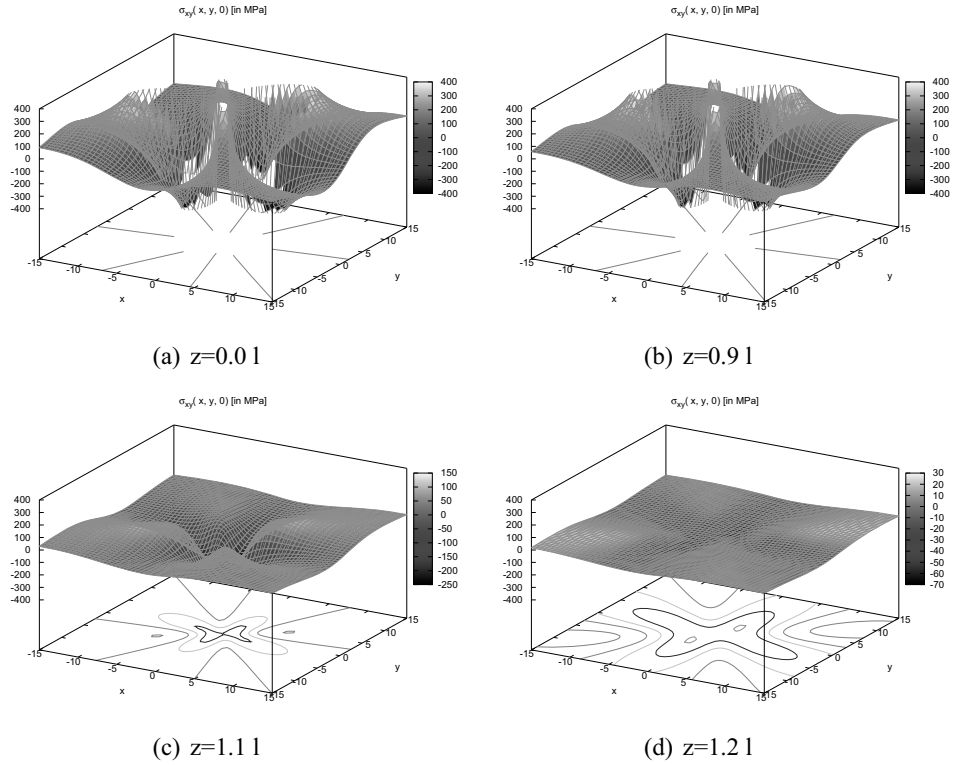

(a) z=0.0 l (b) z=0.9 l

(c) z=1.1 l (d) z=1.2 l

Figure 1. Stress field dependency on the z-axis distance from the plane of dipolar loop

With employment of a cut-off distance for σ_{xy} computation, which was set to 50 nm[3], the profiling results were much better. CPU time spent in computation of σ_{xy} fell down to about 60%, while the unchanged (i.e. still not using the threshold) interaction force among dipolar loops arised to 20%.

As was already written, the numerical scheme uses analytical formulae for evaluation of the stress field generated by a single dipolar loop and the interaction force between a pair of dipolar loops. Both of these are complex formulae which proved to be time expensive to evaluate. More precisely, they are fast to evaluate for a single set of parameters, but we need to evaluate them very often. This leads to 93% and 5% of all CPU time of the computation. Obviously, these numbers depend on the exact setting of the test simulation; they will change with a different setting of the number of segments of the dislocation curve and the number of dipolar loops. Just for imagination, in the setting we profiled, a particular time step of Runge-Kutta method consists of 159960 evaluations of the stress field and 360 evaluations of interactions between a pair of dipolar loops. Therefore, the

[2]The computational program developed to implement numerical simulation of dislocation dynamics

[3]Where such a cut-off value comes from? We will explain later in this section

first motivation for improving the speed of the algorithm came from the fact we wanted to run our model with a bigger amount of dipolar loops. The second motivation was the speed itself which was not good even for a very small amount of dipolar loops.

2.1 Optimizing the stress field evaluation

There is a simple idea how to make the stress field evaluation faster. The stress field is evaluated many times during the algorithm, and many times it evaluates to a value which is near to zero. This is because of the fact that the stress field is of a short-range type and vanishes very quickly as the distance from the generating dipolar loop is growing. Thus, putting a threshold distance into the algorithm seems to be straightforward. We simply neglect the stress generated by a dipolar loop if the point, at which we want to evaluate the stress, is far enough from the dipolar loop. However, it is not an easy task to setup the threshold value properly. We have to make it small enough to speed-up the computation, but we should not make it too small as that can lead to inaccurate simulation results. Obviously, the threshold distance depends on all the parameters of the stress field formula. The rest of this section will use following setting of physical parameters: $\mu = 80$ GPa, $\nu = 0.31, b = 0.26$ nm, $l = 30$ nm, $h = 2$ nm.

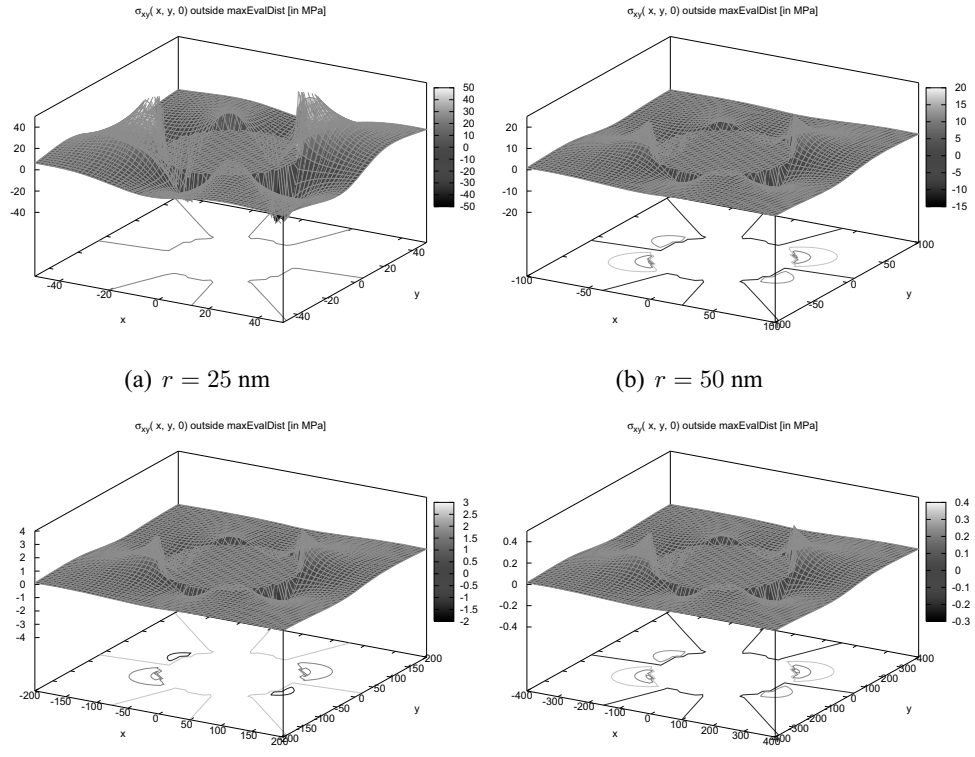

(a) $r = 25$ nm (b) $r = 50$ nm

(c) $r = 100$ nm (d) $r = 200$ nm

Figure 2. Minimum and maximum values of the stress field beyond a circular threshold

Fig 1 shows the stress field of a dipolar loop of type V_1 at several planes below and above the position of the centre of dipolar loop. It can be seen that the stress field is changing rapidly in the closest neighbourhood of the centre of the dipolar loop generating the field, whereas it vanishes fast as the distance from the loop is growing. Let us see what we will miss if we neglect the stress field beyond some threshold distance from the centre of a dipolar loop. To get some imagination, see Fig 2 showing the stress field outside the circles of various radiuses. To be more precise, each figure shows the stress field values outside the circle of a particular radius, whereas the values inside the circle are set to zero. This allows us to compare the minimal and maximal values available at different distances from the centre of the dipolar loop. Only the plane $z = 0$ is showed in Fig 2 as the absolute minimum and maximum values of stress field fall down with growing distance from this plane. Hence, the other planes are not important for the idea which follows.

Table 1. Minimal and maximal values of the stress field outside of a circle around the centre of a dipolar loop, evaluated in planes $z = 0$, $z = l$, and $z = -l$.

	$z = 0$ nm		$z = \pm l$ nm	
Threshold radius r	min σ_{xy}	max σ_{xy}	min σ_{xy}	max σ_{xy}
25 nm	-60 MPa	80 MPa	–	–
50 nm	-15 MPa	20 MPa	-15 MPa	15 MPa
100 nm	-2 MPa	3 MPa	-1.5 MPa	2.5 MPa
200 nm	-0.3 MPa	0.4 MPa	-0.2 MPa	0.4 MPa
300 nm	-0.08 MPa	0.12 MPa	-0.08 MPa	0.12 MPa

Tab 1 shows the minimal and maximal values of the stress field beyond the threshold distance (outside the circle of radius r). We can see that the stress field values beyond the 200 nm radius are at least 7 times smaller than beyond the 100 nm radius. However, the area of the interaction in the annulus between 200 nm and 300 nm radiuses is much larger than the area of the annulus between 100 nm and 200 nm radiuses. What error we make if we neglect the stress field in the annulus bounded between radiuses r_0 and r_1? In fact, we are in 3D, but the dislocation curve can glide only in a slip plane. To estimate the error, we do the following. First, we assume that the maximum stress field value in the annulus is achieved in the whole annulus. Note this is a big overestimate. Second, consider the fact that the stress field of a dipolar loop interacts with segments of dislocation curve in the simulation. The force influence would be the biggest if all the curve segments would be oriented the same (i.e. the dislocation curve would be a straight line). However, this would not fit into the annulus as the typical length of the dislocation curve is several micrometres. Therefore, assuming a circular dislocation curve inside the annulus, and ignoring the real orientations of the segments, we commit another two overestimates. The first one is that the segments are obviously not oriented the same; the second one is that though such a circular curve is rather long, it is surely not real. Nevertheless, assume a circular dislocation curve in the middle of the annulus, i.e. the length of the curve would be $2\pi(r_0 + r_1)/2$.

Using all the above information, we can evaluate upper estimates of the total force acting on a dislocation curve in the annulus (the force is generated by a dipolar loop), and, vice versa, the total

force acting on that dipolar loop (as a reaction of the dislocation curve). From Tab 2 we pick the value for a threshold distance – 50 nm.

Table 2. Neglected force estimation in several annuluses

r_0	r_1	Dislocation curve length	Force estimate
25 nm	50 nm	250 nm	5.2 nN
50 nm	100 nm	450 nm	2.5 nN
100 nm	200 nm	1000 nm	0.78 nN

Acknowledgements

The authors were partly supported by Nečas Center for Mathematical Modeling, project LC06052 of the Ministry of Education of the Czech Republic.

References

[1] S.B. Angenent and M.E. Gurtin. Multiphase thermomechanics with an interfacial structure 2. evolution of an isothermal interface. *Arch. Rat. Mech. Anal.*, 108:323–391, 1989.

[2] G. Dziuk. Convergence of a semi discrete scheme for the curve shortening flow. *Mathematical Models and Methods in Applied Sciences*, 4:589–606, 1994.

[3] F. Kroupa. Long-range elastic field of semi-infinite dislocation dipole and of dislocation jog. *phys.stat.sol.*, 9:27–32, 1965.

[4] K. Mikula and D. Ševčovič. Evolution of plane curves driven by a nonlinear function of curvature and anisotropy. *SIAM J. Appl. Math.*, 61(5):1473–1501, 2001.

[5] V. Minárik and J. Kratochvíl. Dislocation dynamics - analytical description of the interaction force between dipolar loops. *Kybernetika*, 43(6):841–854, 2007.

[6] V. Minárik, J. Kratochvíl, and K. Mikula. Numerical simulation of dislocation dynamics by means of parametric approach. In M. Beneš, J. Mikyška, and T. Oberhuber, editors, *Proceedings of the Czech Japanese Seminar in Applied Mathematics*, pages 128–138. Faculty of Nuclear Sciences and Physical Engineering, Czech Technical University in Prague, Prague, 2005, ISBN 80-01-03181-0.

[7] V. Minárik, J. Kratochvíl, K. Mikula, and M. Beneš. Numerical simulation of dislocation dynamics. In M. Feistauer, V. Dolejší, P. Knobloch, and K. Najzar, editors, *Numerical Mathematics and Advanced Applications, ENUMATH 2003 (peer reviewed proceedings)*, pages 631–641. Springer Verlag, 2004, ISBN 3-540-21460-7.

A Discrete Dislocation Approach to Grain Boundary Diffusion

Can Ayas, Erik Van der Giessen

Zernike Institute for Advanced Materials, University of Groningen, Nyenborgh 4, 9747 AG Groningen, The Netherlands; C.Ayas@rug.nl

ABSTRACT

Stresses, and their relaxation, in thin films at size scales on the order of (sub)micrometers are critical to the mechanical reliability of small devices. In this study we present a discrete dislocation dynamics framework to describe diffusional stress relaxation. We find a nearly linear relationship between the relaxed, residual tensile stress and grain size. The origin lies in the amount of diffused material and the opening profile along the grain boundary.

1. Introduction

Thin films in the (sub)micron scale are routinely used in today's electronic applications. Plasticity and related mechanical properties of these small devices originate from the inelastic deformation mechanisms at this length scale. Several papers in the literature have reported that tensile stresses in polycrystalline thin films can be relaxed by diffusion of material from the surface into the grain boundaries (see for example [1]). Gao et al. [2] investigated diffusional stress relaxation by using the continuum description of dislocations. Here we investigate the same phenomena with discrete dislocations dynamics. In the future this allows for a seamless coupling of grain boundary diffusion to the description of dislocation plasticity as in [3].

2. Model

We consider an infinitely wide thin film in plane-strain that is perfectly bonded to a very thick elastic substrate, as illustrated in figure 1. The film has thickness h and comprises columnar grains of width d. Periodic boundary conditions apply to the sides of a unit cell with width w, while the top surface is traction free.

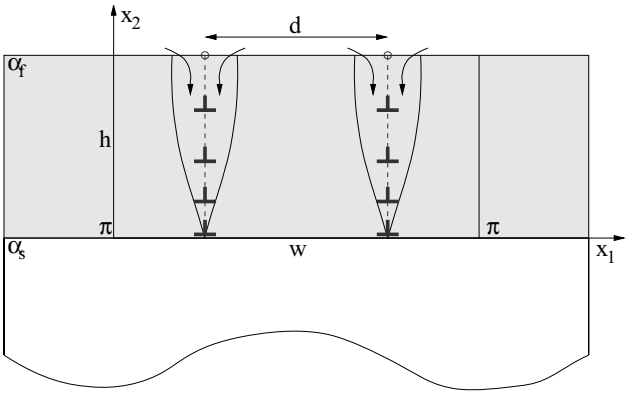

Figure 1: Schematic of the problem where π denotes the periodicity at the sides of the unit cell.

Diffusion is modeled by a 'climb-like' motion of edge dislocations that nucleate from the top of each grain boundary. The governing equations for 'climb' are obtained by using the principle of

virtual work of dislocated body in connection with the Peach-Koehler force and Fick's law. We use the dislocation fields in half-infinite space given in [4] to account for the top surface being traction-free. Due to space limitations the elaborate presentation of the formulation is left to another paper. The tensile stress distribution along the grain boundary translates into Peach-Koehler forces on all individual dislocations, which then move towards the film/substrate interface with a mobility determined by the grain boundary diffusion coefficient. A possible origin of the initial tensile stress, is the cooling the film/substrate system which possesses a thermal expansion mismatch which we consider here. Assuming isotropic elasticity for all grains, this induces an initially homogeneous stress of $\sigma_0 = E^* \Delta T(\alpha_s - \alpha_f)$, where E^* is the plain strain elastic modulus of the film material, ΔT is the change in temperature, and α_f and α_s are the thermal expansion coefficients of film and substrate respectively. Diffusion halts at the grain boundary root, which is implemented by taking the film/substrate interface to be impenetrable to dislocation motion (as in [3]). To avoid having to model diffusion along the top surface we take surface diffusion to be much faster than grain boundary diffusion.

3. Results & Discussion

To demonstrate the effect of microstructure on stress relaxation behavior, we consider films of the same thickness ($h = 0.5\mu$m) but with different grain sizes. Figure 2 presents the film average stress $\langle \sigma_{11} \rangle^f$ after steady state has been reached for diffusion, as a function of grain size. In this state of completed diffusion, stacks of dislocations are lined-up with the grain boundaries. Although the dislocations have attained their equilibrium positions, a non-zero film average tensile stress persists. This is due to both the attractive force on the dislocations by the free surface, and the nearly exponential decay of compressive stress fields of dislocation walls in the x_1 direction. As a consequence, regions of high stress exist in between grain boundaries, as demonstrated in figure 3.

From figures 2 and 3 it can be seen that grain size plays a crucial role on grain boundary

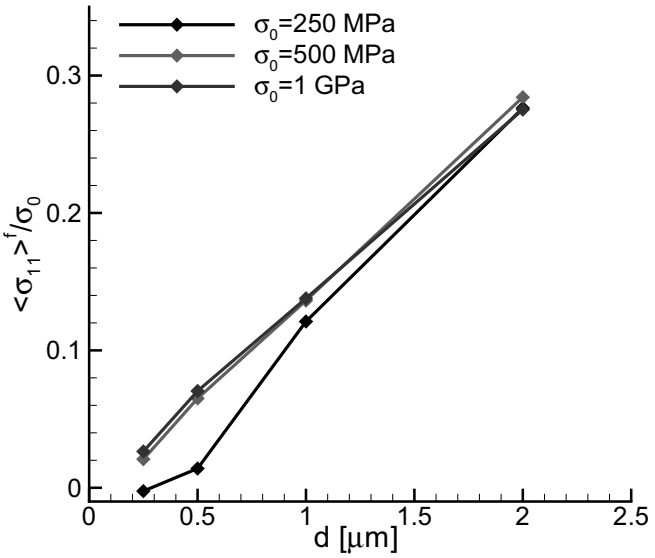

Figure 2: Steady state values of film average stress, normalized with the initial stress σ_0, for films with different grain sizes.

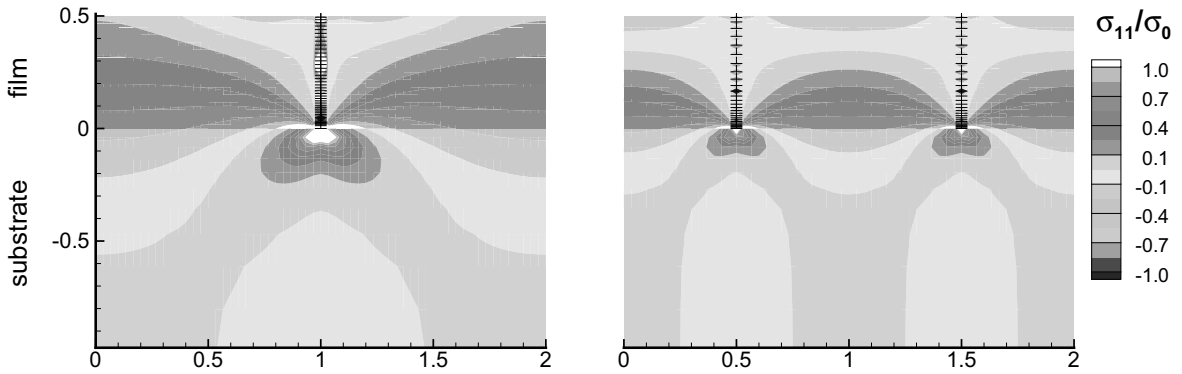

Figure 3: Residual stress distributions after relaxation from $\sigma_0 = 500$MPa for two different grain sizes.

diffusion. For large grains, i.e. widely spaced grain boundaries, diffusion seems to relax the stresses only locally and the overall residual stress level is still several percents of the initial stress. As the grains become finer, the residual stress decreases almost linearly with d.

Associated with the size-dependent residual stress is the effect of grain size on the distribution of dislocations, i.e. the distribution of diffused material, see figure 4. The amount of diffused material per grain decreases with decreasing d and therefore lower back stresses along the evolving grain boundary dislocation structure arises. When d is large the back stresses due to the stronger pile ups prohibits segregation of dislocations near the grain boundary root but instead makes them spread along the whole boundary. As the grain size is refined it is also observed that the kinetics of diffusion speeds up owing to simultaneous diffusion through many boundaries. Increasing σ_0 which is the initial driving force for diffusion has the same effect on the kinetics.

Not only the total amount of diffused material but also its distribution along the grain boundary is seen to be affected by grain size. In order to quantify the grain boundary shape we introduce the following measure

$$\xi = \frac{1}{\delta(h)h}\int_0^h \delta(x_2)dx_2 \tag{1}$$

where $\delta(x_2)$ is the grain boundary opening at x_2: the larger ξ, i.e. the closer to 1, the more uniform is the grain boundary opening. As seen in figure 4, the grain boundary opening profile for large grains is more V-shaped, with ξ being significantly smaller than 1. When grains become columnar the opening tends to become more U-shaped (ξ increases), tending towards the opening profile of a single dislocation at the grain boundary root. This trend is also observed for the other σ_0 values. On the other hand, for a fixed grain size, the grain boundary opening becomes slightly more U–shaped with decreasing σ_0. The explanation for this is, that less diffusion is necessary for relaxation from a lower σ_0, so that the back stress from the dislocation pile up at the root of the grain boundaries is smaller and dislocations manage to propagate closer to the interface.

Gao et al. [2] reported that grain boundary opening shape is nearly independent of the grain size and can be approximated by the crack face displacement of a mode I crack. Indeed, the profile for $d = 1\mu$m in figure 4 agrees well with such a displacement field, which is superimposed onto discrete solution. However in this study we have observed that the grain boundary shape is quite sensitive to the grain size and also depends on the initial stress. This dependence originates from

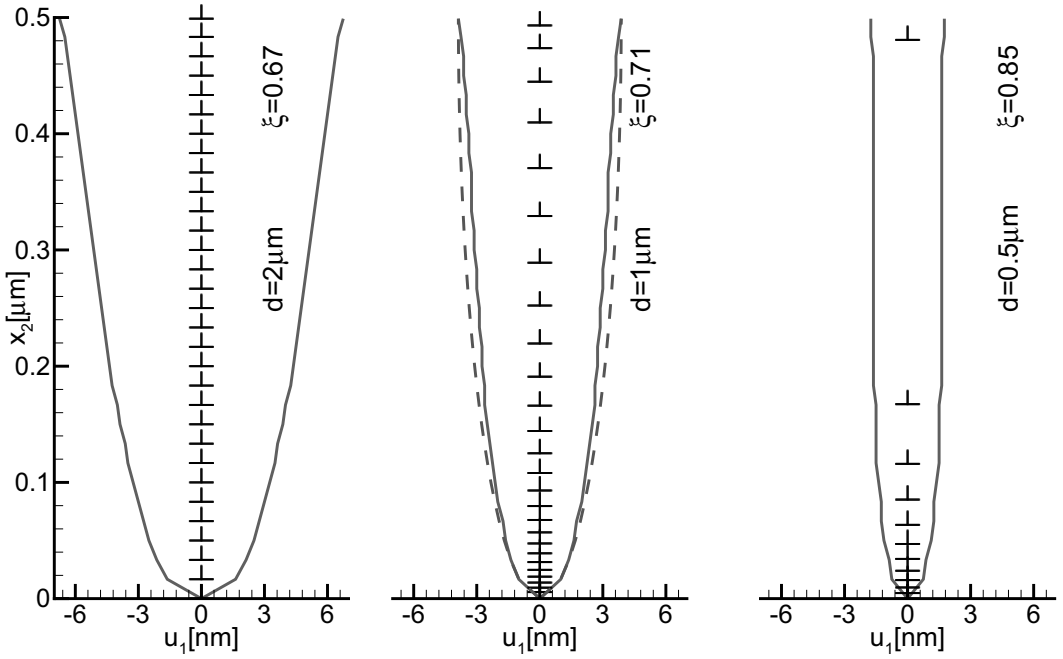

Figure 4: Grain boundary shapes $\delta(x_2)$ together with grain boundary dislocations at steady state for films with grain sizes varying from $d = 2\mu$m to $d = 0.5\mu$m.

the discritization of flux by using a finite and constant value for b.

For the computations presented above, we have omitted the image stress contribution to the Peach-Koehler force arising from the dislocation itself. The implementation of this contribution introduces a critical stress for dislocation nucleation, which will be the next step in this model.

Acknowledgments

Financial support by the European Commission NANOMESO project no. 16710 is gratefully acknowledged.

References

[1] D. Weiss, H. Gao, E. Artz, Constrained diffusional creep in UHV-produced copper thin films, Acta Mater., **49**, 2395 (2001)

[2] H. Gao, L. Zhang, W. D. Nix, C. V. Thompson, E. Artz, Crack-like grain-boundary diffusion wedges in thin metal films, Acta Mater., **47**, 2865 (1999)

[3] C. Ayas, E. Van der Giessen, Dislocation dynamics simulations of the relaxation of intrinsic stress in thin films, Phil. Mag. (in press), DOI: 10.1080/14786430801986647.

[4] L. B. Freund, The mechanics of dislocations in strained-layer semiconductor materials, Advances in Applied Mechanics, **30**, 1 (1993).

Atomistic Calculations Of The Formation, Stability And Mobility Of A Non Dissociated 60° Dislocation In Silicon

Julien Godet[1], Sandrine Brochard[1], Tristan Albaret[2], Laurent Pizzagalli[1]

[1]PHYMAT, University of Poitiers CNRS, BP 30179, F-86962 Futuroscope Chasseneuil Cedex, France
[2]LPMCN, University of Lyon CNRS, F-69622 Villeurbanne Cedex, France
(E-mail: sandrine.brochard@univ-poitiers.fr)

ABSTRACT

There have been very few investigations related to the non-dissociated 60° dislocation in zinc-blende materials. The main reason is that it dissociates in two Shockley partials at high temperature, in the usual experimental conditions, in the ductile domain. Also, at low temperatures, although non-dissociated dislocations have been shown to exist, most studies have focussed on the screw dislocation, since it is expected to govern the plasticity. Nevertheless, recent theoretical investigations have shown that a large stress applied to a surface step could lead to the formation and propagation of a perfect 60° dislocation in silicon, at low temperature, growing the need for a better characterization of this defect.
We present here the results of atomistic simulations, performed with first principles, tight-binding and interatomic potential calculations, of the formation, stability and mobility of a non-dissociated 60° dislocation in silicon. First, it is shown that while a glide core is much more stable than a shuffle core, only the latter can move under the effect of an applied stress. The mechanism underlying dislocation mobility is analyzed. Regarding nucleation, we show that a shuffle 60° dislocation can form at a surface step, but also in the vicinity of a crack front, suggesting that this defect could have a major influence on the mechanical behavior of covalent materials.

Coupling Molecular Dynamics and Kinetic Monte-carlo Simulations to Model the Carbon Snoek Peak in Ferrite

Michel Perez[1], Sébastien Garruchet[2]

[1]Université de Lyon - MATEIS - INSA ; [2]Université de Bourgogne, France
(E-mail : Michel.Perez@insa-lyon.fr, sebastien.garruchet@u-bourgogne.fr)

ABSTRACT

Molecular statics, molecular dynamics and kinetic Monte-Carlo are used to model the carbon Snoek peak in ferrite. Using an inter-atomic EAM potential for the Fe–C system, saddle point energies for the diffusion of carbon have been evaluated under uniaxial stress by molecular statics. These energies have been reintroduced in a kinetic Monte-Carlo scheme to predict the repartition of carbon atoms in different octahedral sites. This repartition leads to an anelastic deformation calculated by molecular dynamics, which causes internal friction (the Snoek peak) for cyclic stress. This approach leads to quantitative predictions of the internal friction, which are in good agreement with experiments. This work is an example of how coupling two different and complementary approaches, namely Monte-Carlo and Molecular Dynamics, can provide a compelling framework to model the kinetics of point defects (C atoms in Fe) organization within a external cyclic stress field. It has been published recently in Computational Materials Science (doi:10.1016/j.commatsci.2007.11.004).

A New Model of Plasticity Development in Solids

Lev B. Zuev and Svetlana A. Barannikova

Institute of Strength Physics and Materials Science, SB RAS
634021, Tomsk, Russia. (E-mail: lbz@ispms.tsc.ru)

ABSTRACT

In the framework of the proposed two-component plastic deformation model, a change-over in the patterns of autowave processes of plastic flow evolution and a transition to fracture is attributed to the specific features of the interaction between information and dynamic subsystems.

1. Introduction

Abundant experimental evidence [1, 2] shows that the plastic deformation would exhibit a localization behavior all the way from yield point to failure, which manifests itself in the emergence of localization patterns. This is due to the deforming medium undergoing self-organization, with each pattern type observed for a given stage corresponding to the acting work hardening law (Fig. 1). Such data has been obtained with the help of speckle-photography technique described in detail elsewhere [3].

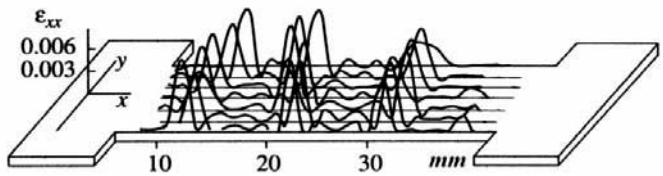

Figure 1. A typical example of plastic flow localization pattern (autowave)

2. The structure of localized plastic flow nucleus

Of particular interest is the data on the local strain distribution in the localization zone at. An analysis of the plastic distortion tensor components for γ-Fe single crystals oriented in the $[\bar{3}77]$ shows that with growing total deformation level, the nuclei of local elongation ε_{xx}, local shear ε_{xy} and local rotation ω_z will evolve in a self-concerted manner within the above zone. Thus at ε_{tot} = 0.035 the maxima $\varepsilon_{xx}(x,y)$, $\varepsilon_{xy}(x,y)$, and $\omega_z(x,y)$ have one and the same co-ordinate x (Fig. 2 a); at ε_{tot}= 0.042 the maxima ε_{xy} and ω_z will shift to the right relative to ε_{xx}. As soon as ε_{tot} becomes equal to 0.049, the component ε_{xx} will reach its maximal value, while $\varepsilon_{xy}=0$ and $\omega_z=0$ become equal to zero (Fig. 2 b), i.e. the shears and rotations of opposite signs will become accommodated. As soon as the components $\varepsilon_{xx}(x,y)$, $\varepsilon_{xy}(x,y)$ and $\omega_z(x,y)$ in the localization zone become rearranged, the solitary localized plastic flow nucleus will start moving. A similar changeover in the behavior of distortion

tensor components occurs several times, while the deformation zone is traveling from the movable towards the immovable grip of the machine.

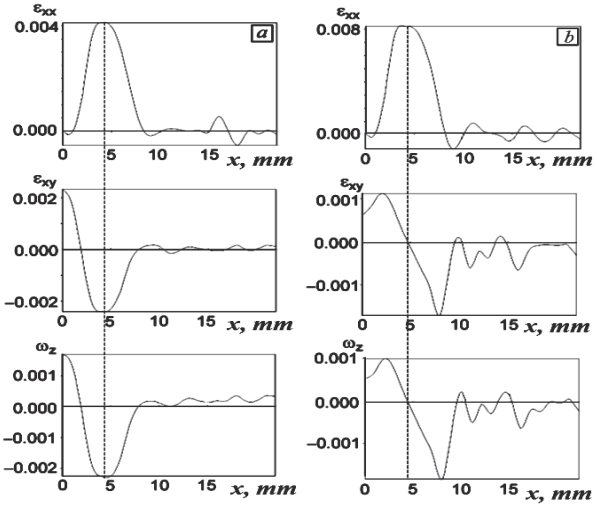

Figure 2. The evolution of local elongation for γ-Fe single crystal $[\bar{3}77]$

3. Two-component plastic deformation model

To address the processes responsible for the distinctive features of localization pictures, a two-component model is proposed. The basic assumption of the model is that the deforming medium separates spontaneously into information and dynamic subsystems [4]. The information subsystem comprises a set of acoustic emission pulses generated in the course of flow; the dynamic subsystem incorporates elementary plastic deformation and is responsible for the form changing proper. A distinguishing feature of the model is the implication that the subsystems would interact with one another in the following way. In the course of deformation, generation of acoustic pulses would occur to initiate new dislocation shears, which, in turn, are accompanied by acoustic emission. By the tensile loading of the test specimen, the process of plastic flow occurs by stages with a change-over in the acting deformation hardening laws.

4. Discussion of results

The multistage plastic flow curve $\sigma(\varepsilon)$ (here σ is the stress and ε is the strain) can be conveniently given by

$$\sigma(\varepsilon) = \sigma_0 + \theta\varepsilon^n, \tag{1}$$

where $\sigma_0 = const \approx \sigma_{0.2}$ and $\theta = d\sigma/d\varepsilon$ is the work hardening coefficient. Depending on the work hardening law $\theta(\varepsilon)$ acting at a given stage, the parabola exponent n from (1) takes on different values for the following stages: yield plateau $(\sigma = const)$, n = 0; linear work hardening $(\sigma \sim \varepsilon)$, n = 1; parabolic (Taylor's) work hardening $(\sigma \sim \varepsilon^{1/2})$, n = ½; pre-failure $(\sigma \sim \varepsilon^n)$, n < ½. Using the exponent n, it is easy to distinguish stages on the plastic flow curve. The total deformation, $\varepsilon \sim t$; therefore, the evolution and distinctive features of plastic flow localization patterns can be conveniently described by use of dependencies $X(t)$, where X is the position of localized deformation nucleus (zone) and t is the loading time. Such dependences obtained for stages (ii), (iii) and (iv) is shown in Fig. 3 for Fe-3wt.% Si alloy.

At the yield plateau stage the deforming specimen ($n = 0$) comprises two coexisting material volumes, i.e. an elastically deformed and a plastically deformed one, which are separated by a moving Lüder's band front. Acoustic emission investigation was performed at the yield plateau for the deforming specimens of low carbon steel. It is found that an area ~10 mm in width, which generates acoustic pulses, coincides with a band that can be observed with the unaided eye. Thus, the deformation-related events that occur at the yield plateau are generally considered in the context of conventional Lüder's band models. These are expected to localize on the interface between the elastically stressed and the plastically deformed specimen volume. Thus in the elastically stressed specimen volume there are no stress concentrators capable of generating shears; hence in the absence of acoustic emission no plastic deformation can be initiated in this zone.

At the stage of linear work hardening in the deforming specimen there forms a set of equidistant localized deformation nuclei (phase autowave), which are traveling in a concerted manner at a constant rate V_{aw} [1, 2] given by

$$V_{aw} \approx \frac{B}{\eta} \cdot \frac{V_S}{\theta}, \tag{2}$$

where V_S is the propagation rate of ultrasound waves, B is the coefficient of viscous drag of dislocations and η is the dislocation viscosity of the crystal, which is determined from damping experiments. The quantity B controls the motion of dislocations over the local barriers, with the moving dislocations not interacting with the defects; this is the function of density of the phonon and electron gases in the crystal. The investigations of ultrasound rate were carried on, for example, for polycrystalline Al. It was found that for the stage of linear work hardening, $V_S = const$ and $\eta = const$; hence from (2) follows that $V_{aw} \approx const$.

At the stage of Taylor's work hardening ($n = ½$) cross-slip processes bring about avalanche-like growth of dislocation density within the localized flow nuclei with a resultant increase in the dislocation viscosity η so that, in accordance with (2), the nuclei's velocity would tend to zero, i.e. $V_{aw} \approx 0$. The registration of acoustic pulses in these experiments was carried on simultaneously with the plotting of plastic flow curve $\sigma(\varepsilon)$ for the deforming specimens. Matching of the two sets of experimental data has revealed the occurrence in the material volume of equidistant stationary zones that are distinguished by high density of ultrasound pulse emission.

At the stage preceding specimen fracture (pre-failure stage), each localized deformation nucleus would resume motion at a constant rate of its own, which depends on the distance between the place of its nucleation and the zone of future failure: the farther away the place of nucleation, the higher the nucleus' rate. At the pre-failure stage the straight lines $X(t)$ (nuclei's position *vs* time) would form bundles, with the co-ordinates X^* and t^* of bundle centers indicating, respectively, the place and the instant of time at which specimen failure is bound to occur. Thus, from the onset of pre-failure stage, the localization nuclei would move in a concerted manner, which enables their simultaneous "arrival" at the same place. This implies that the location of failure and the specimen life are determined by the processes involved in the earlier stages of plastic flow. Finally, only one flow nucleus would survive: it is a forerunner of failure whose place of initiation pinpoints the location of future macroscopic necking and viscous failure. The motion of localized plasticity nuclei is attributed to a decrease in the coefficient of work hardening from (2), which is observed at the final plastic flow stage, and to concurrent growth of ultrasound rate V_S, which was determined experimentally in [1].

In the framework of the model being developed, the emergence of new localized plasticity patterns at the pre-failure stage might correspond with the condition of interference of the acoustic emission pulses of active deformation nuclei already in existence. At the end of pre-fracture stage the system of localized plastic flow nuclei (Fig. 3) would collapse [4] to bring

the plastic deformation to an end and to cause viscous crack initiation. A transition from stable plastic flow (linear and Taylor's stages of work hardening) to the pre-failure stage followed by macroscopic necking and viscous failure might be regarded as "collapse" of the plastic flow process or else as merging of localization nuclei in the location of future failure due to a change in the deforming medium properties in the course of plastic flow. Such transition can be considered as "loss" of deformation stability.

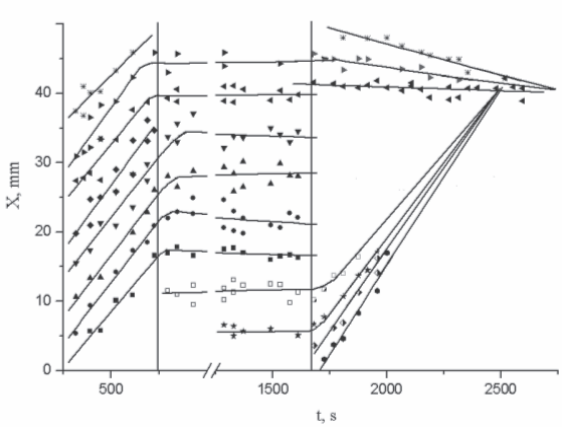

Figure 3. Diagram $X(t)$ obtained for a BCC alloy specimen; alloy Fe-3 wt.% Si

Conclusions

Thus, the evolution of plastic flow localization patterns is found to exhibit certain regularities. On the base of data obtained a new method of monitoring is being developed, which allows one to predict the instant of time and the location of failure in loaded materials and articles made from the same materials. It has been established that this method has sufficient accuracy. Special check-up experiments were conducted, which showed a good fit between the experimental critical points, which are suggestive of imminent failure, and the analogous critical points at the intersection of extrapolated $X(t)$ plots.

Acknowledgements

This work was partly supported by the grant given to S.A. Barannikova by the President of the Russian Federation (No. MD-278.2008.8).

References

[1] L.B. Zuev, "Wave phenomena in low-rate plastic flow in solids", Annalen der Physik, **10,** 956 (2001).
[2] L.B. Zuev, "On the waves of plastic flow localization in pure metals and alloys", Annalen der Physik, **16,** 286 (2007).
[3] L.B. Zuev, S.N. Polyakov, V.V. Gorbatenko, "Instrumentation for speckle interferometry and techniques for investigating deformation and fracture", *Proceedings of SPIE*, **4900** (Part. 2), 1197 (2002).
[4] B.B. Kadomtsev, *Dynamics and Information*, Moscow, UFN Editorial Board, 1997.

2D-Stress analysis during crack-crazing patterns interactions

Seddiki, H and Chabaat, M

Built Environment Research Laboratory, Civil Engineering Faculty, University of Sciences and Technology Houari Boumediene, B.P. 32 El Alia, Bab Ezzouar, Alger 16111, Algeria
(E-mail: mchabaat2002@yahoo.com, hseddiki2007@yahoo.fr)

ABSTRACT

In this study, interactions between a macrocrack and a surrounding layer of crazing patterns are considered. Analysis of the stress field distribution induced during these interactions is based on the resolution of some differential equations along with appropriate boundary conditions. It is proven throughout this study that the crazes growth occurs along directions parallel to the minor principal stress axis and constitutes an important toughening mechanism. Thus, the mode I Stress Intensity Factor (SIF) is employed to quantify the effects of this damage on the main crack and that crazes closer to the main crack dominate the resulting interaction effect and reflect an anti-shielding of the damage while a reduction constitutes a material toughness.

1. Introduction

There is sufficient experimental evidence that in most cases, a propagating crack is surrounded by a damage zone which often precedes the crack itself. This zone usually consists of slip lines or shear bands in metals, microcracks in ceramics and polymers, and crazes in amorphous polymers [1]. Thus, the existence of these defects affects progressively the propagation of cracks already present in some materials. Thus, analysis of the distribution of surface crazes in the vicinity of a stationary edge crack in a polystyrene (PS) sheet in tension has shown that the craze growth occurs along directions parallel to the minor principal stress axis. This behaviour has been thoroughly documented and extensively discussed in a number of papers [2-4].

2. Problem formulation

Considering a two dimensional, linear elastic solid containing an edge crack of length L and a surrounding layer of crazing patterns as shown in Fig. 1. For a semi-infinite body under uniform traction, distant from and normal to the crack and considering Cartesian coordinates with the origin at the crack tip, the elastic stress field is given as follows [5].

$$\begin{Bmatrix} \sigma_{xx} \\ \sigma_{yy} \\ \sigma_{xy} \end{Bmatrix} = K_I/(2\pi r)^{1/2} \begin{Bmatrix} \varphi_{xx}(\theta) \\ \varphi_{yy}(\theta) \\ \varphi_{xy}(\theta) \end{Bmatrix} + \sigma_\infty \qquad (1)$$

The first term of Eqn. (1) expresses an asymptotic stress field near the singularity. The additional terms are homogeneous material stresses.

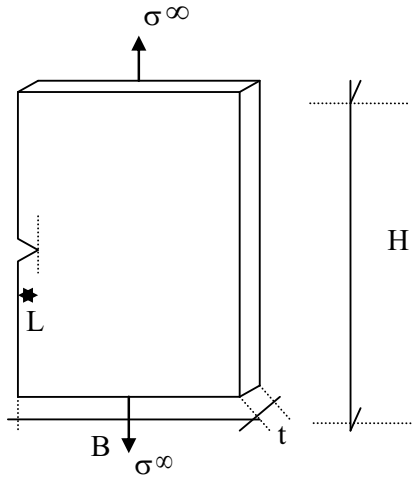

Figure 1: Geometry of the problem for general formulation.

3. Principal stress trajectories

According to Mohr's theory, principal stresses are orthogonal and act on a plane where shear stresses vanish. Then, by using geometrical transformations, differential equations related to the principal stress trajectories along with prescribed boundary conditions are obtained as;

$$\Sigma_{1,2} = y'_{1,2} = -1/\tan 2\beta \pm 1/\sin 2\beta, \quad \theta = \theta_0 = [-\pi, \pi] \text{ and } [\, r_{1,2} = r_{01,02}\,] \qquad (2)$$

where, $\beta = 1/2 \arctan(((-\sin\theta \cos(3/2\,\theta))/(\sin\theta \sin(3/2\,\theta) + (1/A)\sqrt{r}))$

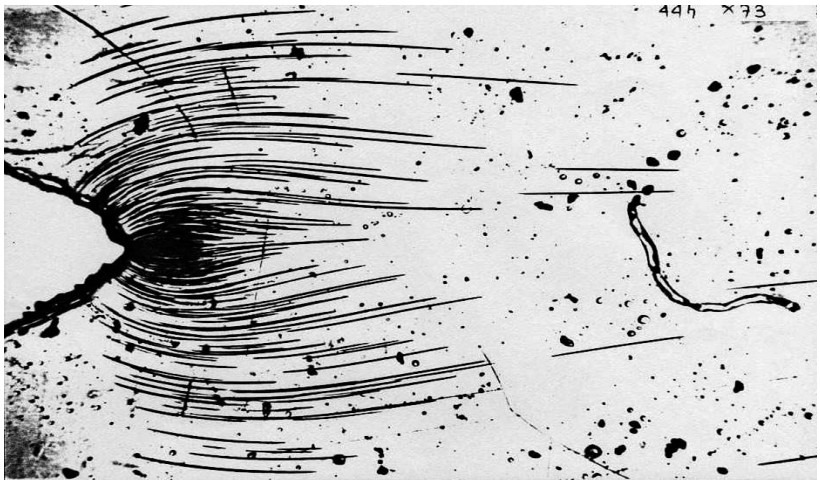

Figure 2: Microscopic observations of crazes in (PS) under tension (taken from [4]).

Using Eqn. (2), a computer program was set up to plot various functions of the principal stresses. Maximum and minimum principal stresses trajectories are plot in Figs. 3 b, c and 4 b, c as continuous curves. Each point is labelled according to its magnitude, and the field for θ is surveyed close to the crack tip, meaning, for values of $r \in V(0)$. It is clear from Fig. 3 a and 4 a that trajectories for major and minor isostresses at given distances from the crack tip are very nearly perpendicular to each others.

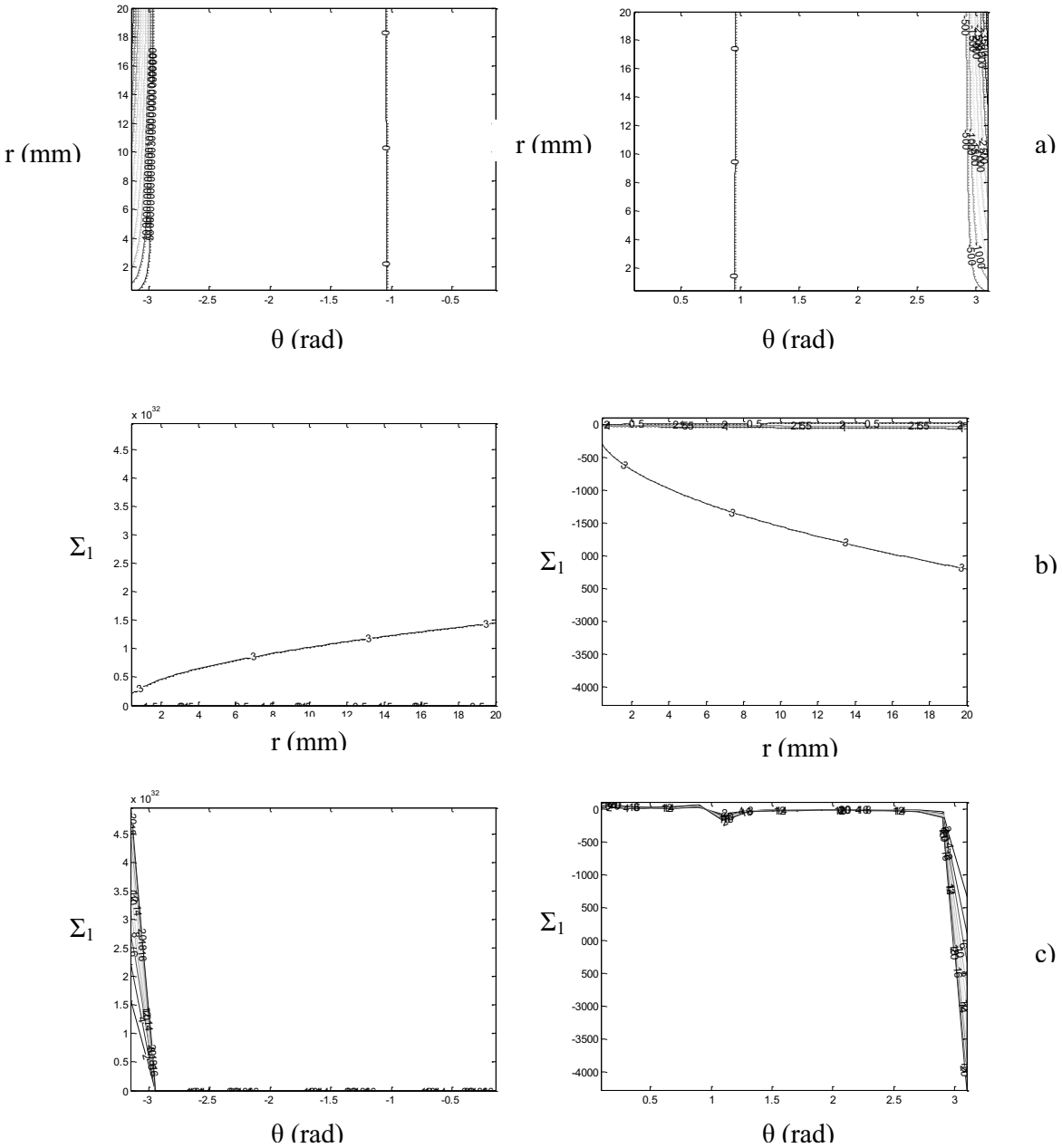

Figure 3: Reduced major principal stress Σ_1 for $r \in V(0)$

a) curves for maximal isostress field
b) versus position of the crazing patterns r.
c) versus the orientation of the crazing patterns θ.

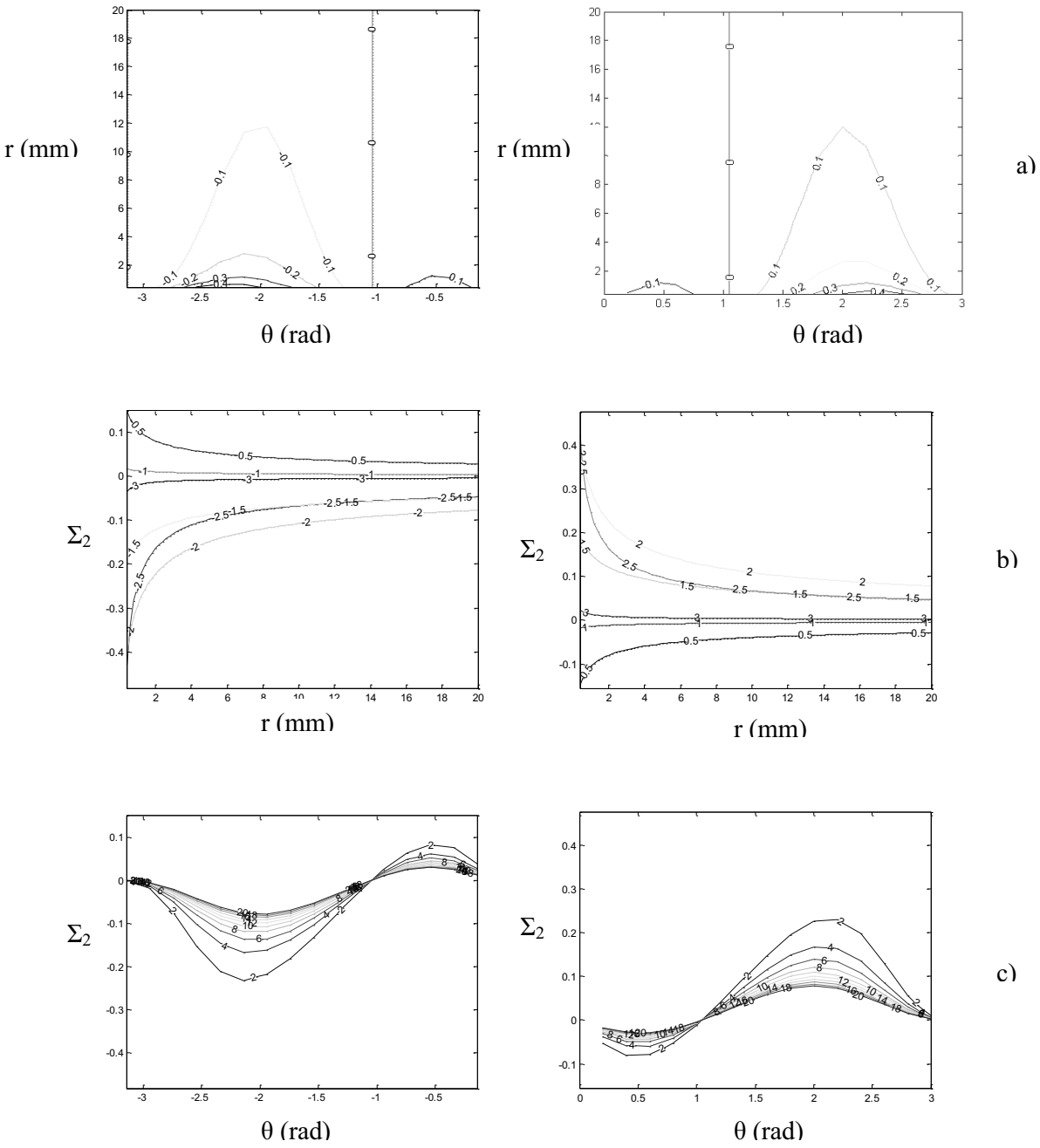

Figure 4: Reduced minor principal stress Σ_2 for $r \in V(0)$

a) curves for minimal isostress field
b) versus position of the crazing patterns r.
c) versus the orientation of the crazing patterns θ.

4. Stress intensity factor

The Stress Intensity Factor (SIF) for a fissured plane medium under mode I is defined as follows;

$$K_I = \lim_{r \longrightarrow 0} [\sigma_{yy} (2\pi r)^{1/2}] \quad (3)$$

Using the aboves stress field, the SIF becomes;

$$K_I/K_0 = 1.12 (\pi.L). \cos \theta/2 (1 + \sin \theta/2 \sin (3/2) \theta) \quad (4)$$

Here, K_0 is the stress intensity factor in absence of damage.

On the basis of these reduced principal stresses, the mode I SIF (K_I/K_0) is drawn versus the length of the main crack as shown in Fig. (7). Here, K_0 stands to the SIF due to remotely load in the absence of the damage zone consisting of crazing patterns. It is proven, herein, that existing crazes closer to the main crack dominate the resulting interaction effect and reflect an anti-shielding of the damage while a reduction constitutes a material toughness

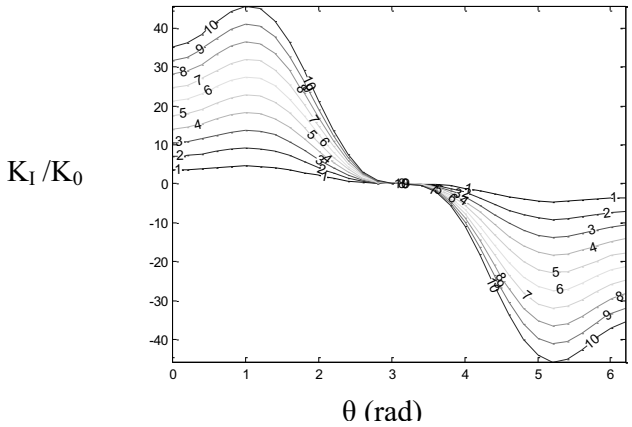

Figure 5: Variation de K_I / K_0 function of the position of crazing patterns.

5. Conclusion

Analysis of the distribution of surface crazes in the vicinity of a stationary edge crack in a polystyrene (PS) sheet in tension has shown that the craze growth occurs along directions parallel to the minor principal stress axis. It shown throughout this study that the stress field distribution in the vicinity of the main crack is obtained by the resolution of some differential equations along with appropriate boundary conditions. Reduced principal stresses trajectories are established according to Mohr's criteria. It is proven, herein, that the mode I stress intensity factor is employed to quantify the effects on a crack of the damage consisting of crazing patterns.

References

[1] B. Bevis and D. Hull, “Craze distribution around cracks in polystyrene”, International Journal of Materials Science, **5,** p. 983 (1970).

[2] *A.* Chudnovsky, I. Palley and E. Baer, “Thermodynamics of the quasiequilibrial growth of crazes”, International Journal of Materials Science, **16**, p. 35 (1981).

[3] D. Post, Proceedings of Society for Experimental Stress Analysis **12,** p. 99 (1954).

[4] J. Botsis, A. Chudnovsky and A. Moet, “Fatigue crack layer propagation in polystyrene”, International Journal of Fracture*,* Parts I and II, **33**, p. 263 (1987).

[5] M. Chabaat, “Comparison of minimal principal stress trajectories with craze distribution in an amorphous polymer”, International Journal of Fracture*,* **37**, p. 47 (1988).

[6] N. Tada, P. C. Paris and G. R. Irwin, The Stress Analysis of Cracks Handbook, Del Research Corporation, Hellertown, PA (1973).

A Dynamical for Flow Localization in Irradiated Materials

Silvester Noronha[1], Nasr Ghoniem[2], Garani Ananthakrishna[3]

[1]AREVA NP Inc, Lynchburg, VA, [2]University of California- Los Angeles, CA
[3]Indian Insititute of Science, Bangalore, India
(E-mail: silvester.noronha@areva.com)

ABSTRACT

When subjected to prolonged irradiation, metals tend to harden and non uniform deformation occurs. This localized deformation degrades the mechanical behavior of materials and cause premature failure due to plastic instability or cracks. The irradiation induced aging and related microstructural evolution can be modeled using well known dislocation transformation reactions and dislocation-defect interactions. A dislocation transformation model with mobile dislocations, forest dislocations and vacancy clusters (stacking fault tetrahedra) is proposed. Rate equations for the evolution of densities of mobile dislocations, forest dislocations and vacancy clusters lead to a coupled set of nonlinear differential equations. For a range of relevant physical parameters like irradiation dose and temperature these equations admit periodic solutions called limit cycles. When spatial dependency is considered they exhibit localized deformation for a range of irradiation dose. The behavior of this localized deformation as a function of irradiation dose and relevant parameters will be reported.

New Strengthening Mechanism of Cu Precipitate in BCC Fe

Zhengzheng Chen[1], Nicholas Kioussis[1], Nasr Ghoniem[2]

[1]Department of Physics, California State University, Northridge, CA 91330; [2]Department of Mechanical and Aerospace Engineering, University of California Los Angeles, CA 90095 (E-mail: satchel1979@gmail.com)

ABSTRACT

We performed the molecular dynamics (MD) simulations on mobility of screw dislocation in BCC Fe with presence of BCC structure Cu precipitates. The results show that the dislocation is pinned at the interface if Cu precipitate is large enough to change the atomic structure of dislocation core. When dislocation moves to the interface, the segment inside the Cu will experience a polarized-core → nonpolarized-core process. This process requires extra stress and thus curves dislocation line. This polarized-based mechanism of the pinning effect gives good estimation of bow-out angle and increasing stress consisting with experiments.

Neutron and proton irradiation cause hardening and embrittlement to ferritic steels serving as reactor pressure vessel (RPV). One of the main reasons for this irradiation-induced hardening phenomenon is the nucleation and growth of Cu precipitates. Because of the low solubility of Cu in Fe at low temperatures, Cu-rich precipitates can easily nucleate and then begin to coarsen and grow under thermal ageing. Small-sized Cu precipitates with BCC structure respond to the strengthening of RPV steel. Recently, Nogiwa *et al*. used *in situ* transmission electron microscope (TEM) to observe the interaction between ultrafine Cu precipitates and dislocations [1]. They found that dislocations are curved and pinned by these ultrafine precipitates. Accordingly, BCC Cu precipitates serve as obstacles to dislocation movement. Though clear observation is available, the mechanisms of Cu precipitate strengthening is still an open question Recent atomic simulations emphasized the necessity to investigate detailed atomic structure instead of considering continuum elasticity theory only [2, 3]. Recently, Shim *et al*. discussed the strengthening mechanism [4]. They found that it is because the structure transformation of Cu that dislocation cannot penetrate into precipitate and forms loops. This work demonstrated the relationship between the geometry transformation and pinning effect of precipitate. However, Nogiwa measured bow-out angle and found the average is 150˚, and did not find loops [1]. This disagreement shows that the details of the mechanism are not fully understood yet.

In this Letter, we perform MD simulations on mobility of <111>a/2 screw dislocation with present of BCC Cu precipitates. The MD simulations are performed with the Finnis-Sinclair potentials fit by Ackland et al. [5]. The size of the entire system is 14.0×12.2×19.9 nm^3 along the X (<110>), Y (<112>), and Z (<111>) directions, respectively, containing 288,000 atoms. Periodic boundary conditions are applied along the Z direction and fixed boundary conditions are employed along the X and Y directions, respectively. Two BCC Cu precipitates are presented with diameters (d) of 2.3 nm and 1.0 nm. A <111>a/2 screw dislocation is generated at the centre of precipitates. The whole system is first thermally equilibrated at 5 K for 30. After that, we

applied 1000 MPa stress σ_{yz} to drive the dislocation to move. The total simulation time is 36 ps, and the time step is 1 fs in all the MD simulations.

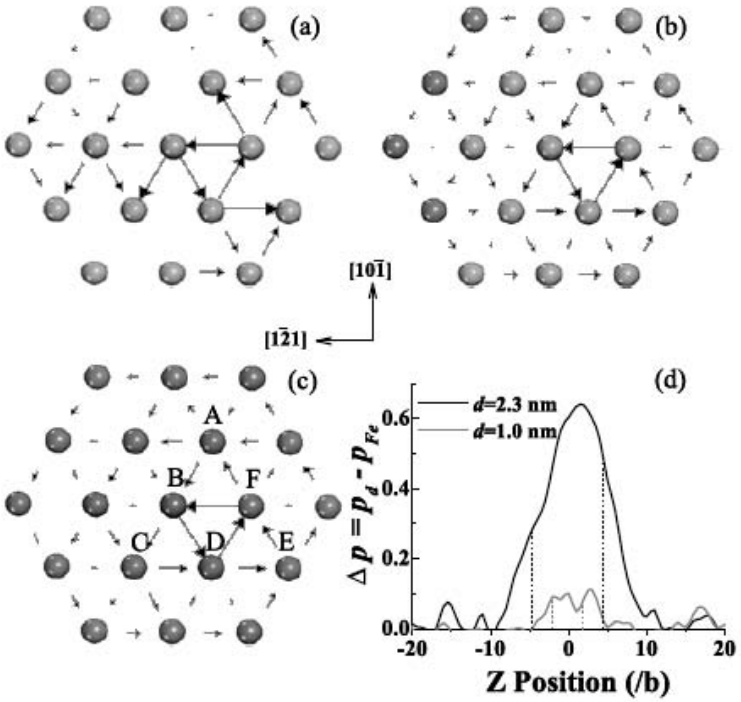

Figure 1. Dislocation core inside a Cu precipitate with (a) d = 2.3 nm; (b) d = 1.0 nm; and (c) d = 0.0 nm (Pure Fe). The red and blue spheres represent Cu and Fe, respectively. (d) Change of dislocation core polarization versus atomic position (normalized to b) along the dislocation line. The black and red curves represent the 2.3 nm and 1.0 nm Cu precipitates, respectively. The vertical dashed lines indicate the precipitate-matrix interface.

The ground core structures inside and outside the precipitate are shown in Fig. 1. The differential displacement (DD) maps are used to visualize the dislocation core. The arrows indicate the relative <111> displacement of neighboring atoms of the dislocation. The length (direction) of the arrow denotes the magnitude (sign) of the displacement difference. Comparing with the core in pure Fe [Fig. 1(c)], the Cu precipitate of d = 2.3 nm dramatically changes the core structure: the displacement field spread only on 3 {110} semi-planes. On the contrary, Cu precipitate of d = 1.0 nm does not change it. There is only marginal change in the precipitate. Fig. 1(d) shows the change of polarization p of dislocation core with respect to Fe, distributing along Z direction. It clearly shows the size-dependent effect on core structure of Cu precipitate. The completed calculation shows that the critical size is d_c = 1.5 nm, which is consistent with TEM result [1].

Fig. 2(a) presents snapshots at different time during the MD simulation with 2.3 nm Cu-precipitate. After 2 ps, the dislocation core inside the precipitate moves via nucleation and migration of kink pairs. When dislocation reaches to the interface, the segments inside the precipitate and in the vicinity region are pinned while those far away from the precipitate move. The dislocation line begins to bow out. At 12 ps, the curvature reaches the maximum. Then, at

14 ps, the dislocation detaches and moves out from the Cu precipitate, and dislocation line restores to straight. The Orowan loop is not observed. The observation clearly shows the key role of interface of precipitate and matrix. It is consistent with the conclusion of Harry [2]. As a comparison, Fig. 2(b) also shows the snapshot of dislocation with 1.0 nm-Cu-precipitate. There is no pinning happens on the interface, the dislocation moves as it is in pure BCC Fe.

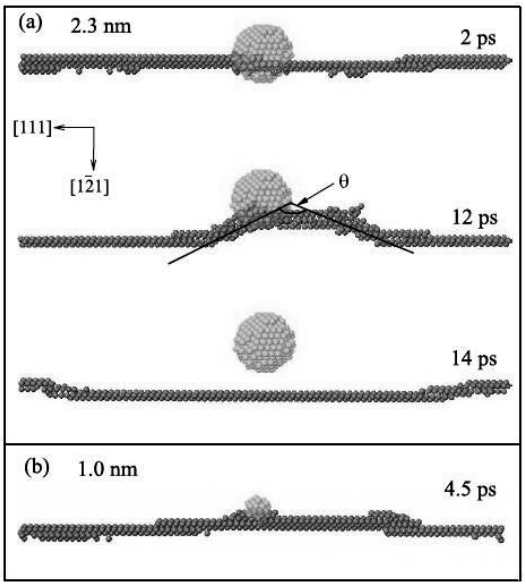

Figure 2. (a) Snapshots of the dislocation core at 2 ps, 12 ps and 14 ps for the 2.3 nm Cu-precipitate. (b) Snapshot at 4.5 ps for the 1.0 nm Cu-precipitate.

We plot DD maps for dislocation at different time in Fig. 3. At 8.5 ps, the dislocation has reached the interface, and the polarized core stays in the precipitate, while a non-polarized core appears on the interface. 3.5 ps later, at 12 ps, only the non-polarized core remains. One should note that the DD map of this core is almost the same as the core structure in BCC Fe under the stress that slightly below the critical stress. This similarity suggests that dislocation line needs to curve to supply the extra stress to transform the core structure. Finally, at 14 ps, the dislocation core totally moves out from the Cu precipitate and shows a non-polarized core structure.

The dislocation can detach from the precipitate when this extra force F_{cr} exceeds the pinning force [2]

$$F_{cr} = \Delta\tau_{cr} Lb \geq F_{pin}, \tag{1}$$

where $F_{pin} = 2\Gamma\cos(\theta/2)$ and L is the precipitate distance along the dislocation line. Here, θ is the bow-out angle, the line tension $\Gamma = \mu b^2/2$, where $\mu = 66.9$ GPa is the shear modulus of Fe calculated by this potential. As shown in Fig. 2(a) $\theta = 128^\circ$, in good agreement with the average value of 150˚ reported in experiments [1]. Thus, we find that $F_{pin} = 2.05\times10^{-9}$ J/m and $\Delta\tau_{cr}$ is 364 MPa for $L = 19.9$ nm, in excellent agreement with the experimental value of 70 MPa for $L = 111$ nm and the theoretical value of 335 MPa for $L = 17$ [2].

We performed MD simulations to study the strengthening effect of Cu precipitates in Fe. The results suggest a novel mechanism associated with the change of dislocation core structure for precipitates larger than a critical size. For larger precipitates, the dislocation needs to first transform its core from polarized to non-polarized, thus resulting in the pinning of the dislocation at the precipitate-matrix interface. The required extra stress is provided by the bowing out of the dislocation line. The calculated values for both the bow-out angle and the extra stress required to detach from the precipitate are excellent consistent with recent TEM experiments.

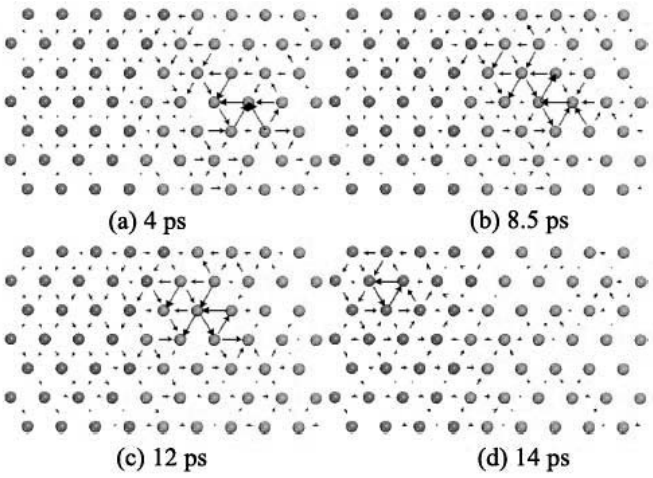

Figure 3. the dislocation core of the 2.3 nm Cu precipitate at (a) 4 ps, (b) 8.5 ps, (c)12 ps and (d) 14 ps, respectively. The red and blue spheres represent Cu and Fe, respectively.

Acknowledgements

We acknowledge valuable discussions with G. Ackland. This research was supported by DOE NERI grant DE-FC07-06ID14748 and NSF-PREM grant DMR-00116566.

References

[1] K. Nogiwa, N. Nita and H. Matsui, "Quantitative Analysis of the Dependence of Hardening on Copper Precipitate Diameter and Density in Fe-Cu Alloy", Journal of Nuclear Materials, **367-370,** 392 (2007).

[2] T. Harry and D. Bacon, "Computer Simulation of the Core Structure of the <111> Screw Dislocation in α-iron Containing Copper Precipitates: II. Dislocation-Precipitate Interaction and the Strengthening Effect", Acta Materialia, **50,** 209 (2002).

[3] Y. Osetsky, D. Bacon, and V. Mohles, "Atomic Modelling of Strengthening Mechanisms due to Voids and Copper Precipitates in α-iron", Philosophical Magazine, **83**, 3623.

[4] J. Shim, Y. Cho, S. Kwon, W. Kim and B. Wirth, "Screw Dislocation Assisted Martensitic Transformation of a BCC Cu Precipitate in BCC Fe", Applied Physics Letters, **90**, 021906 (2007).

[5] G. Ackland, M. Mendelev, D. Srolovitz, S. Han and A. Barashev, "Development of an Interatomic Potential for Phosphorus Impurities in a-iron", Journal of Physics: Condensed Matter, **16**, S2629 (2004).

Molecular Dynamics Simulation Study of Pseudoelastic Effects in Palladium Nanowires

Jijun Lao and Dorel Moldovan

Department of Mechanical Engineering, Louisiana State University, 2504 Patrick Taylor Hall, Baton Rouge, LA 70803, USA (E-mail: jlao1@lsu.edu, moldovan@me.lsu.edu)

ABSTRACT

Using molecular dynamics (MD) simulations we investigate the surface-stress-induced structural transformations and pseudoelastic behavior in palladium crystalline nanowires. For a <100> initial crystal orientation our studies indicate that the surface stress can cause Pd nanowires to spontaneously undergo structural changes with characteristics that are determined by the wire cross-sectional area. Specifically, when the cross-sectional area is below 2.18 nm × 2.18 nm the wire changes spontaneously its crystal structure from the initial fcc structure to a body-centered tetragonal (bct) structure. In wires of larger cross-sectional area (i.e., 2.57 nm × 2.57 nm) the structural transformation is achieved via a spontaneous lattice reorientation leading to an fcc wire with <110> orientation. In both cases, under tensile loading and unloading Pd nanowires transform reversibly between the corresponding transformed structures and the original <100> structure exhibiting pseudoelastic behaviors characterized by comparable, fully recoverable, strains of up to 50%. Moreover, the temperature-dependence of the two pseudoelastic behaviors enables the shape memory effects in Pd nanowires.

1. Introduction

With the miniaturization of electrical, optical, thermal, and mechanical systems the feature size of relevant device components are reduced down to several nanometers. When two spatial dimensions of the systems are in the nanometer range (i.e. nanowire structures) the structural characteristics and stability are strongly influenced by both surface energy and surface stress. Recent atomistic simulation studies have identified two distinct mechanisms that mediate the spontaneous structural changes in metallic nanowires. In certain metals when the cross-sectional area is below $4nm^2$ the surface stress can be large enough to cause a phase transformation that drives the system from the initial fcc structure into a bct structure [1]. Nanowires with larger cross-sectional areas can undergo spontaneous crystal structure reorientation; that is, fcc wires with initial <100> orientations can reorient spontaneously under the effect of surface stress into <110> orientations [2]. Associated with the existence of reversible crystallographic lattice reorientation a novel pseudoelastic behavior in these nanowires was discovered and studied extensively [3]

In this study, using MD simulations, we investigate the fundamentals of both reversible surface-stress-induced fcc to bct phase transformation and reversible <100> to <110> crystal structure reorientation as well as the associated novel pseudoelastic behaviors.

2. Simulation Model and Methodology

The MD simulations were performed using the embedded-atom method (EAM) potential for Pd [4]. Single crystalline Pd [100] nanowires with a square cross section and surface orientation of [100], [010], and [001] were created with initial atomic positions corresponding to the bulk fcc Pd crystal. To investigate the role of the diameter on wire structural stability and mechanical behavior we carried out MD simulations of Pd nanowire systems of various cross-sectional areas. We focused our analysis on three wire systems having original cross-sectional areas of 1.78 nm × 1.78 nm, 2.18 nm × 2.18 nm, and 2.57 nm × 2.57 nm respectively. All wires considered were 31.2 nm in length. Free boundary conditions were used in all directions

3. Results and Discussion

The MD simulation results indicate that due to the presence of large intrinsic surface stresses all three Pd wires undergo spontaneous structural transformations. Namely, at T = 100K the two wires with cross-sectional areas of 1.78 nm × 1.78 nm and 2.18 nm × 2.18 nm respectively undergo phase transformations from the initial fcc to a bct crystal structure whereas the wire with 2.57 nm × 2.57 nm cross-sectional area experiences lattice reorientation into a <110> wire with {111} surfaces. Fig. 1. (a) illustrates the dynamic progression of the fcc to bct phase transformation. During the first 3.0 ps the fcc wire relaxes elastically and contracts longitudinally by about 6.1%. After the elastic contraction a new bct crystalline phase nucleates at the ends and propagates with a speed of approximately 538 m/s toward the center of the nanowire. Fig1.(b) depicts the dynamic progression of structural reorientation in the Pd nanowire. During the first 3.8 ps the wire contracts elastically. After the elastic contraction the lattice reorientation nucleates at the ends and propagates towards the center of the nanowire.

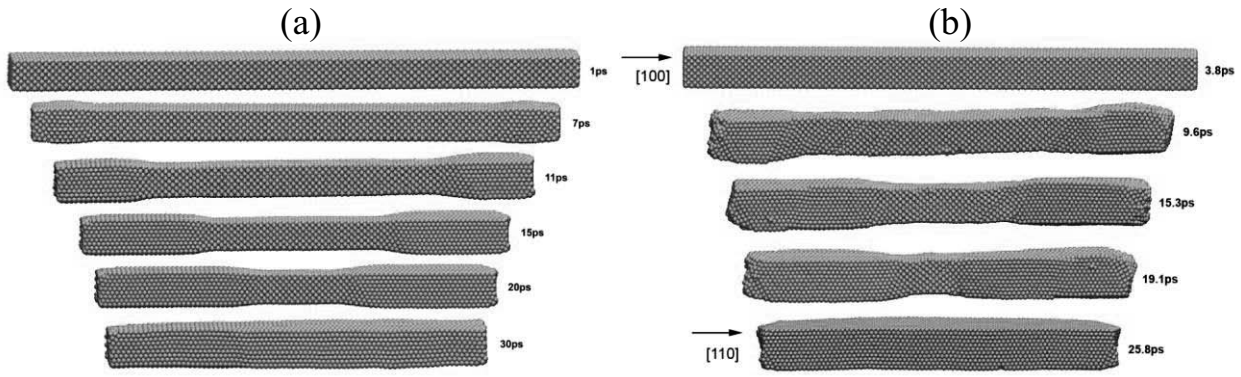

Figure 1. (a) Six snapshots depicting the time evolution of a 1.78 nm × 1.78 nm Pd nanowire during the spontaneous, surface-stress-driven, fcc to bct phase transformation at 100K. Snapshots of the wire at 1, 7, 11, 15, 20, and 30 ps respectively are shown here. (b) Five snapshots depicting the spontaneous crystalline reorientation at 100K in a Pd nanowire of 2.57 nm × 2.57 nm cross sectional area. Snapshots at 3.8, 9.6, 15.3, 19.1, and 25.8 ps respectively are shown here.

After the completion of the spontaneous fcc to bct phase transformation in the 1.78 nm × 1.78 nm wire, the bct wire was loaded in the longitudinal direction to investigate the pseudoelastic behavior. Both tensile loading and unloading studies were conducted under simulated quasistatic conditions. Namely, at each load step the coordinates of all atoms were modified according to a prescribed uniform strain increment of 0.125% (or a strain decrement for unloading) in the length direction.

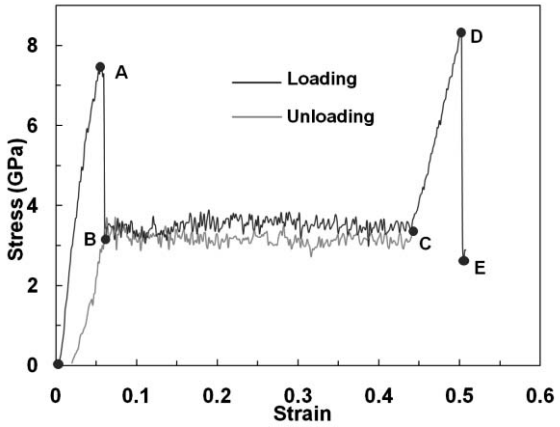

Figure 2. Stress-strain curve for the 1.78 nm x 1.78 nm Pd wire undergoing reversible bct to fcc phase transformation during loading and unloading at 100K.

Fig. 2 shows the stress-strain curves for the 1.78 nm × 1.78 nm wire during loading and unloading at 100K. The curves indicate that the Pd wire is indeed very ductile with fracture strains of approximately 50%. Point B on the curve indicates the nucleation of the fcc phase at the ends of the bct wire. The subsequent motion of the newly nucleated fcc regions marks the beginning of the bct to fcc phase transformation; process which is also associated with the plateau region of the stress-strain curve. At point C the entire wire has been converted to the fcc structure. Interestingly, there is no strain hardening during this stage of deformation.

The 1.78 nm × 1.78 nm fcc wire transforms spontaneously back to the 2.196 nm × 2.196 nm bct configuration via phase change mediated by short range atomic rearrangement processes in reverse to what is described above when the temperature is above a certain value. The curve depicted in red in Fig.2 traces the stress-strain relationship during the controlled simulated quasistatic unloading of the fcc wire. The spontaneous fcc to bct phase transformation occurs only when the temperature is above a critical value Tc. If the temperature is below Tc, the fcc wire configuration is stable. Our MD simulations indicate that the critical temperature, Tc, for the Pd nanowires investigated is around 22.5K

Fig. 3 shows the stress-strain curve obtained during loading and unloading at 100K of the 2.57 nm × 2.57 nm Pd wire that undergoes reversible <110>/{111} to <100>/{100} lattice reorientation. Detailed analysis of similar pseudoelastic behavior has been carried out extensively in Au, Cu and Ni nanowires by Liang et al. [3] and by Park et al. [5]. Comparison of the two stress-strain curves (Fig. 2 and Fig 3), quantifying the two pseudoelastic behaviors mediated by different mechanisms, indicate that there are both similarities and differences between the two systems. Namely, although both transformations can achieve similar levels of

strains they differ qualitatively and quantitatively in the plateau regions. While the loading stress-strain curve for the lattice reorientation-controlled pseudoelastic behavior exhibits a small strain hardening over the range of strains delimited by the begin and the end stage of the reorientation process (see Fig. 3), no such phenomena is observed on the corresponding portion of the stress-strain curve for the fcc to bct phase transformation-controlled pseudoelastic behavior (see Fig.2).

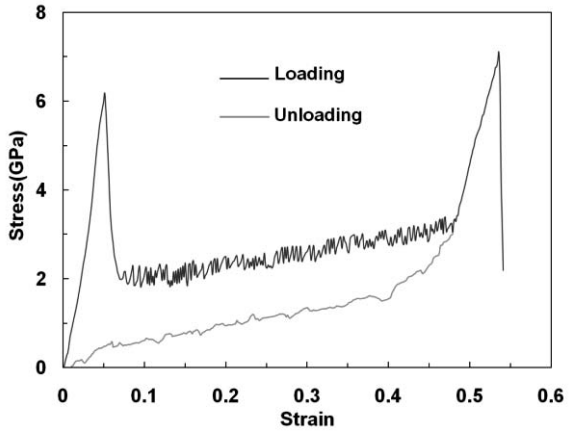

Figure 3. Stress-strain curve for the 2.57 nm x 2.57 nm Pd wire during loading and unloading at 100K.

4. Conclusions

We have shown that depending on the cross-sectional area the surface stress can cause palladium nanowires to undergo either spontaneous phase transformation from fcc to bct structure or <100> to <110> crystal structure reorientation. In both cases under tensile loading and unloading Pd nanowires transform reversibly between the corresponding crystalline structures and the initial <100> structure exhibiting novel pseudoelastic behaviors characterized by fully recoverable strains of up to 50%.

Acknowledgements: This work was supported in part by NSF-EPSCoR (Grants #: EPS-0701491 and EPS-0346411). J.L. was supported by a Graduate Fellowship from LONI Institute.

References:

[1] J. Diao, K. Gall and M. L. Dunn, "Surface-stress-induced phase transformation in metal nanowires", Nature Materials **2**, 656 (2003).
[2] J. Diao, K. Gall, and M. L. Dunn, "Surface stress driven reorientation of gold nanowires", Physical Review B **70**, 075413 (2004).
[3] W. Liang, M. Zhou, and F. Ke, " Shape memory effect in Cu nanowires", Nano Letters **5**, 2039 (2005).
[4] S. M. Foiles, M. I. Baskes, and M. S. Daw, "Embedded-atom-method functions for the fcc metals Cu, Ag, Au, Ni, Pd, Pt, and their alloys", Physical Review B **33**, 7983 (1986).
[5] H. S. Park, K. Gall, and J. A. Zimmerman, "Shape memory and pseudoelasticity in metal nanowires", Physical Review Letters, **95**, 255504 (2005).